Molecular Determinants of Multiple Sclerosis Spinal Cord Pathology

Alex David Waldman

St. John's College, University of Oxford

National Institutes of Health Oxford-Cambridge Scholars Program

Emory Medical Scientist Training Program

Supervisors:

Professor Gabriele De Luca

Dr. Michael J. Lenardo

A Thesis Submitted for the Degree of

Doctor of Philosophy

Hilary Term 2023

Abstract:

Multiple sclerosis (MS) is a chronic inflammatory, demyelinating, and degenerative disorder of the central nervous system (CNS). Disease progression commonly presents as a relentless myelopathy, nominating the spinal cord as an essential anatomical site to investigate in detail. In the current thesis, we leveraged the power of deeply endophenotyped post-mortem and clinical MS cohorts to better understand the molecular determinants of spinal cord pathology. Pathologically, we assessed the interplay between demyelination, inflammation, and neurodegeneration. We observed that demyelination was common, highly inflammatory, and related to clinical measures of disability even at late disease stages. Lesions commonly spared the subpial surface and were vascularly-associated, arguing against a pathological gradient of spinal cord demyelination. We also observed that axonal loss in the normal-appearing white matter motor tracts was a common feature of MS spinal cord pathology. Spinal cord cross-sectional area at end-stage disease woefully underestimated the extent of axonal loss. Activated myeloid cell inflammation but not lesion load was predictive of more severe axonal loss. Given that biomarkers of axonal loss have remained elusive, we also performed proteomics on post-mortem cerebrospinal fluid (CSF), a translational biospecimen. Network analysis identified a signature, enriched in opsonins, that segregated with the degree of axonal loss and presence of spinal cord demyelination. We subsequently performed validation studies of this signature using a well-characterised clinical MS cohort. While this signature distinguished MS and control patients, it did not relate to measures of clinicoradiographic disability. These findings underscore the insensitivity of clinicoradiographic assessments in the short-term and highlight the power of a pathology-driven approach to biomarker discovery. Taken together, our findings nominate vascular dysfunction, CSF opsonins in the perivascular space, and activated myeloid cells as key players in the pathogenesis of MS spinal cord pathology.

Publications and Presentations Related to Thesis:

Publications

1. **Waldman, A.D.**, Catania, C., Pisa, M., Jenkinson, M., Lenardo, M., & De Luca, G.C. 2022. Histopathological Characterization of Staged Lesion Topography in the Multiple Sclerosis Spinal Cord. *medRxiv*

Oral Presentations

1. The Prevalence and Topography of Staged Demyelinated Lesions in the Multiple Sclerosis Spinal Cord
   - **October 2022**, Virtual, National Institutes of Health Laboratory of Immune System Biology Seminar (invited talk) | **June 2022**, Virtual, American Society of Investigative Pathology (invited talk) | **February 2022**, Virtual, Brain Conference 2022 | **July 2021**, Virtual, National Institutes of Health Oxford-Cambridge Scholars Annual Workshop

Poster Presentations

1. **A. Waldman**, C. Catania, M. Pisa, M. Jenkinson, GC. De Luca, The prevalence and topography of spinal cord demyelination and inflammatory activity in multiple sclerosis
   - **October 2022**, Amsterdam, Netherlands, Congress of the European Committee for Treatment and Research in Multiple Sclerosis (ECTRIMS) | **July 2022**, Paris, France, Federation of European Neuroscience Societies (FENS) Forum | **July 2022**, Swansea, Wales, MS Frontiers | **November 2021**, Virtual, European Charcot Foundation Annual Meeting: MS at the Extremes (*Young Investigator Award: Basic Sciences*)
2. **A. Waldman**, P. Charles, R. Fischer, GC. De Luca, Intrathecal opsonins and spinal cord axonal loss in multiple sclerosis
   - **November 2022**, Baveno, Italy, European Charcot Foundation Annual Meeting: Progressive MS from Pathology to Treatment (*Young Investigator Award: Investigations*), **February 2022**, Virtual, Americas Committee for Treatment and Research in Multiple Sclerosis (ACTRIMS) Forum 2022

Publications and Presentations Unrelated to Thesis:

Publications

1. Kubo, S., Fritz, J.M., Raquer-McKay, H.M., Kataria, R., Vujkovic-Cvijin, I., Al-Shaibi, A., Yao, Y., Zheng, L., Zou, J., **Waldman, A.D.**, Jing, X., Farley, T.K., Park, A.Y., Oler, A.J., Charles, A.K., Makhlouf, M., AbouMoussa, E.H., Hasnah, R., Saraiva, L.R., Ganesan, S., Al-Subaiey, A.A., Matthews, H., Flano, E., Lee, H.H., Freeman, A.F., Sefer, A.P., Sayar, E., Çakır, E., Karakoc-Aydiner, E., Baris, S., Belkaid, Y., Ozen, A., Lo, B., Lenardo, M.J. 2022. Congenital iRHOM2 deficiency causes ADAM17 dysfunction and environmentally directed immunodysregulatory disease. *Nat Immunol* 23(1): 75-85.
2. **Waldman, A.D**., Fritz, J.M., & Lenardo, M.J. 2020. A guide to cancer immunotherapy: from T cell basic science to clinical practice. *Nat Rev Immunol* 20: 651-668
3. Zhong, J., **Waldman, A.D**., Kandula, S., Eaton, B.R., Prabhu, R.S., Huff, S.B. & Shu, H.K.G. 2020. Outcomes of whole brain radiation with simultaneous in-field boost (SIB) for the treatment of brain metastases. *J Neurooncol* 147(1):117-123.
4. Wetzel, J.S., **Waldman, A.D**., Buster, B., Texakalidis, P., Eshraghi, S.R., Wheelus, J., Reisner, A., & Chern, J.J. Survival and Failure Trends of Cerebrospinal Fluid Shunts with Distal Slit Valves: Comparative Study and Literature Review. 2019. *J Neurosurg Pediatr* 13: 1-8.
5. Sadigh, G., Saindane, A.M., **Waldman, A.D**., Lava, N.S., & Hu, R. Comparison of Unenhanced and Gadolinium-Enhanced Imaging in Multiple Sclerosis: Is Contrast Needed for Routine Follow-Up MRI? 2019. *AJNR Am J Neuroradiol* 40(9): 1476-1480.
6. Cengiz, P., Zafer, D., Chandrashekhar, J.H., Chanana, V., Bogost, J., **Waldman, A**., Novak, B. Kintner, D.B., & Ferrazzano, P.A. Developmental differences in microglia morphology and gene expression during normal brain development and in response to hypoxia-ischemia. 2019. *Neurochem Int* 127: 137-147.

Oral Presentations

1. A Crash Course on the American Physician Scientists Association (APSA)
   - **June 2022**, Virtual, American Society of Investigative Pathology (invited talk)
2. iRHOM2 Deficiency Resulting in ADAM17 Dysregulation and Chronic Cavitary Pulmonary Infections
   - **September 2019**, Bethesda MD, National Institutes of Allergy and Infectious Diseases Genomics and Immunology Brown Bag

Poster Presentations

1. **A. Waldman**, K. Binder, G.C. De Luca, M.J. Lenardo, Extreme outcomes in multple sclerosis: Rare variation to the rescue
   - **June 2019**, Oxford, UK, National Institutes of Health Oxford-Cambridge Scholars Annual Workshop | **February 2019,** Bethesda, MD, National Institutes of Health Graduate Student Symposium
2. **A. Waldman**, J. Rosenthal, J.C. Howell, L. Schwartz, T. Ozturk, R. Hu, W.T. Hu, W.R. Tyor, Sexually dimorphic multiple sclerosis pathogenesis
   - **May 2019**, Seattle, WA, The Consortium of Multiple Sclerosis Centers Annual Meeting

Dedication:

I dedicate this work to my grandmother, Lila Waldman, who passed away during my final year of studies. The love, support, and generosity she demonstrated throughout my upbringing made me the person I am today and set the stage for me to go on this long educational journey. She displayed tremendous perseverance as a Jewish female working within institutions of higher education beginning in the 1940s. Her guiding hand allowed me to embrace my LGBTQ+ identify and taught me to always work hard in the face of adversity. Completing this degree would not have been possible without her positive influence.

Acknowledgements:

This thesis was made possible by the support of many individuals. First, I would like to thank my supervisors, Professor Gabriele De Luca (University of Oxford) and Dr. Michael Lenardo (National Institutes of Health). They were instrumental to the success of my thesis and my professional development more broadly. I cannot express how grateful I am for the support I have been provided, especially in the face of personal and professional difficulties that arose.

I would also like to thank my peers in the De Luca and Lenardo research groups. I can only hope that our paths cross again and wish each of you the best of luck in your future career endevors. The data and intellectual foundation of this work can be traced back to past members of both research groups and I would like to thank all the individuals who laid the groundwork for my scientific journey. I particularly want to thank Sydney Yee, Adele Smart, Jill Fritz, Lixin Zheng, and Kyle Binder for technical skills training. I also thank Greg Halliwell, a final year honours medical student, for allowing me the opportunity to serve as his research mentor. It was a pleasure working with you and I am so happy to see you pursuing a PhD at Cambridge. I look forward to continued collaboration. I also cannot express enough gratitude to Aimee Avery, Jonathan Pansieri, Marco Pisa, and Cecilia Catania for close collaboration and support. The work in this thesis would not have been possible without our joint efforts.

I would be remissed if I did not recognize my past scientific mentors: Professor Peter Ferrazzano, Professor Pellin Cengiz, Professor Qiang Chang, Dr. Janet Batzli, and Dr. Michelle Harris. Your mentorship and influence led me to pursue a dual degree and I cannot thank you enough for your longitudinal support.

I am humbled to have the opportunity to work with human samples and data derived from the UK MS Tissue Bank and Swiss MS Cohort Study. The selfless sacrifice made by donors and

their families has made this work possible and does not go unoticed. I also wish to thank the UK MS Tissue Bank leadership team and scientific staff, Richard Reynolds, Richard Nicholas, Djordje Gveric, and Marta Camba, and the Principal Investigators of the Swiss MS Cohort Study, Ludwig Kappos and Jens Khule.

This work would also not have been possible without an international team of collaborators. Mapping of demyelinated lesions was performed in collaboration with the Wellcome Centre for Neuroimaging at the University of Oxford. Thank you to Mark Jenkinson for training me in the use of FSL software. Post-mortem proteomics experiments involved guidance from the Target Discovery Institute at the University of Oxford and the Proteomics Core at Emory University. Thank you to Simon Davis, Georgina Berridge, Phil Charles and Roman Fischer from the University of Oxford for assistance with sample preparation and mass spectrometry data processing. I also would like to thank Nicolas Seyfried and Eric Dammer for guidance with downstream network data analysis. Linking clinical CSF proteomics with clinicoradiographic disability measures involved individuals from University of Basel, University College London, and University of Oxford. Thank you to Jens Khule, David Leppert, Pascal Benkert, Eline Willemse, Johanna Oechtering, Cristina Granziera, Lester Melie Garcia, and Charidimos Tsagkas from the University of Basel for your assistance in extracting clinicoradiographic data from MS patients in the Swiss MS Cohort Study. I also want to thank Ferran Prados, Marcello Moccia, Frederik Barkoff, and Olga Ciccarelli from University College London for guidance in tabulating spinal cord atrophy from legacy brain MRI images. I am also grateful to Daniel Anthony and Fay Probert from the University of Oxford for computational assistance and generation of SomaScan® CSF proteomics data in collaboration with Novartis.

Thank you to the Biocomputational and Biostatiscal Branch within the National Institutes of Allergy and Infectious Diseases, namely Jon Fritzi, Poorani Subramanian, Michael Bast, and Sergei Ponomarev for your education in statistical and biocomputational concepts.

I am also grateful for the strong administrative support I received from Maria Hessie, Nicole Yung, Sarah Weber, Kim Bradley, Karen Hennigan, and Kim Tindal whilst traversing a complex international doctoral degree as an National Institutes of Health trainee. Thank you to the National Institutes of Health Oxford-Cambridge Program Leadership team and Executive Committee. I particularly want to highlight Katie Stagliano, Kristi Porter, Racquel Collins-Milinkovich, Kara Rothberg, Ashley Moore, Alan Sher, Lisa Cunningham, Sonja Best, Daniel Reich, and Michael Dustin. Your support has never wavered and has been instrumental in ensuring I had the necessary resources to complete my degree in a timely manner even in the face of COVID-related disruptions. I also cannot express enough appreciation for the International Biomedical Research Alliance Leadership team, including Randi Balletta, Alexandra Ambrico. You have provided me with unique professional development experiences that I will never forget and have allowed me to better understand my future career goals.

Throughout my dual degree, I am grateful for the support I have been provided from Emory University Faculty, namely Dr. Jason Schneider and Dr. William Tyor, and members of the Medical Scientist Training Program leadership team, including Robert Gross, Joanna Bonsall, Anita Corbett, Ann Chahroudi, Paul Garcia, Cathy Quinones-Maseo, Erica Weaver, Mary Horton, Andrew Neish.

To my friends, new and old, near and far, thank you for staying by my side throughout this journey. You never failed to lend a supportive ear over many cocktails. You made a safe space for me to seek refuge from scientific difficulties.

Last and certainly not least, I thank my family for serving as a constant source of love and support. Thank you to my mom, Susan Waldman, for always acting as my “worry sponge” and talking me off the ledge when the going got tough. Thank you to my dad, Jay Waldman, for grounding me when my confidence was shaken. Thank you to my second set of parents, Rocio and Arturo Blanco, who helped raise me and shape me into the person I am today. I also want to give a massive thank you to my brother, Chase Waldman, his wife and my sister, Jenna Waldman, and my neice, Ellie Waldman, for fun moments of escape when difficulties arose.

Statement of Originality:

I declare that, unless otherwise stated, this thesis is entirely my own work and describes my own research.

Alex David Waldman
St. John's College, Oxford

Table of Contents:

List of Tables *12*

List of Figures ..... *1Error! Bookmark not defined.*

Abbreviations *15*

1. Introduction *17*

1.1 Multiple Sclerosis Overview **17**
1.1.1 Background and Significance 17
1.1.2 Signs and Symptoms 17
1.1.3 Diagnostic Criteria 18
1.1.4 Clinical Course 18
1.1.4.1 Susceptibility 18
1.1.4.2 Natural History 21
1.1.4.3 Disability Measurement Scales 22
1.1.4.4 Prediction of Clinical Outcome 24
1.1.5 Treatment and Management 25

1.2 Pathogenesis **26**

1.3 Neuropathology of Multiple Sclerosis **26**
1.3.1 Demyelination 26
1.3.2 Inflammation and Glial Biology 27
1.3.3 Neurodegeneration 28

1.4 Neuroimaging in Multiple Sclerosis **30**
1.4.1 Radiographic Features of Multiple Sclerosis 30
1.4.2 Neuroimaging Limitations 32

1.5 Molecular Biomarkers in Multiple Sclerosis **33**
1.5.1 Significance of Protein Molecular Biomarkers 33
1.5.2 Proteomic Technologies 34
1.5.3 Protein Biomarkers in Multiple Sclerosis Cerebrospinal Fluid 35

1.6 Thesis Overview **37**

2. The Prevalence and Topography of Demyelination in the Multiple Sclerosis Spinal Cord *39*

2.1 Introduction **39**

2.2 Materials and Methods **40**
2.2.1 Study Population 40
2.2.2 Neuropathological Assessment 41
2.2.3 Statistical Analysis 43

2.3 Results **44**
2.3.1 Cohort Demographics 44
2.3.2 Prevalence of Spinal Cord Demyelination and Inflammatory Activity 44
2.3.3 Concordance of Spinal Cord Lesion Presence Between Levels 46
2.3.4 Topography of Spinal Cord Demyelination and Inflammatory Activity 46
2.3.5 Prevalence and Extent of Subpial Demyelination 47
2.3.6 Clinicopathological Relationships 51

2.4 Discussion **53**

3. Neuropathological and Proteomic Relationships with Axonal Loss in the Multiple Sclerosis Spinal Cord *60*

3.1 Introduction **60**

3.2 Materials and Methods 62
3.2.1 Study Population 62
3.2.2 Palmgren Silver Staining 63
3.2.3 Immunohistochemistry 64
3.2.4 Neuropathological Image Annotation and Sampling 65
3.2.5 Histological Image Analysis 66
3.2.6 Post-Mortem Cerebrospinal Fluid Proteomics 69
3.2.7 Data Integration 69
3.2.8 Statistical Analysis 70

3.3 Results 73
3.3.1 Cohort Demographics 73
3.3.2 Quantitative Neuropathology 74
3.3.2.1 MS vs. Controls 74
3.3.2.2 Relationships Between Features of MS Spinal Cord Pathology 75
3.3.3 Cerebrospinal Fluid Weighted Protein Correlation Network Analysis 79

3.4 Discussion 86

4. Clinicoradiographic Exploration of Pathologically-Identified Cerebrospinal Fluid Biomarkers of Spinal Cord Pathology 94

4.1 Introduction 94

4.2 Materials and Methods 95
4.2.1 Study Population 95
4.2.2 Clinical Disability Assessment and Calculation 96
4.2.3 Radiographic Assessment of Spinal Cord Atrophy 97
4.2.4 Cerebrospinal Fluid SomaScan® Proteomics 99
4.2.5 Statistical Analysis 100
4.2.5.1 Clinicopathological Relationships 100
4.2.5.2 Cerebrospinal Fluid SomaScan® Proteomics 100
4.2.5.3 Cerebrospinal Fluid Proteomics Modelling of Age 102

4.3 Results 104
4.3.1 Cohort Demographics 104
4.3.2 Relationships Between Clinical Disability and Spinal Cord Atrophy 105
4.3.3 Targeted Analysis of CSF Proteomic Relationships 107
4.3.4 Cerebrospinal Fluid Determined Age in Multiple Sclerosis 113

4.4 Discussion 115

5. Conclusions and Future Perspectives 120

5.1 Thesis Summary 120

5.2 Ongoing Work and Future Directions 121
5.2.1 Integrated Transcriptomics to Investigate Divergent Molecular Profiles of Grey and White Matter Spinal Cord Tissue 121
5.2.2 Assessment of Wallerian Degeneration in the Multiple Sclerosis Spinal Cord 123
5.2.3 Tissue-Derived Immunohistochemical and Proteomic Relationships with Opsonins 124
5.2.4 Immunoglobulin Specificity Profiling of Post-Mortem Cerebrospinal Fluid 125
5.2.5 Long-Term Follow-Up of Clinical Cohorts and Expansion of Phenotypic Characterisation for Biomarker Discovery 127

6. References 129

List of Tables:

Table 2.1. Spinal Cord Lesion Mapping Cohort Demographics
Table 2.2. Antibodies and Conditions Used for Immunohistochemistry
Table 3.1. Spinal Cord Quantitative Neuropathology Cohort Demographics
Table 3.2. Post-Mortem CSF Proteomics Cohort Demographics
Table 3.3. Antibodies and Conditions Used for Immunohistochemistry
Table 3.4. Purple Module Proteins and Module Membership (kME) Scores
Table 3.5. Purple Module Gene Ontogeny Biological Process Analysis
Table 3.6. Light Cyan Module Proteins and Module Membership (kME) Scores
Table 3.7. Light Cyan Module Gene Ontogeny Biological Process Analysis
Table 4.1. MS and Control Clinical Cohort Demographics
Table 4.2. CSF Proteomics Elastic Net Model Coefficients

List of Figures:

Figure 2.1. Methodological Approach to Assessing Staged Lesion Topography
Figure 2.2. Prevalence of Demyelination in the MS Spinal Cord
Figure 2.3. Pathological Patterns and Topography of Demyelination
Figure 2.4. Location of Demyelinating Pathology
Figure 2.5. Prevalence of Subpial White Matter Demyelination in the MS Spinal Cord
Figure 2.6. Extent of Subpial Demyelination in the MS Spinal Cord
Figure 2.7. Prevalence of Demyelination in the Central Canal of the MS Spinal Cord
Figure 2.8. Distance-Based Lesion Segmentation Analysis of Spinal Cord Demyelination
Figure 2.9. Clinicopathological Relationships Between Demyelination and Clinical Milestones
Figure 2.10. Working Hypothesis of Spinal Cord Demyelination
Figure 3.1. Barrier Site Crosstalk in MS
Figure 3.2. Neuropathology Image Annotation and Sampling
Figure 3.3. Palmgren Silver Image Analysis Pipeline
Figure 3.4. Myeloid Cell Image Analysis Pipeline
Figure 3.5. Approach to Integrate Quantitative Neuropathology with Post-Mortem CSF Proteomics
Figure 3.6. CSF Proteomic Data Pre-Processing Pipeline.
Figure 3.7. Neurodegenerative Differences Between the Control and MS Spinal Cord
Figure 3.8. Myeloid Inflammatory Differences Between the Control and MS Spinal Cord
Figure 3.9. Relationship Between Demyelination, Atrophy, and Axonal Loss in the MS Spinal Cord
Figure 3.10. Relationship Between Myeloid Cell Inflammation and Spinal Cord CSA in MS
Figure 3.11. Relationship Between Adaptive Immune Cell Inflammation and Spinal Cord CSA in MS
Figure 3.12. Relationship Between Demyelination and Total Motor Axon Number in the MS Spinal Cord
Figure 3.13. Relationship Between Myeloid Cell Inflammation and Spinal Cord Total Motor Axon Number in MS
Figure 3.14. Relationship Between Adaptive Immune Cell Inflammation and Spinal Cord Total Motor Axon Number in MS
Figure 3.15. Weighted Protein Correlation Network Relationships with Total Motor Axon Number
Figure 3.16. Protein-Trait Significance and Module Membership Relationships
Figure 3.17. Weighted Protein Correlation Network Relationships with MS Status
Figure 3.18. Weighted Protein Correlation Network Relationships with Demyelination
Figure 3.19. Weighted Protein Correlation Network Relationships with Myeloid Cell Inflammation
Figure 3.20. Working Hypothesis Detailing the Potential Determinants of Axonal Loss in MS
Figure 4.1. Patient Assessment Summary
Figure 4.2. GBSI MRI Analysis Pipeline
Figure 4.3. Nested Cross-Validation Workflow
Figure 4.4. Impact of Increased Follow-Up on Hippocampal GBSI
Figure 4.5. Relationship Between Atrophy and Cross-Sectional MS Disability (ARMSS)
Figure 4.6. Relationship Between Atrophy and Longitudinal MS Disability (nARMSS)
Figure 4.7. Relationship Between Atrophy over 4 years and MS Disease Progression (Presence of PIRA)

Figure 4.8. CSF IgG in Control and MS Patients
Figure 4.9. CSF Complement in Control and MS Patients
Figure 4.10. Relationships Between CSF IgG and Cross-Sectional MS Disability (ARMSS)
Figure 4.11. Relationships Between CSF Complement and Cross-Sectional MS Disability (ARMSS)
Figure 4.12. Relationships Between CSF IgG and Longitudinal MS Disability (nARMSS)
Figure 4.13. Relationships Between CSF Complement and Longitudinal MS Disability (nARMSS)
Figure 4.14. CSF Biomarkers and MS Disease Progression (time to PIRA)
Figure 4.15. CSF IgG and Spinal Cord Atrophy over 1 year in MS Patients
Figure 4.16. CSF IgG and Spinal Cord Atrophy over 4 years in MS Patients
Figure 4.17. CSF Complement and Spinal Cord Atrophy over 1 year in MS Patients
Figure 4.18. CSF Complement and Spinal Cord Atrophy over 4 years in MS Patients
Figure 4.19. CSF Elastic Net Models of Age
Figure 6.1. 10x Genomics Visium Spatial Transcriptomics Technology
Figure 6.2. 10x Genomics Visium Spatial Transcriptomics Workflow
Figure 6.3. Phage Immunoprecipitation Sequencing Workflow

Abbreviations:

ACST	Anterior Corticospinal Tract
ANOVA	Analysis of Variance
ARMSS	Age-Related Multiple Sclerosis Severity Scale
BBB	Blood-Brain Barrier
βAPP	Beta Amyloid Precursor Protein
BSCB	Blood-Spinal Cord Barrier
CDMS	Clinically-Define Multiple Sclerosis
CDW	Confirmed Disability Worsening
CI	Confidence Interval
CIS	Clinically-Isolated Syndrome
CNS	Central Nervous System
CSA	Cross-Sectional Area
CSF	Cerebrospinal Fluid
DAB	3,3'-diaminobenzidine
DTT	Dithiothreitol
EBV	Epstein Barr Virus
EDSS	Expanded Disability Status Scale
ELISA	Enzyme-Linked Immunosorbent Assay
FDR	False Discovery Rate
FLAIR	Fluid Attenuated Inversion Recovery
FMRIB Software Library	FSL
GBSI	Generalised Boundary Shift Integral
GWA	Genome-Wide Association
IAA	Iodoacetamide
LCST	Lateral Corticospinal Tract
LP	Lumbar Puncture
MPRAGE	Magnetisation-Preared Rapid Gradient Echo
MRI	Magnetic Resonance Imaging
MS	Multiple Sclerosis
MSFC	Multiple Sclerosis Functional Composite
MSSS	Multiple Sclerosis Severity Score
MTR	Magentisation Transfer Ratio
NAA	N-Acetyl Aspartate
nARMSS	Normalised Age-Related Multiple Sclerosis Severity Scale
NAWM	Normal-Appearing White Matter
OCBs	Oligoclonal Bands
ODRS	Overall Disability Response Score
ORA	Overrepresentation Analysis
PCR	Polymerase Chain Reaction
PET	Positron Emission Tomography
PIRA	Progression Independent of Relapse Activity

PLP	Proteolipid Protein
PMI	Post-Mortem Interval
PPMS	Primary Progressive Multiple Sclerosis
PRLs	Paramagnetic Rim Lesions
PRMS	Progressive-Relapsing Multiple Sclerosis
QRILC	Quantile Regression of Left-Censored Data
RAW	Relapse-Associated Worsening
RIS	Radiologically-Isolated Syndrome
RRMS	Relapsing-Remitting Multiple Sclerosis
SCT	Spinal Cord Toolbox
SD	Standard Deviation
SE	Standard Error
SELs	Slowly Expanding Lesions
SMSC	Swiss Multiple Sclerosis Cohort
SNR	Signal-to-Noise Ratios
SPMS	Secondary Progressive MS
VALIS	Virtual Alignment of pathoLogy Image Series
WPCNA	Weighted Protein Correlation Network Analysis

1. Introduction

1.1 Multiple Sclerosis Overview

1.1.1 Background and Significance

MS is a chronic inflammatory, demyelinating, and degenerative disorder of the CNS (Reich *et al.* 2018). Affecting nearly 2.8 million people worldwide, it is the most common cause of nontraumatic disability in young adults and disproportionately contributes to healthcare expenditures (Wallin *et al.* 2019, Walton *et al.* 2020, Bebo *et al.* 2022). The aetiology of MS has remained elusive but thought to be due to an interaction between genetic susceptibilities and environmental exposures (Reich *et al.* 2018). Few diseases display more clinical heterogeneity than MS, which likely relates to the relative contribution of different pathological processes and topographical variation (Krieger *et al.* 2016, Kuhlmann *et al.* 2023). However, it has proven difficult to disentangle this heterogeneity and ultimately risk-stratify patients at greatest risk of disability accumulation because current disease biomarkers are limited. Clinically, disease progression, leading to irreversible accumulation of disability, commonly presents as a relentless myelopathy (Correale *et al.* 2016, Giovannoni *et al.* 2017). This suggests that the spinal cord is a central player in disease outcome and represents a critical anatomical site to investigate in detail. Therefore, biomarkers of spinal cord pathology are likely to yield important insights into disease outcome.

1.1.2 Signs and Symptoms

MS manifests as a multitude of symptoms reflecting the distribution and extent of pathological changes. The subcortical white matter, cerebellum, brainstem, spinal cord, optic pathway, cerebral cortex, and deep grey matter structures are all impacted (Reich *et al.* 2018). However, the anatomical site of demyelination cannot always be traced to a clinical event. There are likely compensatory reserve mechanisms that contribute to the dissociation between

demyelination and emergence of clinical symptoms with inflammatory and degenerative changes outside lesions being important contributors (Lassmann 2018). Certain anatomical sites are posited to exhibit more reserve compared to others (Krieger *et al.* 2016). Spinal cord involvement is notoriously more symptomatic than pathology impacting the cerebral hemispheres and is known to contribute to motoric disability that is a prominent and disabling feature underlying disease progression. Therefore, the spinal cord motor pathways are an important anatomical site to study in more detail to unravel mechanisms relevant to disability accumulation.

1.1.3 Diagnostic Criteria

The diagnosis of MS was historically based on clinical findings in which symptoms had to impact two different functional systems (dissemination in space) at two different time points (dissemination in time) (Poser *et al.* 1983). The advent of magnetic resonance imaging (MRI) and use of cerebrospinal fluid testing as paraclinical tools to support the physical examination have increased our sensitivity to fulfil dissemination in space and time criteria to diagnose MS. However, the current 2017 McDonald Criteria for MS diagnosis display only an 83% sensitivity, 39% specificity, and 61% accuracy to predict conversion from clinically-isolated syndrome (CIS) to clinically-definite (CD)MS (Filippi *et al.* 2022). Therefore, novel diagnostic MRI and/or CSF biomarkers are important lines of research to better assist clinicians in the MS diagnostic process.

1.1.4 Clinical Course

1.1.4.1 Susceptibility

The estimated worldwide prevalence of MS is 2.8 million (Bebo *et al.* 2022). Geographic representation is not homogenous, which indicates that environmental exposures likely play a role in susceptibility. However, as a prototypical complex disease, genetic factors are also

known contributors. In fact, it is currently believed that a specific set of environmental exposures in a genetically susceptible host underlies disease onset.

From a demographic perspective, young white females seem to be at highest risk for developing MS. However, biased sampling of early epidemiological studies has underestimated the risk of minority populations. An often-overlooked risk factor for disease susceptibility includes vascular comorbidities which position the blood vessel at centre stage of the disease process (Marrie *et al.* 2015). Vitamin D has also been posited to represent a potentially unifying hypothesis that links epidemiological findings, namely the relationship between MS and 1) birth month and 2) distance from the equator. In fact, biologically, vitamin D is a known essential cofactor for immunological processes. In addition, exposure to pathogens has also been hypothesised to represent an environmental risk factor for MS. Many studies have searched for candidate pathogens and exposure to Epstein-Barr virus (EBV) has proven convincing as a risk factor for MS development (Bjornevik *et al.* 2022). Other pathogens, including *Clostridium perfringens*, also represent interesting candidates (Rumah *et al.* 2013, Wagley *et al.* 2019, Ma *et al.* 2023). However, further studies are required to better understand the contribution of pathogens to MS susceptibility and pathogenesis.

Beyond demographic and environmental factors, familial studies in MS have proven important in advancing our understanding of genetic factors contributing to susceptibility. Familial clustering was first appreciated in the 1890s with a multitude of more contemporary studies providing support to these results (Dyment *et al.* 2004). Recently, worldwide prevalence of familial MS, defined as having at least one blood relative with MS, was estimated to be 12.6% (Harirchian *et al.* 2018). The *HLA-DRB1*1501/HLADRB5*0101* haplotype has been consistently implicated as the strongest susceptibility locus for MS. Subsequent studies have highlighted a plethora of modest susceptibility alleles (*IL7RA*, *IL2RA*, *CLEC16A*, *CD58*, *CD6*,

IRF8, *KIF21B*, *TMEM39A*, *TNFRSF1A*) with more recent genome wide association (GWA) studies expanding the number of susceptibility alleles to 233 (Gregory *et al.* 2007, Australia *et al.* 2009, International Multiple Sclerosis Genetics 2009, Bush *et al.* 2011, International Multiple Sclerosis Genetics 2013, International Multiple Sclerosis Genetics *et al.* 2013, Leone *et al.* 2013, Damotte *et al.* 2014, Traboulsee *et al.* 2014). However, common variation (present at an allele frequency of ≥ 1%) in these loci only explains ~20% of the heritability of MS, leaving a large fraction of "missing heritability" to discover (Gregory *et al.* 2007, Australia *et al.* 2009, International Multiple Sclerosis Genetics 2009, Bush *et al.* 2011, International Multiple Sclerosis Genetics 2013, International Multiple Sclerosis Genetics *et al.* 2013, Leone *et al.* 2013, Damotte *et al.* 2014, Traboulsee *et al.* 2014, Mitrovic *et al.* 2018, Consortium 2019). In fact, a rare-variant association study identified coding variants in 6 new loci that contribute an additional 5% to MS heritability (Mitrovic *et al.* 2018). While there is substantial overlap in the MS genetic architecture with that of autoimmune conditions, MS-related variants identified via association studies have not included key genes involved in immune tolerance (i.e., *AIRE* and *FOXP3*) that characterise susceptibility to other autoimmune conditions (Gregory *et al.* 2007, Australia *et al.* 2009, International Multiple Sclerosis Genetics 2009, Bush *et al.* 2011, International Multiple Sclerosis Genetics 2013, International Multiple Sclerosis Genetics *et al.* 2013, Leone *et al.* 2013, Damotte *et al.* 2014, Traboulsee *et al.* 2014). Whole-exome sequencing of multiplex families has nominated *CYP27B1* (encoding vitamin D activating 1-a hydroxylase), *TYK2* (tyrosine kinase-2), and *NLRP1* (influencing inflammasome oligomerization and assembly) as potential novel rare variants contributing to susceptibility. However, subsequent biochemical validation has been limited due to cost and resource limitations (Ramagopalan *et al.* 2011, Doherty *et al.* 2012, Dyment *et al.* 2012, Maver *et al.* 2017).

1.1.4.2 Natural History

MS has classically been described as a two-phase disease. The 1996 consensus guidelines defined the MS phenotypes as relapsing-remitting (RR)MS, secondary progressive (SP)MS, primary progressive (PP)MS, and progressive-relapsing (PR)MS (Lublin *et al.* 1996). Onset of the RR phase peaks in the second and third decade of life during which patients exhibit periods of focal CNS inflammation, resulting in demyelination and observable gadolinium-enhancing lesions on T1 MRI that may manifest as clinical relapses. Subsequent periods during which active inflammation subsides and remyelination begins leads to the relative relief of symptomology (remissions). Within 25 years, the vast majority of RRMS patients later evolve into a phase of SPMS characterised by a more neurodegenerative phenotype in which there is little to no respite from the accumulation of symptoms and disability. A minority of patients (approximately 15%) present, commonly in the fourth decade of life, with progressive inflammation and disability accumulation at disease onset (Confavreux *et al.* 2006). This disease subtype was further classified into PPMS if frank relapses were not evident and PRMS if relapses were an accompanying feature.

In 2013, the MS classification criteria were revised (Lublin *et al.* 2014). CIS and radiologically isolated syndrome (RIS) were added as pre-MS entities. CIS is defined as a singular MS relapse. Lack of dissemination in time distinguishes this category from CDMS. RIS represents patients in which there is radiographic evidence of lesions consistent with MS in the absence of clinical attacks. It is now well-accepted that these clinical classifications exist on a spectrum. Therefore, the 2013 classification also added modifiers of disease activity and progression to define patient phenotypes more specifically.

The marked clinical heterogeneity of MS makes the application of simplistic classification schemes insufficient. For example, clinical, radiographic, pathological, and immunologic

studies have failed to identify any biological differences between SPMS and PPMS leading some to believe that these entities should not be distinct clinical categories (Lublin *et al.* 2014). In addition, the conversion from RRMS to SPMS is not easily defined, which complicates matters further (Lorscheider *et al.* 2016). One model that aims to better classify the heterogeneity and dynamic aspects of MS disease course is the topographical model (Krieger *et al.* 2016). The topographical model envisages the dynamic clinical course of MS as a pool of water broken up into 3 different anatomical sites. Each pool consists of water at different depths to represent functional reserve. This topographical information underscores the fact that distinct nervous system sites have differing clinical thresholds and capacities for repair. In fact, the spinal cord is known to be a site with a relatively smaller clinical threshold and functional reserve. To extend this model further, there has recently been a call for a mechanism-driven framework to define MS that operationalises the disease as a spectrum in which patients harbour different contributions from distinct pathological processes (Kuhlmann *et al.* 2023). Given these considerations, this thesis will explore spinal cord pathology, including its underlying mechanisms, evolution, and clinical and radiographic manifestations.

1.1.4.3 Disability Measurement Scales

The expanded disability status scale (EDSS) is the most commonly used metric of neurological impairment in the MS field (Kurtzke 1983). Neurological impairment is measured within 8 functional systems (Pyramidal, Cerebellar, Brainstem, Sensory, Bowel and Bladder, Visual, Cerebral, and Other). Each system receives a score ranging from 0 (no impairment) to 5 or 6 (maximal impairment). A composite score ranges from 0 (no impairment) to 10 (death due to MS). However, while the EDSS provides a general framework for quantifying disease severity, its use is limited by many factors (Kosa *et al.* 2018). The difference between intervals on the EDSS scale is not equal, making disease trajectory interpretation difficult. Statistically, even though the EDSS is ordinal in nature, it is commonly treated as a linear continuous scale which

may lead to statistical aberrations. The scale is also biased towards pyramidal function, especially beyond a score of 4. EDSS scoring is based off a subjective neurological examination, which leads to profound inter-rater variation and a lack of sensitivity. In fact, only about 10% of individuals demonstrate increases in EDSS per year.

Given the heterogeneity and limitations of the EDSS, multiple methods have been devised to try and scale the cross-sectional EDSS by a metric of time, either disease duration or age. The progression index is a simple ratio of EDSS to disease duration (Cendrowski 1986). The multiple sclerosis severity score (MSSS) extends this concept further. The MSSS corresponds to the decile of EDSS values of a historical dataset of individuals who share the same disease duration (Roxburgh *et al.* 2005). Given the difficulties in assessing disease onset and capturing the true disease duration of a patient, the age-related multiple sclerosis severity score (ARMSS) uses age as a normalising factor instead (Manouchehrinia *et al.* 2017). However, these cross-sectional measures still lack the sensitivity to predict future disease trajectories. Longitudinal measures that tabulate slopes or areas under the curve of these cross-sectional progression metrics may better reflect disease progression but exposure to disease-modifying therapies confounds the ability to understand the true disease trajectory of each patient (Manouchehrinia *et al.* 2021). Adjustments for therapy using meta-analysed datasets have been used but are not widely applicable (Weideman *et al.* 2017a, Weideman *et al.* 2017b).

To increase sensitivity and reduce reliance on the EDSS, multiple composite measures have been proposed, including the Multiple Sclerosis Functional Composite (MSFC), Overall Disability Response Score (ODRS), and Combinatorial Weight-Adjusted Disability Score (CombiWISE) (Kosa *et al.* 2016, Tiftikçioğlu 2018, Chang *et al.* 2022). However, these are cumbersome to tabulate making widespread use limited. However, the use of digital

applications for recording and tabulating these scores may address this limitation in part (Kosa *et al.* 2018).

1.1.4.4 Prediction of Clinical Outcome

Natural history studies and subsequent meta-analyses have been used to better understand the determinants of clinical outcome in MS. Demographic features including older age of onset and male sex have been demonstrated to confer a poor prognosis. The topography of the first clinical attack, namely the presentation of motor symptoms from spinal cord involvement, is also a known correlate of poor outcome (Confavreux *et al.* 2006). Interestingly, the prognostic value of relapse number early in the disease course has been the subject of debate. While some studies have demonstrated that relapse rate prior to entrance into the progressive phase associates with a worse outcome (Weinshenker *et al.* 1991, Scalfari *et al.* 2014), this relationship has not always been replicated (Confavreux *et al.* 2000, Tremlett *et al.* 2009). The reason behind these discrepant findings may lie in the topography of relapse. It is important to note that early exposure to high-efficacy disease-modifying therapies, which operate mainly to reduce relapse rate, is associated with a better outcome and delayed conversion to SPMS (Brown *et al.* 2019, Tedeholm *et al.* 2022). However, the impact of disease-modifying therapies has been demonstrated to be age-dependent (Weideman *et al.* 2017b). Interestingly, the vast majority of patients exhibit disability accumulation independent of new relapses, termed silent progression or PIRA (University of California *et al.* 2019, Kappos *et al.* 2020, Lublin *et al.* 2022), and early PIRA has been shown to be a strong predictor of long-term outcome (Tur *et al.* 2023). Taken together, these findings suggest that relapse-dependent and relapse-independent mechanisms likely contribute to long-term outcome in MS.

Similar to susceptibility, both modifiable and non-modifiable risk factors are known to contribute to disease progression. One important non-modifiable risk factor is the presence of

vascular comorbidities which predicts a more aggressive disease course and severe pathology (Marrie *et al.* 2009, Marrie *et al.* 2010, Geraldes *et al.* 2020). Genetics represent an important non-modifiable risk factor involved in disease progression. In fact, a recent study confirms that carriage of the *HLA-DRB1*1501* susceptibility allele leads to a faster rate of disability progression (Brownlee *et al.* 2022). In addition, two recent GWA studies have implicated CNS-intrinsic mechanisms in the pathogenesis of disease progression (Baranzini *et al.* 2022, Jokubaitis *et al.* 2022).

1.1.5 Treatment and Management

The treatment and management of MS has come a long way over the past 25 years (Callegari *et al.* 2021). The first drugs to be approved for the treatment of RRMS were the interferon-beta preparations. Since then, an additional 10 classes of drugs have been approved with various administration routes including injectable, oral, or infused (glatiramer acetate, mitoxantrone, natalizumab, fingolimod/siponimod/ponesimod/ozanimod, cladribine, monomethyl fumarate/dimethyl fumarate/diroximel fumarate, teriflunomide, ocrelizumab/ofatumumab, ublituximab-xiiy, alemtuzumab). Hematopoietic stem cell transplant has also been shown to be of benefit though the risks limit broad use at this time. Overall, the current suite of approved immunomodulatory and immunosuppressive therapies are most effective at reducing the number of relapses. However, the neurodegenerative component of the disease remains unchecked and CNS inflammation commonly persists despite the impact of these therapies on immune system function, leading to disease progression. Therefore, current efforts must be made to target the pathogenic mechanisms of smouldering neuroinflammation and neurodegeneration to successfully halt disease progression.

1.2 Pathogenesis

The pathophysiology of MS has been shown to be complex and heterogeneous. In fact, the pathogenesis has been subject to considerable debate. Two overarching hypotheses have been purported, termed outside-in and inside-out paradigms (Luchicchi *et al.* 2021). The outside-in hypothesis theorises that the inflammatory response is primary and peripherally-activated autoreactive immune cells, namely T and B cells, gain license to enter the CNS and promote inflammatory demyelination. On the other hand, the inside-out paradigm hypothesises that the inflammatory reaction is secondary to a primary neurodegeneration. However, regardless of the vantage point, the pathology of MS is characterised by the triad of demyelination, inflammation, and neurodegeneration (Lassmann 2018).

1.3 Neuropathology of Multiple Sclerosis

1.3.1 Demyelination

The first descriptions of MS pathology date back to the early 1800s (Lassmann 2005). The loss of the myelin sheath surrounding white matter axons was appreciated as one of the most predominant features of the disease process. These demyelinating lesions were demonstrated to centre around venous blood vessels with inflammatory cells in the perivascular space. More contemporary studies began to classify lesions histologically. The most recent classification system categorises the inflammatory nature of lesions as active, mixed active/inactive, or inactive (Kuhlmann *et al.* 2017).

Lesions are identified and further characterised using immunohistochemical techniques. Luxol fast blue was originally used to detect demyelination histochemically but has since been replaced by myelin protein immunohistochemistry due to improved sensitivity for the detection of lesions, especially in grey matter structures (Gilmore *et al.* 2006, Kuhlmann *et al.* 2017).

Activated myeloid cell immunohistochemistry can be used to stage lesions by their inflammatory activity. Active lesions are observed as hypercellular throughout the region of demyelination while inactive lesions display scant inflammatory activity and are "burnt-out.". Mixed/active inactive lesions exhibit features of both active and inactive lesions. Activity is observed at the lesion edge and the lesion core is hypocellular. It is important to note that lesions of all stages have the capacity for remyelination though mixed active/inactive lesions appear to have impaired remyelination ability (Heß *et al.* 2020). However, characterisation of remyelination proves challenging in human material (Neumann *et al.* 2020).

The criteria for lesion staging described above is most easily applied to white matter lesions. Inflammation is more pronounced in white compared to grey matter, which makes delineation amongst categories easier. In particular, the cerebral cortex displays a less inflammatory signature compared to deep grey matter structures and the spinal cord (Revesz *et al.* 1994, DeLuca *et al.* 2013, Haider *et al.* 2014, Reali *et al.* 2020). Therefore, cerebral cortical lesions are commonly classified by their location. Subpial lesions impact the surface of the cortex. Intracortical lesions impact multiple layers of the cortical ribbon but do not extend into the adjacent subcortical white matter, while leukocortical lesions have both a grey and white matter component.

1.3.2 Inflammation and Glial Activation

The inflammatory aspects of MS have been well-documented in MS pathological specimen (Lassmann 2018). As described above, the inflammatory environment can be used to characterise lesions. Perivascular inflammation that spreads into the lesional parenchyma is commonplace with a diverse inflammatory signature composed of adaptive immune cells (T and B cells), myeloid cells (infiltrating monocytes and resident microglia), and other glia (astrocytes and oligodendrocytes). Importantly, inflammation is not relegated to just the lesion.

In fact, normal-appearing areas without myelin loss display inflammatory infiltration. These areas tend to demonstrate an inflammatory signature that is more myeloid and glial in nature, though adaptive immune activation is still observed. Beyond the parenchyma and perivascular space, immunological niches resembling tertiary lymphoid follicles have been identified in the meninges of MS cases. Interestingly, these areas are typically juxtaposed to areas of demyelination, innate immune activation, and neurodegeneration (Serafini *et al.* 2004, Magliozzi *et al.* 2007, Magliozzi *et al.* 2010, Howell *et al.* 2011, Choi *et al.* 2012, Bevan *et al.* 2018, Magliozzi *et al.* 2022). These follicles have also been demonstrated to harbour EBV components (Serafini *et al.* 2007). The meningeal inflammatory reaction indicates that soluble factors, detectable in the CSF, may participate in the MS pathophysiological process.

More contemporary single-cell studies have been able to further delineate the phenotype of inflammatory cells within lesions and normal-appearing tissues. For example, tissue-resident memory cells and specialised populations of microglia and astrocytes have been identified using these next-generation profiling techniques (Jäkel *et al.* 2019, Park *et al.* 2019, Ramaglia *et al.* 2019, Schirmer *et al.* 2019, Fransen *et al.* 2020, Wheeler *et al.* 2020, Absinta *et al.* 2021). However, these studies are typically done on a restricted number of tissue samples, typically in cerebral grey/white matter, and on cases that have limited pathological characterisation.

1.3.3 Neurodegeneration

Given the predominance of lesional pathology, MS has traditionally been thought of us a prototypical primary demyelinating disease. However, neurodegenerative pathology, especially of the axon, was also described in early accounts of the disease (Lassmann 2005). These early descriptions focused on axonal pathology within the lesion. Axonal swelling and the formation of terminal end bulbs, visible using traditional histochemical stains, were signs of axonal injury. These findings were later confirmed by immunohistochemical means. Beta

amyloid precursor protein (βAPP) was first shown in traumatic brain injury specimen to accumulate at sites of injury (Gentleman *et al.* 1993). Mechanistically, βAPP undergoes fast axonal transport and is typically not visible by immunohistochemistry. However, in the context of axonal injury, βAPP transport ceases and accumulation can be visualised immunohistochemically. βAPP+ axons were first observed within MS lesions, a finding which correlated with the degree of inflammation within the lesional environment (Ferguson *et al.* 1997), though inactive lesions were also later demonstrated to be a source of βAPP+ axons (Bitsch *et al.* 2000, Kornek *et al.* 2000, Kuhlmann *et al.* 2002). While it is thought that axonal injury may be reversible, some axons are known to be transected (Trapp *et al.* 1998) leading to frank axonal degeneration. More recent studies have also identified the importance of grey matter neurodegeneration within the cortex, deep grey matter, and spinal cord, as a predominant feature of pathology (Geurts *et al.* 2008).

The distribution of lesional pathology alone does not explain the constellation of symptoms within a given patient. More contemporary work has highlighted the role of normal-appearing tissue in the accumulation of disability. In fact, the processes of axonal injury (Bitsch *et al.* 2000, Kornek *et al.* 2000, Kuhlmann *et al.* 2002) and neuroaxonal loss (Ganter *et al.* 1999, Lovas *et al.* 2000, Bjartmar *et al.* 2001, DeLuca *et al.* 2004, DeLuca *et al.* 2006, Gilmore *et al.* 2009, Petrova *et al.* 2018, Petrova *et al.* 2020) are not restricted to lesions. In addition, pathological studies of PPMS cases, where inflammatory demyelination is less pronounced, have also identified profound neuroaxonal injury and loss (Revesz *et al.* 1994, Tallantyre *et al.* 2009). Taken together, these findings suggest the importance of non-lesioned sites in the pathogenesis of neuroaxonal degeneration. However, whether neuroaxonal loss in normal-appearing tissues represents a primary neuroaxonopathy or Wallerian degeneration arising from lesioned interconnected sites is still subject to debate.

1.4 Neuroimaging in Multiple Sclerosis

1.4.1 Radiographic Features of Multiple Sclerosis

Neuroimaging is a useful paraclinical tool for the diagnosis of MS and its prognostication. Conventional and advanced sequences have been used to image the demyelinating, inflammatory, and neurodegenerative components of MS with varying success. However, at this time, our current neuroimaging tools are unable to approximate the resolution of post-mortem neuropathological assessment (Filippi *et al.* 2019).

White matter lesions are commonly observed as hyperintensities when using proton-density, T2-weighted, and fluid-attenuated inversion recovery (FLAIR) MRI scans. However, relying too heavily on this feature when diagnosing MS and not appropriately excluding mimics may lead to overdiagnosis (Geraldes *et al.* 2018, Solomon *et al.* 2019). T2 hyperintensities that harbour a central vein, visualised using susceptibility-weighted imaging sequences, increase diagnostic specificity. However, these sequences are not routinely obtained clinically and have only been successfully applied supratentorially (Sati *et al.* 2016, Wattjes *et al.* 2021). 10-30% of focal white matter hyperintensities also appear hypointense on T1-weigted MRI scans (Filippi *et al.* 2012). MRI-pathology correlation studies indicate that these hypointense lesions represent end-stage tissue destruction (van Walderveen *et al.* 1998). In comparison to white matter lesions, grey matter lesions, especially those found in the cerebral cortex, have proven to be harder to image. T1, T2, and FLAIR sequences do not possess enough contrast to readily identify grey matter lesions. The advent of more advanced neuroimaging techniques, including double-inversion recovery, phase-sensitive inversion recovery, and three-dimensional magnetisation-prepared rapid acquisition with gradient echo, and the use of higher field strengths have marginally improved detectability (Kilsdonk *et al.* 2016).

Traditional T2-weighted scans do not readily distinguish the inflammatory status of lesions. Instead, T1-weight scans with gadolinium contrast enhancement, a marker of blood-brain-barrier disruption, are commonly used for this purpose. This approach allows for the visualisation active inflammatory lesions. However, the temporal nature of contrast enhancement is heterogeneous making accurate estimation of active lesion load difficult (Cotton *et al.* 2003). Gadolinium enhancement in the leptomeninges has also been observed in the MS brain (Absinta *et al.* 2015). However, this feature is not specific to MS and the specificity of its histological correlate has been debated. Recent developments have also made the detection of mixed active/inactive lesions easier *in vivo*. Longitudinal assessment of patient cohorts and novel segmentation and registration methods have made it possible to identify a subtype of mixed/active inactive lesions terms 'slowly-expanding lesions' (SELs) (Dal-Bianco *et al.* 2017, Elliott *et al.* 2019). In addition, susceptibility-weighted sequences have also been used to identify paramagnetic-rim lesions (PRLs) that correspond to iron-containing macrophages at lesion rims (Absinta *et al.* 2019). However, these two MRI features that are hypothesised to represent mixed active/inactive lesions do not fully correspond. In fact, it has been estimated that only 54% of PRLs are SELs and only 7% of SELs are PRLs (Calvi *et al.* 2023). This is not surprising given that pathological studies have demonstrated that mixed active/inactive lesions represent a heterogeneous lesional population (Kuhlmann *et al.* 2017). Beyond T1, T2, and susceptibility-weighted imaging, positron emission tomography (PET) has also been used to characterise myelin integrity through the use of a [^{11}C]PiB tracer (Bodini *et al.* 2016). In tandem, the inflammatory landscape of MS can be assessed with microglial-specific tracers. In fact, recent work using PET approaches has highlighted that normal-appearing tissue inflammation is common and that inflammation persists within lesions (Hamzaoui *et al.* 2023).

Neuroimaging has also been used to understand the neurodegenerative component of MS. As mentioned above, T1 hypointensities have been shown to correlate with axonal loss and tissue destruction (Filippi *et al.* 2012). Magnetisation transfer ratio (MTR) sequences and magnetic resonance spectroscopy measuring the neuronal marker, N-acetyl aspartate (NAA), have also been demonstrated to reflect tissue damage within and outside of lesions (van Walderveen *et al.* 1998, Leary *et al.* 1999, De Stefano *et al.* 2001, Filippi *et al.* 2003, Petzold *et al.* 2011). Volumetric assessment, cross-sectionally and longitudinally, is also thought to reflect the degenerative component of MS with rates of atrophy demonstrating prognostic value. Importantly, regional heterogeneity in atrophy and its prognostic potential has been observed with spinal cord atrophy demonstrating higher predictive value than other sites (Pagani *et al.* 2005, Casserly *et al.* 2018, Eshaghi *et al.* 2018). Volumetric assessments have also been used to estimate CNS reserve in MS patients. Cross-sectional measures of total intracranial volume and spinal cord canal volume have been taken to represent the maximal size of the brain and spinal cord, respectively, and larger values were shown to be protective against disability accumulation (Sumowski *et al.* 2016, Sastre-Garriga *et al.* 2023).

1.4.2 Neuroimaging Limitations

While the utility of neuroimaging assessment in MS cannot be disputed, there are several important limitations. T2 hyperintensities are commonly misattributed to MS (Geraldes *et al.* 2018). MRI has limited resolution when compared to histological assessment for detecting all the pathological hallmarks of MS (Filippi *et al.* 2019). Even with advanced sequences, CSF interference makes detection of pathology at fluid interfaces difficult which particularly impacts our ability to identify subpial cerebral cortical and spinal cord pathology. At this time, inflammatory lesion activity (i.e. active, mixed active/inactive, inactive) cannot be confidently staged using MRI. While PET imaging shows promise, it is hampered by poor resolution.

Sequences with a basis in susceptibility-weighing cannot easily be applied to the spinal cord where pathology is common and known to impact disability. The use of volumetric assessments is also not ready for clinical application for many reasons (Sastre-Garriga *et al.* 2020). Technical factors, including the choice of acquisition protocol, gradient distortion, intrascanner/interscanner variability, and patient movement all contribute to image quality and can add significant noise to any volumetric assessment. Confounding biological factors, including age, sex, CNS morphology, hydration status, hormonal fluctuations, comorbidities, and lifestyle factors can contribute to volume estimates, though the extent to which these factors contribute and how best to address these confounds remains to be seen. Within the MS CNS, suppression of fulminant inflammation can be erroneously characterised as atrophy but rather represents pseudoatrophy. These issues are further amplified when trying to measure small effect sizes and volume changes of small structures like the spinal cord.

1.5 Molecular Biomarkers in Multiple Sclerosis

1.5.1 Significance of Protein Molecular Biomarkers

Proteins are the downstream effector molecules in the vast majority of biological processes and expression has not been shown to be reliably correlated with transcripts (Schwanhäusser *et al.* 2011). In addition, protein identification and assessment are extremely important clinically. 90% of the currently approved drugs target a protein and 85% of the human proteome remains untargeted. Beyond drug discovery, proteins are also integral to the invention of novel diagnostic and prognostic tests. Currently, over 100 million immunoassays targeting proteins are performed per year with new immunoassays being constantly developed (Wishart *et al.* 2006, Uhlén *et al.* 2015).

1.5.2 Proteomic Technologies

Two broad classes of proteomic technologies are currently widely used for quantification. These include mass spectrometry and affinity-based assays. Mass spectrometry approaches can be further subdivided into top-down and bottom-up paradigms with the aim of measuring intact and proteolytically digested peptides, respectively. Given the complexity of measuring native proteins due to their complex structure, the bottom-up format is the most common mechanism by which mass spectrometry-based proteomics is performed. In order to achieve deeper profiling of proteolysed material, mass spectrometry is typically coupled to a form of protein separation. Historically, SDS-PAGE gels were used though the advent of ultraperformance nano liquid chromatography has improved the ability to profile the proteome of precious samples with limited quantity (Sen *et al.* 2021).

Conversely, affinity-based assays use targeted capture reagents and quantify native proteins. These include antibodies and aptamers. The enzyme-linked immunosorbent assay (ELISA) represents one of the most common proteomic profiling techniques which can be performed in various formats (direct, indirect, sandwich, or competitive). More sensitive ELISA assays, including the SIMOA bead-based ELISA for neurofilament light chain (NfL), have been developed (Hendricks *et al.* 2019). However, the issue with the ELISA approach when performing discovery-based biomarker research lies in its targeted nature. Companies like Luminex have attempted to increase proteomic coverage through development of multiplexed ELISA platforms. However, these assays are still limited in the number of proteins that can be quantified per sample. Proximity-extension assays, like OLINK, represent a second affinity-based approach. Two antibody-oligonucleotide conjugates are used to bind each protein of interest. The oligonucleotides from each paired conjugate hybridise and serve as templates for polymerase-chain reaction (PCR) extension. The requirement of matched conjugate protein binding ensures specificity of the reaction. This extension step creates a double-stranded DNA

molecule with a unique sequence specific to the targeted protein. Quantification of the DNA molecule is proportional to the concentration of protein in the sample and performed using quantitative PCR or next-generation sequencing. Currently, the maximum number targets that can be measured in each sample with this technology is 384. Similar to the OLINK approach, SomaScan® leverages the power of oligonucleotides. However, rather than use antibody conjugates, the oligonucleotides, termed aptamers, bind protein targets directly. The newest assay from SomaLogic has the power to detect ~7,000 proteins per sample.

1.5.3 Protein Biomarkers in Multiple Sclerosis Cerebrospinal Fluid

Assessment of CSF has revealed itself to be a useful tool to understand MS. In fact, CSF analysis forms part of the diagnostic criteria. CSF-specific oligoclonal bands (OCBs), representing an intrathecal polyclonal immunoglobulin-mediated response, are observed in nearly 95% of MS patients and can be used to meet the dissemination in time criterion (Chu *et al.* 1983, Thompson *et al.* 2018). The IgG index, found to be elevated in 70% of MS patients, represents another measure of an intrathecal antibody-response that is also commonly measured clinically. It is calculated by normalising the ratio of CSF to serum IgG to the CSF to serum ratio of albumin, a measure of blood-brain barrier (BBB) breakdown (Simonsen *et al.* 2020). Kappa free light chain index serves as an emerging diagnostic biomarker that has improved sensitivity and specificity over OCBs and is easier to measure in a standardised fashion without subjectivity (Duell *et al.* 2020). In order to distinguish MS from neuromyelitis optica spectrum disorders previously thought to fall under the MS umbrella, anti-aquaporin-4 and anti-myelin oligodendrocyte protein antibody titers are also measured routinely in the clinic. However, these tests are commonly performed in serum due to improved sensitivity (Ziemssen *et al.* 2019).

While protein CSF biomarkers are currently being used in the clinic to aid in MS diagnosis, no CSF biomarkers are currently being used for prognostication. However, studies have identified multiple promising candidates. As described above, the presence of intrathecal immunoglobulin production represents a diagnostic biomarker in MS. Many studies have also investigated how intrathecal immunoglobulins relate to disease course. Both intrathecal IgG (Stendahl-Brodin *et al.* 1980, Izquierdo *et al.* 2002, Imrell *et al.* 2006, Tintore *et al.* 2015, Vecchio *et al.* 2019) and intrathecal IgM (Villar *et al.* 2003, Perini *et al.* 2006, Villar *et al.* 2008, Ozakbas *et al.* 2017, Oechtering *et al.* 2021, Oechtering *et al.* 2022) have been shown to associate with a higher relapse rate and increased disability accumulation. Given the central role of neuroinflammation in MS pathogenesis, the concentration of inflammatory cytokines/chemokines have also been investigated as potential biomarkers of MS progression. In particular, CXCL13 has been demonstrated to associate with EDSS, relapse rate, and cortical damage (Khademi *et al.* 2011, Magliozzi *et al.* 2018). In addition to adaptive inflammatory molecules, proteins of glial origin, inclduing GFAP and Chitinase 3-Like 1, have also been shown to predict MS disease course (Petzold *et al.* 2002, Comabella *et al.* 2010, Axelsson *et al.* 2011, Martínez *et al.* 2015). Beyond inflammation, CSF NfL has also been investigated as a potential biomarker of disease activity and progression. NfL serves as a marker of axonal damage and has been demonstrated to associate with smouldering neuroinflammation post-mortem (van den Bosch *et al.* 2022). Clinical studies of CSF have demonstrated that NfL is elevated during relapses (Norgren *et al.* 2004) and has the potential to predict clinicoradiographic progression (Bhan *et al.* 2021). However, serum NfL seems to have better predictive potential (Kosa *et al.* 2022b). Therefore, research has shifted to the study of serum levels given the non-invasive nature of its sampling as compared to CSF. Overall, while the CSF biomarkers of progression described above are promising, future work must be done to identify new candidates for testing that are specific to underlying pathophysiological processes.

1.6 Thesis Overview

This thesis aims to better understand the determinants of spinal cord pathology in MS. We address this overarching goal with three complementary approaches. First, we employ traditional neuropathological tools to characterise demyelination, inflammation, and axonal loss in the MS spinal cord. We next couple these outcomes with post-mortem CSF proteomics to identify pathologically-relevant biomarkers of spinal cord pathology. Lastly, we attempt to validate our biomarkers in living MS patients through deep clinicoradiographic phenotyping and CSF proteomic profiling. Through the use of this novel and integrative approach, we advanced our understanding of the complex interplay between demyelination, inflammation, and degeneration in the spinal cord and demonstrated that these features can be linked by the perivascular unit and molecular alterations found within the CSF. Analysis of our complementary autopsy and living MS cohorts underscored the importance of deep endophenotyping to assess MS disease progression and reaffirmed the sensitivity that only pathological characterisation can provide.

This thesis is structured in the form of three results chapters comprised of the following sections:

1. Introduction
2. Materials and Methods
3. Results
4. Discussion

The specific aims of each scientific chapter are described below:

Chapter 2: To assess the prevalence and topography of demyelination staged by the degree of inflammatory activity in the MS spinal cord using a large human autopsy cohort of 119 MS cases.

Chapter 3: To characterise the complex relationships between demyelination, inflammation, and axonal loss in the MS spinal cord with CSF molecular alterations in a subset of well-characterised MS cases (used in Chapter 2) and controls.

Chapter 4: To examine whether the CSF biomarkers of axonal loss identified in chapter 3 predict MS status and clinicoradiographic outcome in a cohort of 132 living MS patients and 66 controls.

Chapter 5: This final chapter summarises the key findings of this thesis and describes ongoing and future work to address outstanding questions brought about by this research.

2. The Prevalence and Topography of Demyelination in the Multiple Sclerosis Spinal Cord

2.1 Introduction

[1]The demyelinated lesion is the central hallmark of MS pathology (Rindfleisch 1863, Charcot 1865, Vulpian 1866, Dawson 1916, Fog 1950, Fog 1965). While lesions were originally thought to be specific to the white matter, early studies quickly realised that the grey matter was not spared (Dawson 1916, Bø *et al.* 2003, Gilmore *et al.* 2006). Heterogeneity in the extent and distribution of demyelination along the length of the neuraxis is a major contributor to the accumulation of irreversible disability (Reich *et al.* 2018, Kerbrat *et al.* 2020). The spinal cord represents a key anatomical site where demyelinating pathology underlies the sensorimotor manifestations that predominate the clinical profile of the disease, especially during the progressive phases (Rovaris *et al.* 2000).

The aetiopathogenesis of demyelinated lesions in MS is still the subject of much debate. Early neuropathological observations elegantly demonstrated that spinal cord lesion topography mirrors the architecture of the venous system (Dawson 1916, Fog 1950, Adams *et al.* 1987). Subsequent work by David Oppenheimer illustrated that lesions exhibited a strong predilection for the upper cervical cord in close opposition to the denticulate ligaments where tensile forces transmitted to the vasculature are likely strongest (Oppenheimer 1978). In contrast to this vascular-centric view of spinal cord lesion pathogenesis, more recent MRI studies have observed an outside-in gradient

[1] The text and figures found within this chapter have already published in *MedRxiv* (Waldman *et al.* 2022) and are being reproduced for the purposes of this thesis with minor modifications as per the MSD graduate school guidelines.

of demyelination in the cervical spinal cord that is most pronounced at surfaces in close opposition to the CSF.

Given the lack of consensus regarding the distribution and extent of spinal cord demyelination, we performed the largest neuropathological characterisation of staged lesion topography along the length of the spinal cord to address this fundamental question. Compared to MRI approaches, neuropathology affords improved sensitivity for lesion detection and provides enhanced resolution to classify lesions by level of activity. Overall, this chapter aimed to characterize the prevalence and distribution of staged lesions in the MS spinal cord and relate these observations to clinical milestones obtained during life.

2.2 Materials and Methods

2.2.1 Study Population

A post-mortem cohort (n=119) of pathologically-confirmed MS cases derived from the UK MS Tissue Bank was available for study. Cases were selected based on the availability of formalin-fixed-frozen, paraffin-processed cervical, thoracic, and lumbar spinal cord material. Demographic, clinical, and pathological information were extracted from post-mortem reports (**Table 2.1**). Ethical approval was obtained (REC# 08/MRE09/31+5) and Human Tissue Act Guidelines were followed.

Table 2.1. Spinal Cord Lesion Mapping Cohort Demographics

		Multiple Sclerosis (*n*=119)
Number of Samples	*Cervical*	*102*
	Thoracic	*115*
	Lumbar	*106*
Disease Type*	*Primary Progressive*	14
	Secondary Progressive	100
	Progressive-Relapsing	4
	Relapsing-Remitting	1
Age (Mean ± SD)		61.7 ± 12.5
Sex (M:F)		36:83
Disease Duration in Years (Mean ± SD)*		28.4 ± 11.2
Time to Wheelchair (Mean ± SD)*		17.3 ± 10.3
PMI in Hours (Mean ± SD)		16.7 ± 6.6

*Data missing for disease duration (*n*=6) and time to wheelchair (*n*=20)

2.2.2 Neuropathological Assessment

Characterisation of lesion distribution and inflammatory activity was performed using the workflow described in **Figure 2.1**.

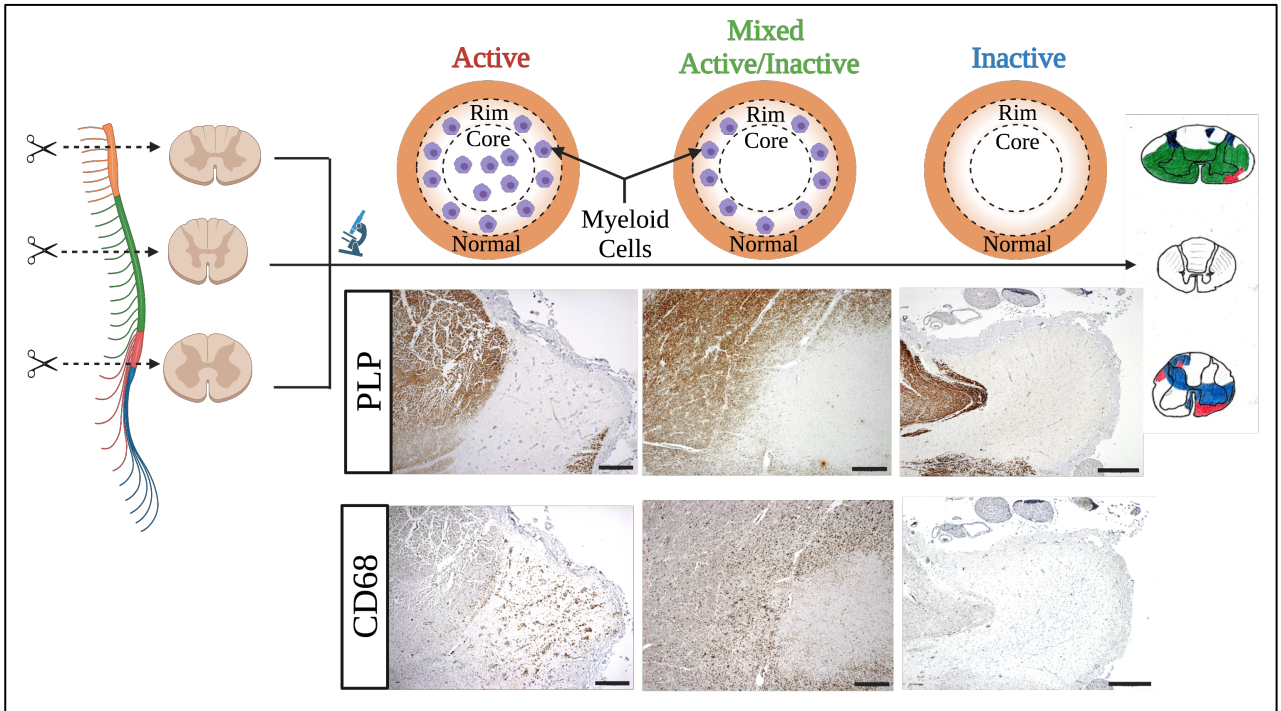


Figure 2.1. Methodological Approach to Assessing Staged Lesion Topography. Spinal cord material from the cervical, thoracic, and lumbar region was sectioned and processed for immunohistochemistry to stain for myelin (PLP) and myeloid cells (CD68). Light microscopy was used to identify areas of complete myelin absence and infiltration by myeloid cells was used to stage each lesion (scale bars: 0.5mm). Staged lesions were carefully drawn onto standardized templates prior to downstream computational analyses.

Formalin-fixed-frozen, paraffin-processed material from the cervical, thoracic, and lumbar spinal cord was serially sectioned (6μm thick) before immunohistochemical evaluation of demyelination and myeloid cell inflammation by proteolipid protein (PLP) and CD68 primary antibodies, respectively. Immunohistochemical optimisation determined the appropriate antigen retrieval method, primary antibody concentration, and incubation conditions for staining (**Table 2.2**).

Table 2.2. Antibodies and Conditions Used for Immunohistochemistry

Antibody	Clone	Classification	Antigen Retrieval	Dilution	Block	Incubation	Supplier	Catalogue
PLP	plpc	Mouse Monoclonal	Microwave, Citrate pH 6	1:1000 (TBST)	None	1hr RT	BioRad	MCA839G
CD68	PGM1	Mouse Monoclonal	Microwave, Citrate pH 6	1:100 (TBST)	None	1hr RT	DAKO	M0876

Tissue was first deparaffinised and rehydrated. Endogenous peroxidase activity was quenched with 3% hydrogen peroxide prior to heat-induced antigen retrieval. Staining was performed using the semiautomatic Shandon Sequenza system. The Dako REAL™ EnVision™ Detection System (K500711-2) was used for 3,3'-diaminobenzidine (DAB) detection. Sections were counter-stained with hematoxylin. Omission of primary antibodies confirmed the specificity of the immunoreactions.

Slides were viewed on an Olympus BX43 Brightfield Microscope. Areas of demyelination were defined by complete loss of myelin in PLP-stained sections. Inflammatory activity of demyelinated lesions was assessed using established criteria (Kuhlmann *et al.* 2017). In short, lesion activity was classified broadly as 1) active, 2) mixed active/inactive, and 3) inactive by histologically assessing the abundance and distribution of myeloid cells in CD68-stained sections. Specifically, active lesions were defined by the presence of homogenous CD68+ hypercellularity throughout the lesion, mixed active/inactive lesions by a hypocellular lesion core and rim of CD68+ cells along

the border, and inactive lesions by a relative paucity of CD68+ cells throughout the lesion. Active and mixed/active inactive lesions were subsequently collapsed to represent inflammatory lesions. Lesions classified by stage of inflammatory activity were drawn by a trained microscopist onto standardised templates of cervical, thoracic, and lumbar spinal cord levels ensuring that proportional lesion location and size were respected. A subset of cases was also assessed by a trained neuropathologist and consistent inter-rater reliability was observed. Representative histology images were captured using a Zeiss AxioCam MRc Color Camera. Hand-drawn lesion maps were digitised using the FMRIB Software Library (FSL) for downstream analyses.

2.2.3 Statistical Analysis

Graphical representations of all results were created in Prism 9 and imported into BioRender to create figure panels. Statistical analysis of prevalence and lesion extent data was performed in RStudio Version 1.4.1717. Lesion presence and proportion of the subpial circumference affected were used as an input for mixed effects logistic and linear regression, respectively, using the glmmTMB package. Models included fixed effects terms of spinal cord level and lesion stage, where relevant, with a random effect of case. The emmeans package was used to extract estimated marginal means and assess the significance of pairwise comparisons (Searle *et al.* 1980). A bias adjustment based on the value of sigma (standard deviation of the random effect) was applied. P-values were adjusted using the multivariate adjustment method. An adjusted p-value of 0.05 was used to define statistically significant comparisons. In addition, using the survival package, multivariate cox proportional hazards models were fit to understand the effects of lesion presence, inflammatory activity, and subpial lesion presence on clinical milestones obtained during life (time from onset wheelchair and time from onset to death) whilst controlling for sex and age of onset.

FSL was used to generate lesion frequency heatmaps. The Randomise function was used to perform permutation-based voxel-wise analysis with 500 permutations to identify lesion predilection sites for inflammatory and inactive lesions. Distance-based lesion segmentation was performed according to the method described in Ouellette *et al.* 2020. In short, 10 concentric trajectories (termed bins) were drawn onto the cervical, thoracic, and lumbar template in FSL. For each patient, the normalised lesion fraction (lesional area within each bin divided by the area of the bin) was calculated. A one-way ANOVA was used to test for differences across bins in lesion area for each level separately. Post-hoc tests with Dunnet's correction were used to assess differences between all bins and bin 5 (the innermost bin furthest from the CSF).

2.3 Results

2.3.1 Cohort Demographics

A total of 119 progressive MS cases contributed 102 cervical, 116 thoracic, and 107 lumbar spinal cord sections to the study for analysis. Cases with varied demographic profiles were included to maximise generalisability of the results (**Table 2.1**). In short, 83 cases were female (69.7%) and 36 were male (30.3%) with a mean age of 61.7 ± 12.5, disease duration of 28.4 ± 11.2 years, and time from onset to wheelchair of 17.3 ± 10.3 years. The mean post-mortem interval for the cohort was 16.7 ± 6.6.

2.3.3 Prevalence of Spinal Cord Demyelination and Inflammatory Activity

Across the cohort, 91/119 (76.5%) of cases harbored at least one lesion in the spinal cord with 80/91 (87.9%) exhibiting inflammatory demyelinating activity (active or mixed active/inactive lesions) (**Figure 2.2A**). Contrasts derived from logistic regression mixed models indicated that lesions were more likely to be present in the cervical spinal cord compared to the lumbar region

(OR=10.01, SE=3.96, p=0.0056) (**Figure 2.2B**). Inflammatory sections predominanted over those that were found to be inactive at all spinal cord levels (Cervical: Probability=0.84, SE=0.065, p=0.0001; Thoracic: Probability=0.70, SE=0.067, p=0.0031; Lumbar: Probability=0.73, SE=0.074, p=0.0022). However, when comparing across levels, sections from the cervical, thoracic, and lumbar spinal cord were equally likely to be inflammatory (**Figure 2.2C**).

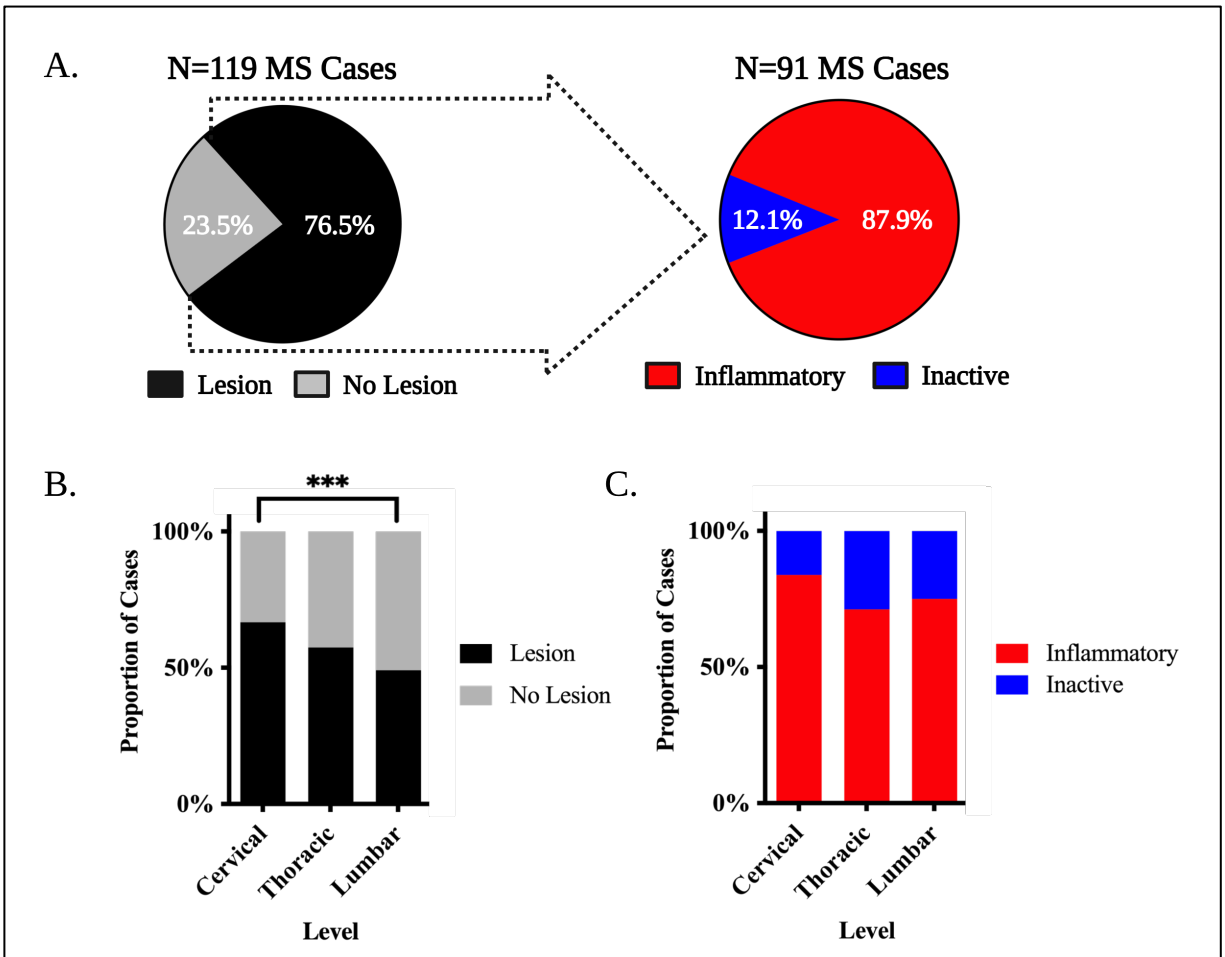


Figure 2.2. Prevalence of Demyelination in the MS Spinal Cord. (A) Pie charts highlighting the observed proportion of cases with spinal cord lesions and those that harbored at least 1 inflammatory (active or mixed/active inactive) lesion. (**B-C**) Stacked bar charts depicting the proportion of MS cases that harbored lesions at each level of the spinal cord irrespective of stage (**B**) and classified by the presence of inflammation (**C**). Proportions represent observed values and the asterisks indicate significant post-hoc pairwise comparisons following logistic mixed modelling and multivariate adjustment for multiple comparisons (*p<0.05; **p<0.01; ***p<0.001; ****p<0.0001).

2.3.3 Concordance of Spinal Cord Lesion Presence Across Levels

Given that radiographic imaging of the entire spinal cord poses challenges, especially in resource-limited settings, we explored the predictive potential of cervical spinal cord lesions on the identification of lesions in the thoracic and/or lumbar spinal cord. The sensitivity of cervical spinal cord lesions in the prediction of thoracic lesions was high (84.2%) though specificity was poor (59.5%), a finding also seen in the lumbar spinal cord (sensitivity=86.0%; specificity=51.0%).

2.3.4 Topography of Spinal Cord Demyelination and Inflammatory Activity

Representative histological patterns and summarized heatmaps of lesion predilection sites demonstrated that the dorsal columns, lateral corticospinal tracts, and the central canal were consistently affected by lesions. Interestingly, the subpial surface surrounding the spinal cord was spared across all spinal cord levels (**Figure 2.3A and 2.3B**). When stratified by inflammatory activity, inactive lesions predominated in the grey matter while lesions with inflammatory activity were common in the white matter (**Figure 2.3B**).

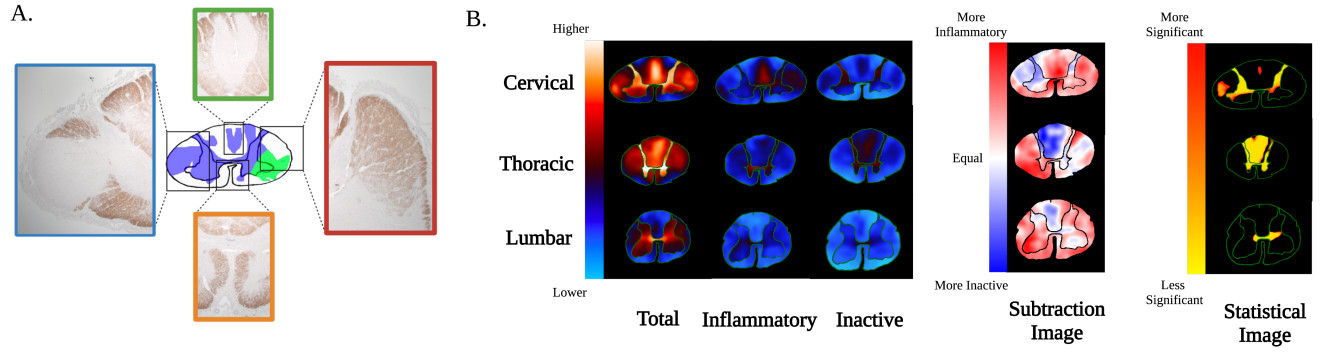


Figure 2.3. Pathological Patterns and Topography of Demyelination. (A) Representative histological images of lesion distribution patterns. The dorsal columns (green box), lateral corticospinal tracts (red box), and the whole grey matter (orange box) were consistently affected throughout the cohort. Interestingly, the subpial surface was commonly spared (red, green, and orange boxes). However, when present, subpial demyelination only affected a limited circumference (blue box). **(B)** Lesion frequency heatmaps of total, inflammatory, and inactive lesions in the cervical, thoracic, and lumbar spinal cord. The subtraction images highlight areas more commonly affected by inflammatory lesions (red), inactive lesions (blue), and those equally affected by both types (white). The voxelwise statistical image demonstrates areas significantly associated with inflammatory status. All areas represented are significantly overrepresented by the inactive class.

A complementary analysis assessing lesion prevalence in the anterior, posterior, and lateral funiculi was undertaken (**Figure 2.4A**). The probability of a lesion affecting the lateral and posterior funiculi was consistently higher than the anterior funiculus (**Figure 2.4B**).

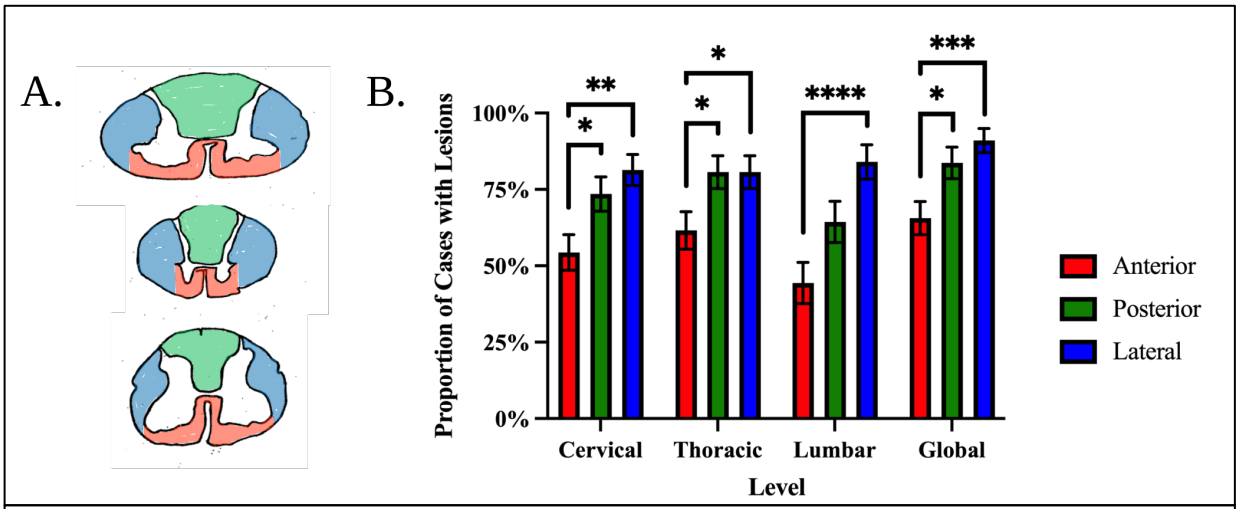


Figure 2.4. Location of Demyelinating Pathology. (A) Anatomical landmarks of the anterior (red), lateral (blue) and posterior (green) funiculi. **(B)** Bar charts depicting the proportion of MS cases that exhibited demyelination of the anterior, posterior, and lateral funiculi at each level of the spinal cord and globally. Proportion values represent estimated marginal means and standard errors derived from mixed logistic regression models. The asterisks indicate significant post-hoc pairwise comparisons after the multivariate adjustment for multiple comparisons (*p<0.05; **p<0.01; ***p<0.001; ****p<0.0001).

2.3.5 Prevalence and Extent of Subpial Demyelination

Given the relative subpial sparing observed in histological sections, a more comprehensive analysis of demyelination at CSF interfaces was undertaken. 76/91 (83.5%) cases with lesions exhibited demyelination of the white matter subpial surface with 61/76 (80.3%) exhibiting inflammatory demyelinating activity (**Figure 2.5A**). Contrasts from derived from logistic regression mixed models indicated that subpial lesions were not significantly more likely to be at any spinal cord level (**Figure 2.5B**). Sections with inflammatory subpial involvement were more common than those that were found to be inactive at all levels. This relationship was significant for the cervical and lumbar levels with borderline significance at the thoracic level (Cervical:

Probability=0.72, SE=0.0714, p=0.0083; Thoracic: Probability=0.64, SE=0.071, p=0.055; Lumbar: Probability=0.69, SE=0.074, p=0.020). However, when comparing across levels, sections from the cervical, thoracic, and lumbar spinal cord were equally likely to have inflammatory subpial disease (**Figure 2.5C**).

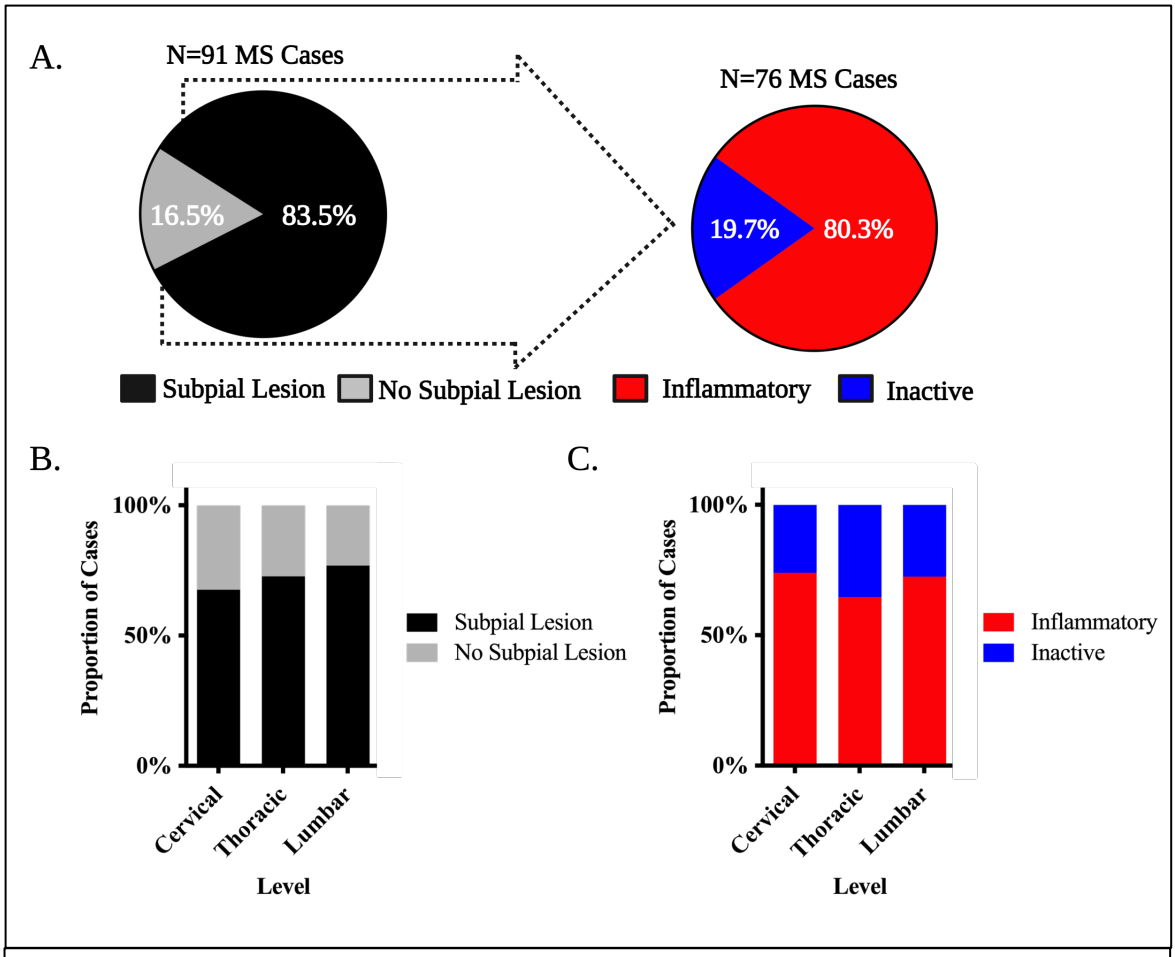


Figure 2.5. Prevalence of Subpial White Matter Demyelination in the MS Spinal Cord. (A) Pie charts highlighting the observed proportion of cases with subpial white matter spinal cord lesions and those that harbored at least 1 inflammatory (active or mixed/active inactive) subpial white matter lesion. (**B-C**) Stacked bar charts depicting the proportion of MS cases that harbored subpial white matter lesions at each level of the spinal cord irrespective of stage (**B**) and classified by the presence of inflammation (**C**). Proportions represent observed values, and the asterisks indicate significant post-hoc pairwise comparisons following logistic mixed modelling and multivariate adjustment for multiple comparisons (*p<0.05; **p<0.01; ***p<0.001; ****p<0.0001).

While subpial demyelination was common, the proportion of the subpial surface affected by lesions (i.e. spinal cord circumference affected by subpial lesions relative to total cord

circumference) was low and did not differ across levels (Cervical: 12.6%, Thoracic: 12.9%, Lumbar: 9.2%) (**Figure 2.6A and Figure 2.6B**). When only considering cases with subpial lesions, the proportion of the subpial surface affected by lesions remained relatively low (Cervical: 29.3%, Thoracic: 32.5%, Lumbar: 26.4%) (**Figure 2.6C and Figure 2.6D**).

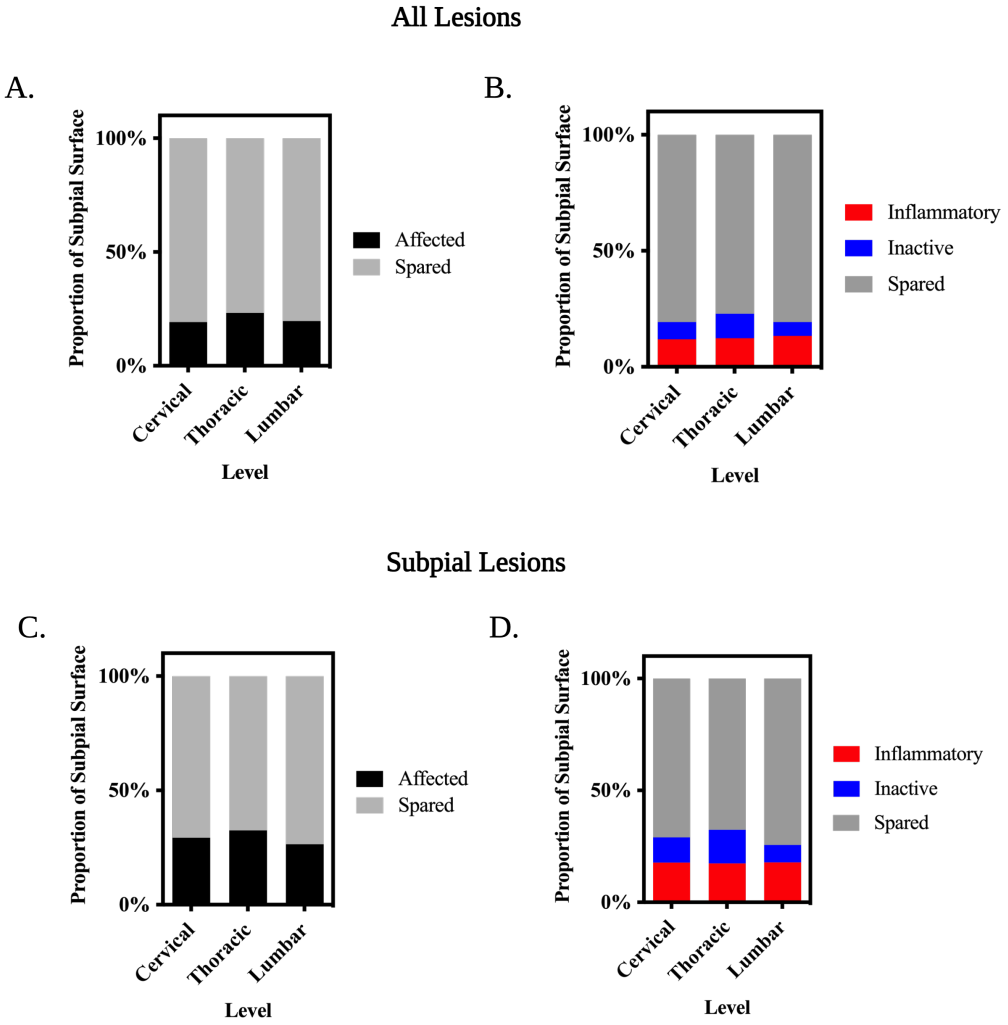


Figure 2.6. Extent of Subpial Demyelination in the MS Spinal Cord. (A-B) Stacked bar charts depicting the proportion of the subpial white matter surface affected by lesions at each level of the spinal cord irrespective of stage (**A**) and classified by the presence of inflammation (**B**) including cases with lesions of all types. **(C-D)** Stacked bar charts depicting the proportion of the subpial white matter surface affected by lesions at each level of the spinal cord irrespective of stage (**C**) and classified by the presence of inflammation (**D**) including only the cases with subpial lesions. Proportions represent observed values, and the asterisks indicate significant post-hoc pairwise comparisons following linear mixed modelling and multivariate adjustment for multiple comparisons (*p<0.05; **p<0.01; ***p<0.001; ****p<0.0001).

We also investigated the central canal, as it represents another CSF fluid interface. 67/91 (73.6%) cases with lesions exhibited demyelination of the central canal with 46/67 (80.3%) exhibiting inflammatory demyelinating activity (**Figure 2.7A**). Contrasts from derived from logistic regression mixed models indicated that central canal lesions were not significantly more likely to be at any spinal cord level (**Figure 2.7B**). Sections with inflammatory central canal involvement were not more common than those that were found to be inactive at all levels.

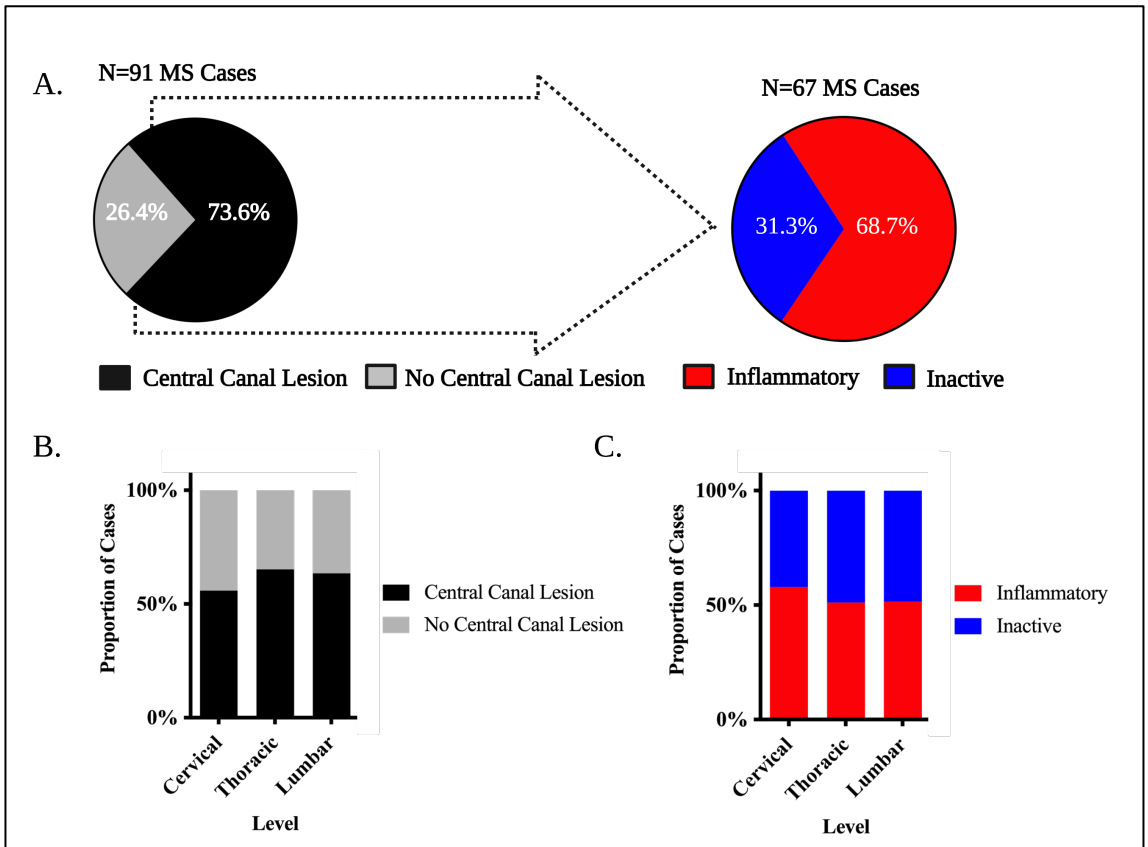


Figure 2.7. Prevalence of Demyelination in the Central Canal of the MS Spinal Cord. (A) Pie charts highlighting the observed proportion of cases with central canal lesions and those that harbored at least 1 inflammatory (active or mixed/active inactive) central canal lesion. (**B-C**) Stacked bar charts depicting the proportion of MS cases that harbored central canal lesions at each level of the spinal cord irrespective of stage (**B**) and classified by the presence of inflammation (**C**). Proportions represent observed values and the asterisks indicate significant post-hoc pairwise comparisons following logistic mixed modelling and multivariate adjustment for multiple comparisons (*p<0.05; **p<0.01; ***p<0.001; ****p<0.0001).

Given that recent MRI work suggested a gradient of spinal cord lesions extending from fluid interfaces inwards (i.e. subpial or central canal to the parenchyma), we decided to recapitulate the analysis by Ouellette *et al.* 2020. One-way ANOVA analysis demonstrated that normalised lesion volumes differed amongst bins at all levels (Cervical: $F=27.59$, $p<0.0001$; Thoracic: $F=29.75$, $p<0.0001$; 19.85; $p<0.0001$). Post-hoc analyses comparing all bins to the innermost bin (i.e. furthest from CSF boundaries) demonstrated a consistent decrease of normalised lesion volumes in the bins positioned furthest to the CSF (bin 1 and bin 10) (**Figure 2.8A, Figure 2.8B, and Figure 2.8C**).

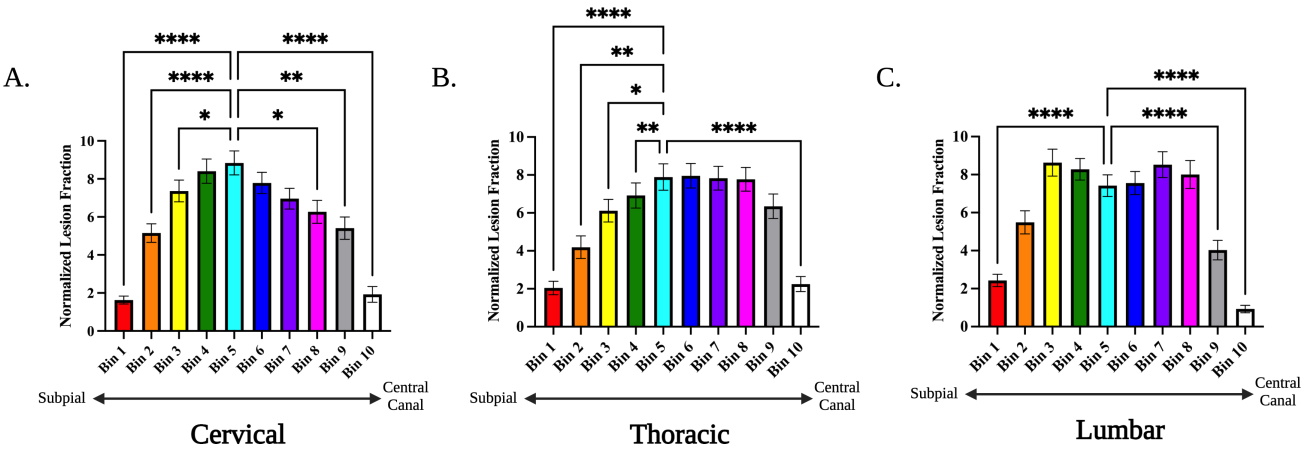


Figure 2.8. Distance-Based Lesion Segmentation Analysis of Spinal Cord Demyelination. Bar charts displaying normalized lesion fractions within concentric trajectories extending from the subpial surface (bin 1) to the central canal (bin 10) in the cervical (**A**), thoracic (**B**), and lumbar (**C**) spinal cord. Differences were assessed within each level individually with a one-way repeated measures ANOVA. Post-hoc comparisons with Dunnett's correction were made compared to bin 5 (the innermost region). The asterisks indicate significant post-hoc pairwise comparisons (*p<0.05; **p<0.01; ***p<0.001; ****p<0.0001).

2.3.6 Clinicopathological Relationships

Given the heterogenous demographics of our large post-mortem cohort, we aimed to understand the relationship between spinal cord demyelination and clinical outcome. Time from disease onset to wheelchair and time from disease onset to death (disease duration) were used as surrogate markers of disease severity and response variables for multivariate cox proportional hazard

analysis (**Figure 2.9**). Given previous data, sex and age of onset were included as covariates in all analyses (Confavreux *et al.* 2006). Cases with lesions anywhere in the spinal cord were more likely to be wheelchair-dependent (HR 2.45, 95% CI 1.43-4.20) or die (HR 2.65, 95% CI 1.61-4.34) at younger ages (**Figure 2.9A and Figure 2.9B**) with lesion activity or subpial location not having any impact (time to wheelchair: lesion activity - (HR 1.01, 95% CI 0.53-1.93; subpial lesion - HR 1.32, 95% CI 0.71-2.44; time to death: lesion activity - (HR 1.78, 95% CI 0.93-3.38; subpial lesion (HR 1.71, 95% CI 0.93-3.13) (**Figure 2.9 C-F**).

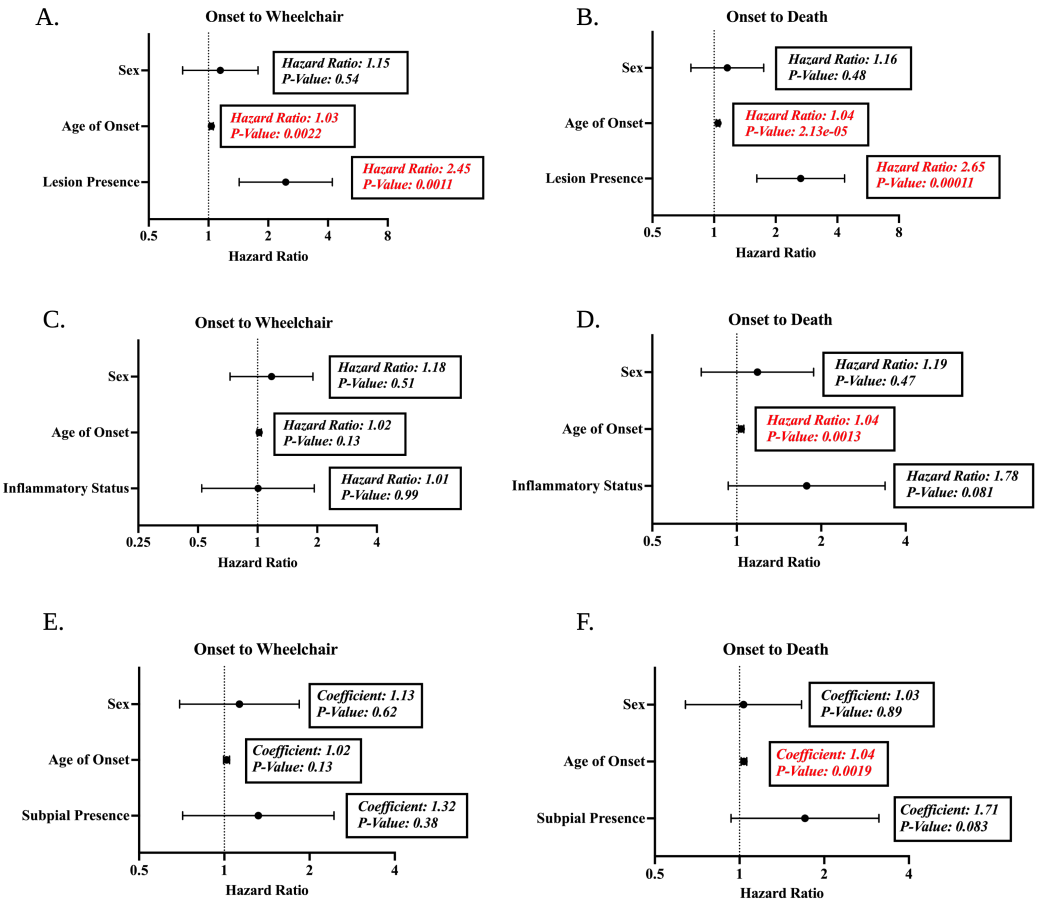


Figure 2.9. Clinicopathological Relationships Between Demyelination and Clinical Milestones. Forest plots displaying the hazard ratio and 95% confidence interval are derived from multivariate cox proportional hazards models controlling for sex and age of onset. The impact of spinal cord lesion presence on the time from MS onset to wheelchair use (**A**) and MS onset to death (**B**) was tested. The impact of inflammatory status was also tested on the time from MS onset to wheelchair use (**C**) and MS onset to death (**D**). Lastly, in cases with lesions, the impact of subpial lesion presence was tested on the time from MS onset to wheelchair use (**E**) and MS onset to death (**F**). Coefficients and p-values are highlighted in red for significant predictors ($p<0.05$) in the models.

2.4 Discussion

Demyelination is a cardinal feature of MS spinal cord pathology that has attracted particular attention over the years due to pathogenic insights that may be gleaned based on its topography. However, the study of spinal cord lesion topography has yielded discrepant interpretations and engendered considerable debate. Therefore, we performed the largest neuropathological characterisation of the extent, distribution, and inflammatory activity of spinal cord lesions. We highlight that lesions in the MS spinal cord are common, and highly inflammatory debunking the traditionally held view that spinal cord lesions are 'burnt out' at end-stage disease. Further, our topographic finding that lesions most commonly affect the posterior and lateral columns with relative sparing of the subpial and central canal interfaces challenges the view that an outside-in gradient of diffusible CSF factors is the main culprit of lesion pathogenesis.

We found that demyelination is common and highly inflammatory in the progressive MS spinal cord. Lesions were found in 91/119 (76.5%) of cases of which 80/91 (87.9%) demonstrated inflammatory activity. While previous MRI work has demonstrated similar prevalence of lesion burden (Bot *et al.* 2004, Weier *et al.* 2012) which has justified spinal cord lesion inclusion in the MS diagnostic criteria and MAGNIMS-CMSC-NAIMS consensus reccomendations (Thompson *et al.* 2018, Wattjes *et al.* 2021), our study provides novel insight into the extent of inflammatory activity in spinal cord lesions at end-stage disease. Our finding of the high prevalence of lesional activity is in line with a recent post-mortem study (Luchetti *et al.* 2018), and provides a critical extension given the focus on the clinically eloquent spinal cord. While MRI studies show that contrast enhancing lesions decrease over the MS lifecycle, it is well established that spinal cord imaging is riddled with technical and physiological challenges that make detection of active lesions, let alone mixed active/inactive ones, difficult (Khaleeli *et al.* 2010, Dal-Bianco *et al.* 2017,

Absinta *et al.* 2019). The fact that the significant majority of lesions at death remain inflammatory, particularly of the mixed active/inactive moiety, challenges the notion that lesions become "burnt-out" in the progressive phase and are not amenable to therapy (Frischer *et al.* 2009, Frischer *et al.* 2015).

Spinal cord lesions preferentially affect the cervical spinal cord. In our cohort, 68/102 cases (66.7%) had a lesion in the cervical cord compared to 66/116 cases (56.9%), and 52/107 cases (48.5%) in the thoracic and lumbar levels, respectively. Previous MRI studies in clinical cohorts have shown a similar prevalence of spinal cord lesions in the cervical cord, but under-estimate the extent of thoracolumbar disease (Bot *et al.* 2004, Weier *et al.* 2012, Poulsen *et al.* 2021). While technical and physiological artifacts reduce the sensitivity of lesion detection in *in vivo* imaging studies, the fact that we studied cases at the end of life where a more significant accumulation of lesion burden is expected could also contribute to this discrepancy. Regardless, our work supports the MAGNIMS-CMSC-NAIMS guidelines that highlight the utility of spinal cord MRI in the monitoring and prognosis of MS (Wattjes *et al.* 2021). What is more, the lack of cervical cord lesions predicted the lack of lesions in the thoracolumbar region of a given case. This data suggests that solely imaging the cervical spinal cord may provide important insights into the status of the thoracolumbar region. Therefore, particularly in resource-limited settings, prognostication and monitoring paradigms using spinal cord MRI could focus on just obtaining images from the cervical level.

We provide novel insight into the distribution and extent of demyelination in the MS spinal cord. In line with previous work, we found that MS cases most commonly have lesions affecting the lateral and posterior columns and central canal (Eden *et al.* 2019). While the majority of MS cases

harboured a subpial lesion (76/91 of cases, 83.5%), the proportion of the subpial surface affected by lesions was low (~30% of cord perimeter). Distance-based lesion segmentation analyses further supported the relative sparing of the subpial surface by showing that lesions most commonly affected the cord at distances furthest away from CSF boundaries (i.e. subpial and central canalicular surfaces). These findings challenge those from a recent MRI study that reported a subpial gradient of demyelination in the spinal cord (Ouellette *et al.* 2020). Several factors could explain this discrepancy. Pathological studies have superior resolution to detect the presence and distribution of lesions, especially at CSF interfaces where imaging artifacts are common. MRI studies of the spinal cord are further challenged by the cord's proximity to mobile tissues and fluids and relative shielding by bone and fat (Bruschi *et al.* 2020). Not to mention, subpial signal changes previously reported on MRI may reflect pathological processes apart from demyelination. Reactive microgliosis is a prime candidate as a subpial gradient of glial cell reactivity has been observed in the post-mortem spinal cord (Grussu *et al.* 2017).

Our topographical analyses of lesion distribution in the MS spinal cord lend support to the vasculature as a key culprit in the pathogenesis of demyelination in the disease. The conflation of data from our lesion probability maps and distance-segmentation analyses show that lesions mirror the vascular network and spare regions juxtaposed to CSF boundaries (Fog 1950, Oppenheimer 1978). These data lend further support to vascular pathology (e.g. blood-brain-barrier disruption) as a likely upstream contributor to the pathogenesis of the demyelinated lesion and argues against an outside-in process of demyelination (Oppenheimer 1978). In fact, while work in the cortex has identified tertiary lymphoid follicles as major drivers of a gradient of cortical demyelination from the subpial surface inward, follicle positivity did not significantly increase the severity of demyelination in the spinal cord (Reali *et al.* 2020). Representative images of demyelination from

the study by Reali and colleagues also demonstrated that large portions of the subpial surface are spared in follicle positive individuals. We also illustrated that the demyelination is underrepresented in the anterior funiculus, an area where CSF stasis and meningeal inflammation is posited to be at its highest. Discordant findings regarding the relative importance of CSF-derived factors and the vascular unit between the brain and spinal cord may be due to inherent topographical differences in 1) the mechanical forces imparted on these structures and 2) the intrinsic permeability of the BBB compared to the blood-spinal cord barrier (BSCB) (Oppenheimer 1978, Bartanusz *et al.* 2011). Overall, our findings suggest topographical differences play a major role in the pathogenesis of demyelination throughout the length of the neuraxis and that vascular mechanisms likely predominate in the spinal cord.

Our distributional analysis also allowed us to investigate differences between the distribution of white and grey matter demyelination in the MS spinal cord. Comparative analyses such as these have historically been inaccessible to MRI-based studies due to contrast and spatial resolution limitations (Moccia *et al.* 2019). In our work, inflammatory lesions commonly affected the white matter while inactive lesions were overrepresented in grey matter. This finding is in line with previous pathological studies that highlight a biologically-relevant difference between the pathogenesis of demyelination in the white and grey matter and continues to support a broader view of demyelination beyond the white matter (Gilmore *et al.* 2006, Gilmore *et al.* 2009). Whether our findings support an entirely different pathogenic mechanism of lesion pathogenesis in grey versus white matter or a capacity for grey matter to better resolve inflammation remains to be seen and is the subject of future work.

Indexed clinical reports with metrics of disease outcome obtained during life allowed us to draw interesting clinicopathologic correlations. When controlling for sex and age of onset, the presence of a spinal cord lesion was an independent predictor of two important clinical endpoints, time from onset to wheelchair and death. These findings confirm the relevance of spinal cord demyelination to MS prognosis purported by MRI studies of clinical cohorts (Sombekke *et al.* 2013, Brownlee *et al.* 2017, Arrambide *et al.* 2018). In contrast to Luchetti *et al.* 2018, cases with inflammatory lesions did not have a significantly worse clinical course compared to those with only inactive ones, a finding potentially explained by the small number of inactive cases in our cohort (n=11). However, it is possible that the impact of lesion presence in an anatomical site with relatively low functional reserve overwhelms the impact of lesion phenotype.

We acknowledge the limitations inherent to post-mortem studies. Our case series are necessarily biased towards the end-stage of the MS disease process. To address this, we included a large number of cases across a wide spectrum of clinical disability. Our focus on the post-mortem spinal cord sampled throughout its length is unique and provides resolution to detect granular cord pathology well beyond that of *in vivo* imaging modalities. This strategy enabled us to not only characterise lesion location more precisely but also to decipher the inflammatory activity of lesions and their distribution. We recognise that our lesion maps represent a static view of a dynamic process and are an extrapolation from individual spinal cord sections that were deemed representative of the cervical, thoracic, and lumbar levels. However, we attempted to mitigate this by transposing lesions for each case into a standard space. While measurement error is possible, anatomical landmarks were used to maintain proportional relationships required for downstream analyses and reliability was assessed with two expert raters. Paired statistical analyses also improved statistical power. In comparison to dedicated spinal cord MRI, our approach did not

allow for the comprehensive profiling of lesion topography throughout the entirety of the spinal cord. However, we placed emphasis on relevant heterogeneity within each section and across levels more broadly (cervical, thoracic, and lumbar). Overall, compared to MRI, our histopathological approach provides increased sensitivity for lesion detection and enhanced resolution for the assessment of inflammatory activity.

In summary, this chapter demonstrates that spinal cord lesions are an important feature of MS pathology. Spinal cord lesions are common, often inflammatory at end-stage disease, portend a worse clinical course, and exhibit a unique topographical pattern. The subpial zone is relatively spared across the cohort and lesion patterns mirror the trajectories of the vasculature (**Figure 2.10**). These findings begin to disentangle the complexities surrounding the relative contributions of the meningeal interface and vascular unit to the pathogenesis of lesions in MS. Our study sets the stage for further exploration of the mechanisms that underlie topographical variation in lesion biology along the length of the MS neuraxis.

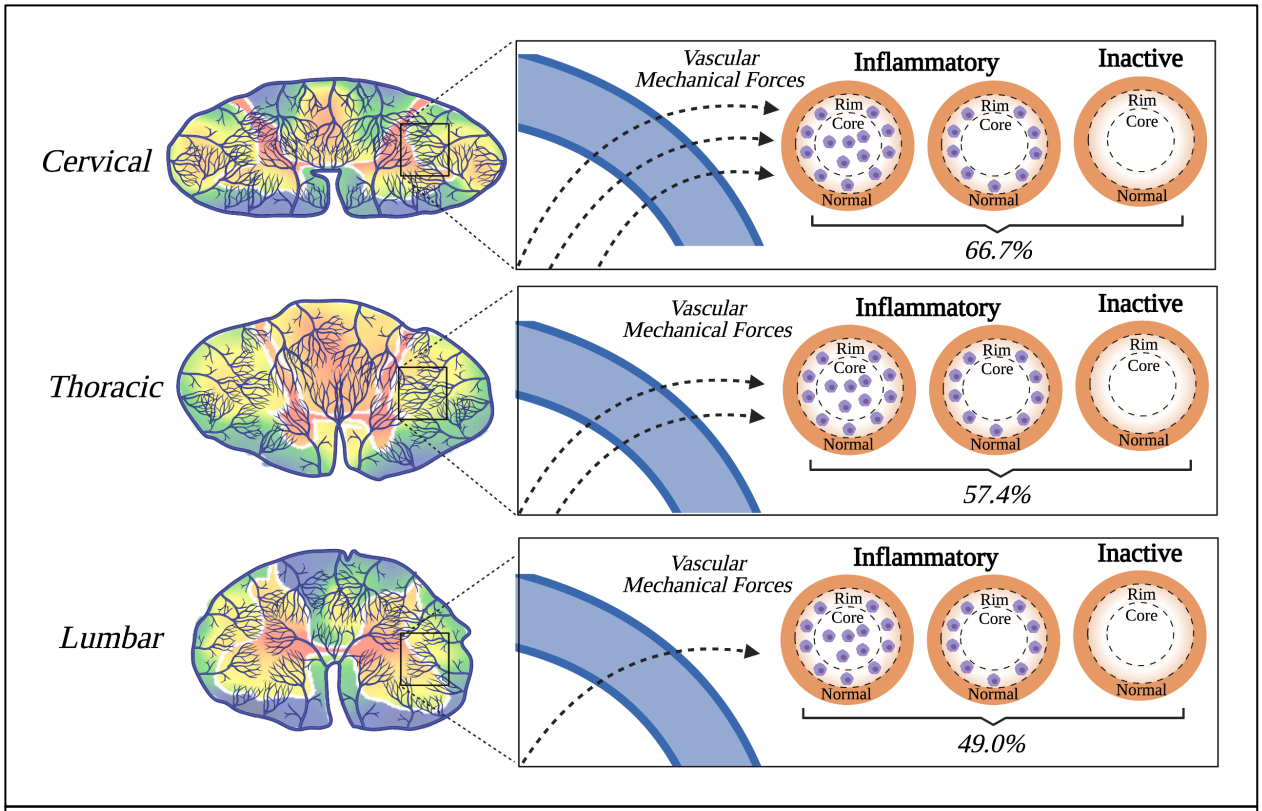


Figure 2.10. Working Hypothesis of Spinal Cord Demyelination. The topography of lesional pathology in the spinal cord across all levels spares the subpial surface and mirrors the distribution of venous drainage. The cervical spinal cord is more susceptible to chronic inflammatory demyelination when compared to the thoracic and lumbar regions. Heterogeneity in mechanical stress along the length of the spinal cord is hypothesised to underlie this enhanced susceptibility. Mobility of the cervical spinal cord is prominent and posited to transmit tensile forces onto the vasculature, ultimately promoting barrier dysfunction, myelinotoxic immune cell infiltration, and diffusion of toxic substances.

3. Neuropathological and Proteomic Relationships with Axonal Loss in the Multiple Sclerosis Spinal Cord

3.1 Introduction

Axonal loss is a predominant feature of MS spinal cord pathology and known substrate of disability accumulation (Ganter *et al.* 1999, DeLuca *et al.* 2004, Tallantyre *et al.* 2010, Petrova *et al.* 2018). However, the determinants of axonal loss have remained elusive. Demyelination has been posited as one candidate driver of neurodegeneration though pathological reports on its relationship with axonal loss have been conflicting (Lovas *et al.* 2000, DeLuca *et al.* 2006, Tallantyre *et al.* 2009, Petrova *et al.* 2018). Inflammation of the CNS parenchyma has also been shown to contribute to the MS neurodegenerative cascade (Androdias *et al.* 2010, Howell *et al.* 2010, Zrzavy *et al.* 2017).

Additional neuropathological studies have implicated disruption of the BBB, BSCB, and blood-CSF barrier as important contributors to MS-related neurodegeneration (Magliozzi *et al.* 2007, Popescu *et al.* 2012, Yates *et al.* 2017, Bell *et al.* 2018, Magliozzi *et al.* 2019). Specifically, fibrinogen, a surrogate of barrier breakdown, is deposited in the progressive MS CNS and associates with neurodegeneration (Yates *et al.* 2017). Further, inflammation in the meningeal and perivascular spaces, where CSF flows, is tightly linked not only to parenchymal inflammation but also to the extent of axonal loss (Androdias *et al.* 2010, DeLuca *et al.* 2013, Reali *et al.* 2020). Taken together, these data suggest that molecular mediators that traverse barrier sites and accumulate in compartments like the subarachnoid space, may be important contributors of inflammatory-related neurodegeneration in the progressive MS spinal cord.

Disruption of these barrier sites (BBB, meninges, perivascular space) allows for unrestricted two-way exchange of effector and bystander molecules, including those that are typically intracellular,

with the parenchyma and surrounding CSF. Therefore, the CSF provides a biologically-relevant repository to identify biomarkers and/or molecular mediators of axonal loss (**Figure 3.1**). However, a unified understanding of the meningeal, perivascular, and parenchymal factors involved in axonal loss and how they interact to promote spinal cord neurodegenerative pathology is not known.

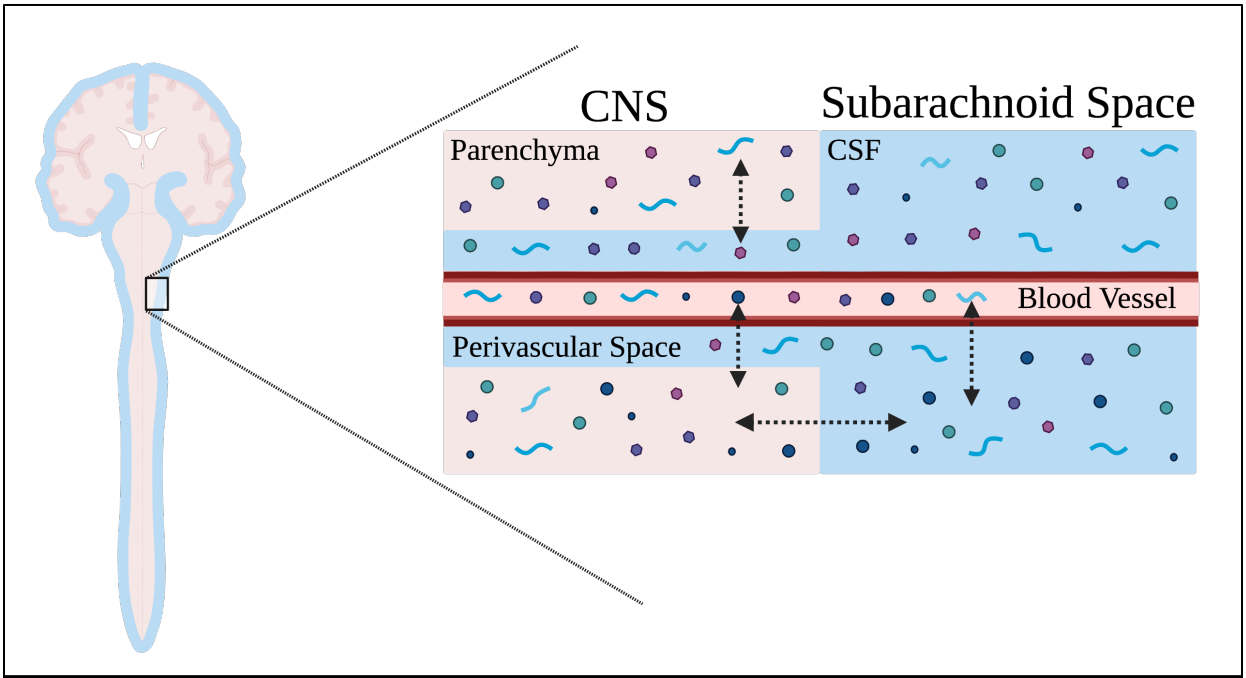


Figure 3.1. Barrier Site Crosstalk in MS. The subarachnoid space, where CSF flows, is contiguous with the perivascular space surrounding vessels in the CNS parenchyma. Barrier dysfunction in pathological conditions, like MS, allows molecules to flow between the blood, CSF, perivascular space, and parenchyma. Therefore, sampling of readily available biofluids (CSF and blood) represents a reservoir of potential biomarkers involved in CNS pathology.

This chapter investigates the relationship between demyelination, inflammation, and degeneration in the MS spinal cord and employs a novel approach of correlating objective quantitative pathological outcomes with CSF protein signatures. This experimental paradigm 1) controls for significant biologic (and likely pathologic) diversity/heterogeneity that has previously limited biomarker discovery and 2) uniquely allows us to evaluate the influence of proteomic variation of

tissues readily accessible during life (CSF) on pathologic changes only detectable, at present, after death.

3.2 Materials and Methods

3.2.1 Study Population

Spinal cord material (cervical, thoracic and lumbar levels) from a human autopsy cohort with pathologically confirmed MS (n=40) and non-neurological disease controls (n=15) was derived from the UK MS Tissue Bank (**Table 3.1**). This cohort represents a subset of cases analysed in the previous chapter.

Table 3.1. Spinal Cord Quantitative Neuropathology Cohort Demographics

		Multiple Sclerosis (*n*=40)	**Control (*n*=15)**	**Difference**
Number of Samples	*Cervical*	*31*	*10*	N/A
	Thoracic	54	*16*	
	Lumbar	31	*8*	
Age (Mean ± SD)		64.2 ± 12.8	78.5 ± 10.0	***(p=0.0004)
Sex (M:F)		13:27	7:8	N/A
Post-Mortem Interval in Hours (Mean ± SD)		17.3 ± 6.8	22.7 ± 12.8	N/A
Disease Type*	*Primary Progressive*	4		
	Secondary Progressive	34		
	Progressive-Relapsing	1		
	Relapsing-Remitting	1		
Disease Duration in Years (Mean ± SD)*		31.3 ± 11.9		
Time to Wheelchair (Mean ± SD)*		19.8 ± 12.2		

*Data missing for disease duration (*n*=2) and time to wheelchair (*n*=8)

Fresh frozen post-mortem CSF was available in the MS cohort and a separate control cohort (n=9) for downstream proteomics to assess the relationships between MS status and pathology (**Table 3.2**). The post-mortem interval for each case was <24 hours. Ethical approval was obtained (REC# 08/MRE09/31+5) and Human Tissue Act Guidelines were followed.

Table 3.2. Post-Mortem CSF Proteomics Cohort Demographics

		Multiple Sclerosis (*n*=40)	Control (*n*=9)	Difference
Age (Mean ± SD)		64.2 ± 12.8	77.7 ± 9.0	**(p=0.0028)
Sex (M:F)		13:27	6:3	N/A
Post-Mortem Interval in Hours (Mean ± SD)		17.3 ± 6.8	27.8 ± 9.5	***(p=0.0006)
Disease Type*	*Primary Progressive*	4		
	Secondary Progressive	34		
	Progressive-Relapsing	1		
	Relapsing-Remitting	1		
Disease Duration in Years (Mean ± SD)*		31.3 ± 11.9		
Time to Wheelchair (Mean ± SD)*		19.8 ± 12.2		

*Data missing for disease duration (*n*=2), and time to wheelchair (*n*=8)

3.2.2 Palmgren Silver Staining

Nitric acid washed glassware was used to make up all reagents and process specimens with the Palmgren silver staining procedure. Fixed-frozen paraffin-embedded spinal cord material was first sectioned (10μm thick) onto superfrost plus glass slides. Slides were baked for 30 minutes at 60°C prior to de-waxing in xylene and rehydration with graded alcohol dilutions (100%, 100%, 90%, 70%). Sections were incubated in Palmgren acid formalin for 10-minutes and washed with distilled water 3 times over 5-minutes. Sections were then incubated in freshly filtered Palmgren silver solution for 45 minutes. The resulting silver solution was drained, and each section underwent reduction using the Palmgren reducer solution heated to 60°C. The sections were washed with distilled water and the reaction was quenched with a 5-minute incubation in a 5% solution of sodium thiosulfate. Sections were washed in distilled water before being dehydrated using graded alcohol dilutions (70%, 90%, 100%, 100%), cleared in xylene, and mounted with DPX.

3.2.3 Immunohistochemistry

Fixed-frozen paraffin-embedded material from the spinal cord was sectioned (6μm thick) onto superfrost plus glass slides. Slides were baked for 30 minutes at 60°C prior to de-waxing in xylene and rehydration with graded alcohol dilutions (100%, 100%, 90%, 70%). Immunohistochemical optimisation determined the appropriate antigen retrieval method, primary antibody concentration, and incubation conditions for staining (**Table 3.3**) Endogenous peroxidase activity was quenched with 3% hydrogen peroxide prior to antigen retrieval. Staining was performed using the semiautomatic Shandon Sequenza system. The Dako REAL™ EnVision™ Detection System (K500711-2) was used for DAB signal development. Sections were counterstained with Harris Haematoxylin (Lecia, 3801560E) before dehydration using graded alcohol dilutions (70%, 90%, 100%, 100%). Sections were then cleared in xylene before mounting with DPX. Negative controls with omission of primary antibody were used to verify the specificity of the immunohistochemical reaction.

Table 3.2. Antibodies and Conditions Used for Immunohistochemistry

Antibody	Clone	Classification	Antigen Retrieval	Dilution	Block	Incubation	Supplier	Catalogue
CD68	PGM1	Mouse Monoclonal	Microwave, Citrate pH 6	1:100 (TBST)	None	1hr RT	DAKO	M0876
TMEM119	N/A	Rabbit Polyclonal	Autoclave, Tris EDTA pH 9	1:1500 (TBST)	None	ON 4°C	Sigma	HPA051870
IBA1	N/A	Rabbit Polyclonal	Autoclave, Citrate pH 6	1:1000 (PBS)	10% FCS	1hr RT	WAKO	019-19741
P2Y12	N/A	Rabbit Polyclonal	Autoclave, Citrate pH 6	1:1500 (DAKO Diluent)	DAKO Serum-Free	ON 4°C	AnaSpec	AS-55042A

3.2.4 Neuropathological Image Annotation and Sampling

Spinal cord sections (immuno)stained with Palmgren silver, PLP, IBA1, CD68, P2Y12, and TMEM119 were slide scanned with the Aperio Scanscope AT Turbo system (Leica Biosystems) prior to processing in QuPath v0.4.3. Palmgren-stained sections were used for masking relevant structures and tracts to undertake an optimised sampling strategy (DeLuca *et al.* 2013) described in **Figure 3.2**.



Figure 3.2. Neuropathology Image Annotation and Sampling. The white matter (yellow) and grey matter (purple) were first masked using QuPath v0.4.3 as a means to tabulate cross-sectional area. The lateral corticospinal tracts (red) were identified by drawing a straight line horizontally across the posterior commissure. The anterior corticospinal tracts (green) were identified by drawing a straight line from the inside edge of the ventral horn. 5 trajectories (black) on each side of the lateral corticospinal tracts and 3 trajectories (white) on each side of the anterior corticospinal tracts were assessed for axonal density and myeloid cell densities.

Specifically, white and grey matter were first delineated and traced followed by lateral corticospinal tracts (LCST) and anterior corticospinal tracts (ACST) using landmarks as previously described (DeLuca *et al.* 2013). Adjacent PLP-stained sections were then overlayed onto the Palmgren-stained section to identify lesional areas. Normal appearing areas (in white or grey matter) were defined as being at least 200μm from a lesion edge regardless of its inflammatory stage on which trajectories of 96,740μm^2 were added (five per LCST and three per ACST). The masks of the identified normal appearing white or grey matter areas were subsequently transferred to serial sections stained for myeloid markers (IBA1, CD68, P2Y12, and TMEM119) using the Virtual Alignment of pathoLogy Image Series (VALIS) python program (Gatenbee *et al.* 2021). This pipeline uses a reference image (Palmgren silver) with a corresponding annotation geoJSON file and target images (IBA1, CD68, P2Y12, and TMEM119) as inputs. Machine learning identifies matching features across serial sections. Rigid and non-rigid registration is then performed before annotation vertices are warped to generate geoJSON annotation files for each target image. Quality control of the newly generated annotation files was performed by loading each image and geoJSON file into QuPath v0.4.3. Annotation adjustments were made by hand, if necessary.

3.2.5 Histological Image Analysis

Area measurements (in mm^2) were calculated using the annotations made in QuPath v0.4.3 on Palmgren silver images. White and grey matter areas were summed to tabulate cross-sectional area (CSA) measurements. Areas of each motor tract (LCST and ACST) on each side of the spinal cord were averaged to generate unilateral estimates of motor tract area.

LCST and ACST trajectories from Palmgren silver-stained sections were extracted as individual images and analysed in batch using a previously developed and optimised pipeline integrating MATLAB (R2019b) and ImageJ (DeLuca *et al.* 2004, DeLuca *et al.* 2013). Palmgren silver images were first contrast enhanced. Axons were then segmented based on colour and sphericity. All images underwent manual quality control of segmentation (**Figure 3.3**) before axonal counts were extracted and converted into axonal densities. Total motor axonal counts were calculated by multiplying motor tract areas by density measures.

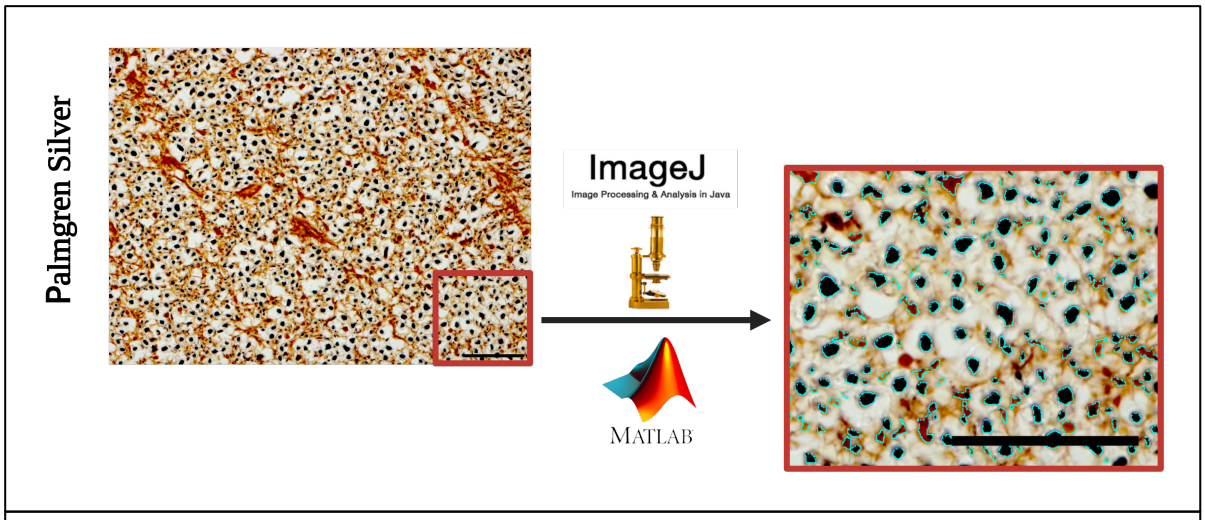


Figure 3.3. Palmgren Silver Image Analysis Pipeline. Plamgren silver images were analysed through integration of MATLAB (R2019b) and ImageJ. Images (scale bars: 50µm) were contrast-enhanced and axons were then segmented based on color and sphericity. All images underwent manual quality control of segmentation before axonal counts were extracted.

LCST and ACST trajectories from myeloid cell stains were analysed directly within QuPath v0.4.3. Four random-forest pixel classifiers were trained to identify DAB deposits derived from immunohistochemical images of the various myeloid cell stains (IBA1, P2Y12, CD68, and TMEM119). Both control and MS areas were included in the training set. Each stain-specific pixel classifier was applied to the entire cohort. All images underwent manual quality control of DAB signal identification (**Figure 3.4**) before area coverage measures were extracted.

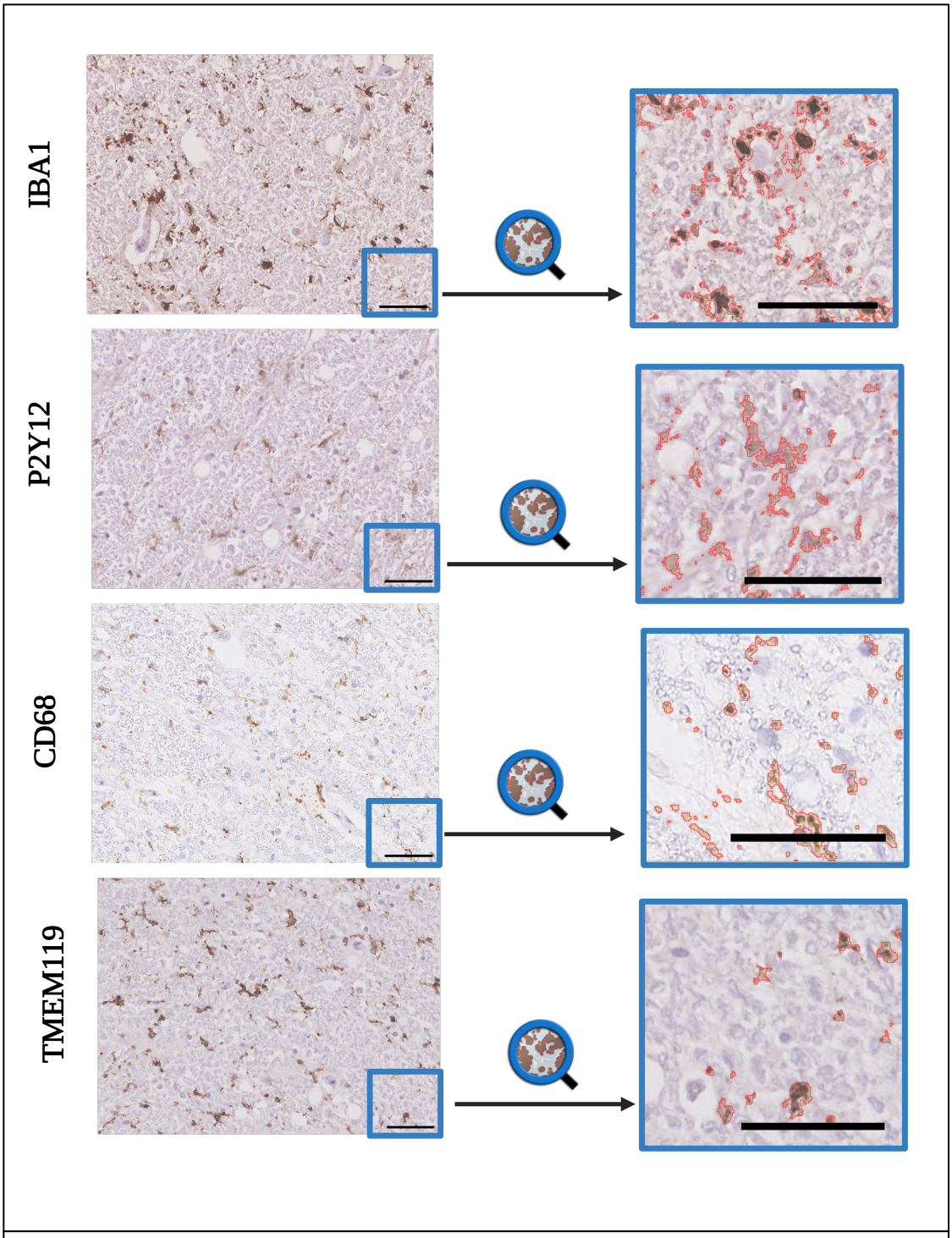


Figure 3.4. Myeloid Cell Image Analysis Pipeline. Immunohistochemical images (scale bars: 50μm) of myeloid cells were analysed using QuPath v0.4.3. Four separate random-forest pixel classifiers were trained to identify 3,3'-diaminobenzidine (DAB) deposits derived from immunohistochemical images of various myeloid cell stains (IBA1, P2Y12, CD68, and TMEM119). Both control and MS areas were included in the training. Each pixel classifier was applied to the entire cohort. All images underwent manual quality control of DAB signal identification before area coverage measures were extracted.

Images of adaptive immune cell markers (CD3 and CD20) were obtained at 200X magnification in the LCST and ACST trajectories described above using an Olympus BX43 Brightfield Microscope coupled to the Zeiss AxioCam MRc Color Camera with AxioVision software (v4.9.1, ZEISS). Cells were counted by hand and reported as cells/mm^2. In addition, CD3+ and CD20+ cells overlaying the entire circumference of each spinal cord section were counted manually at 400X magnification to assess meningeal inflammation (reported as cells/mm).[2] Given the relative paucity of CD20 in our cohort, we devised discrete classes of CD20+ inflammation. Parenchymal CD20+ inflammation was defined as present or absent while meningeal CD20+ inflammation was split into two groups defined as being above or below the median value of the cohort.

3.2.6 Post-Mortem Cerebrospinal Fluid Proteomics

20ul of CSF was diluted up to a volume of 175ul in distilled water. Dithiothreitol (DTT) and iodoacetamide (IAA) were added for the reduction and alkylation of cysteine disulfide bonds, respectively. Proteins were precipitated using a chloroform/methanol extraction. The solid protein pellet was solubilised in 6M urea before dilution by a factor of 6 and proteolysed with trypsin overnight. Peptides were desalted on C1-18 before analysis by nano-UPLC-MS/MS using a Dionex Ultimate 3000 coupled to an Orbitrap Fusion Lumos (Thermo Scientific) with a 60-minute gradient for peptide elution.

3.2.7 Data Integration

Integration of neuropathological and proteomic data was performed according to the workflow described in **Figure 3.5**.

[2] This data was previously generated (DeLuca *et al.* 2013) and shared for the purposes of this work.

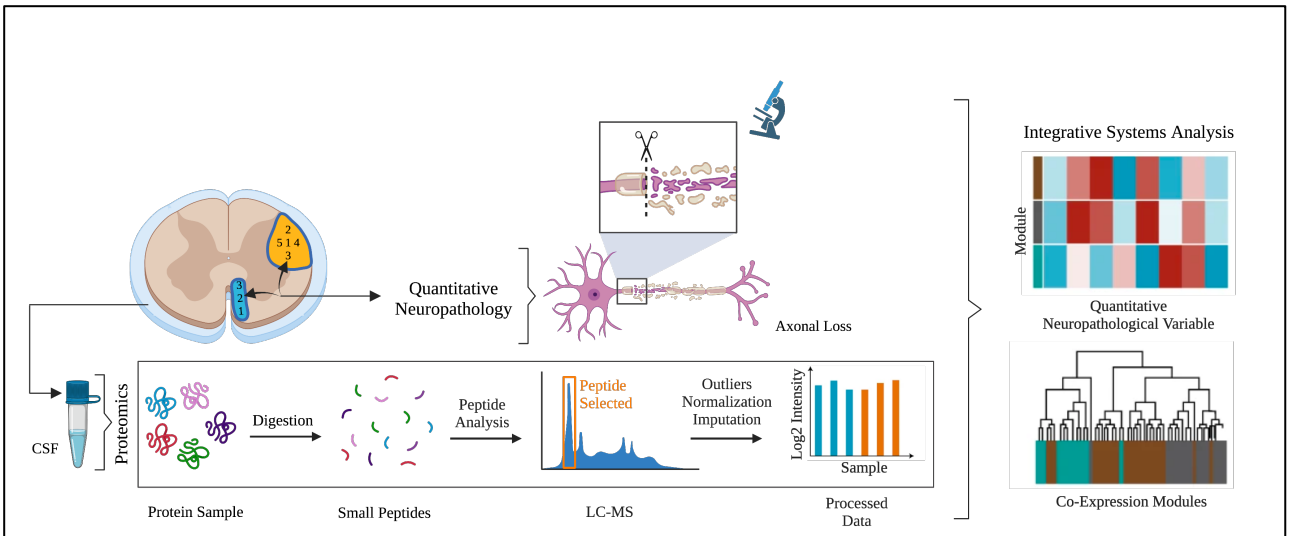


Figure 3.5. Approach to Integrate Quantitative Neuropathology with Post-Mortem CSF Proteomics. Paired cerebrospinal fluid (CSF) and spinal cord tissue was available for analysis. Motor tracts (lateral corticospinal and anterior corticospinal) were assessed immunohistochemically and proteins were extracted from CSF samples and subjected to trypsinisation. Peptides were analysed with liquid chromatography tandem mass spectrometry. CSF proteomics and histochemically derived quantitative outputs were integrated using weighted-protein correlation network analyses to identify protein modules that related to pathological traits of interest.

3.2.8 Statistical Analysis

Graphical representations of all results were created in Prism 9 and imported into BioRender to create figure panels. Statistical analysis of quantitative neuropathology data was performed in RStudio Version 1.4.1717. Differences between discrete variables, including 1) MS and control cases, 2) MS cases with and without lesions, and 3) CD20+ discrete groups, were assessed using linear regression models controlling for covariates (age, sex, and post-mortem interval). Estimated marginal means, standard errors, and contrasts were generated using the Emmeans R package. Relationships between continious variables (CSA, motor axonal density, total motor axonal number, and myeloid marker area coverage) were assessed using the non-parametric Spearman correlation. As pathological traits across levels and tracts were correlated within subjects, all quantitative pathological data was pooled per subject to limit missing data and improve statistical

power. Pooling was performed via arithmetic mean calculation and represented global spinal cord motor tract values. P-values of 0.05 were used to define statistically significant comparisons.

Peptide LC-MS/MS data was imported into MaxQuant for label-free quantitation. After feature alignment, peptides were identified using Mascot (Matrix Sciences) with standard parameters. Results were filtered with a peptide false discovery threshold of 1%, followed by a spectrum quality filer (Score >20). Protein-level data was pre-processed through a robust and novel integration of the following R packages: pMartR, NormalyzerDE, DEP, and WGCNA (Langfelder *et al.* 2008, Oldham *et al.* 2008, Chawade *et al.* 2014, Zhang *et al.* 2018, Stratton *et al.* 2019). In short, contaminants were first identified and removed. Proteins identified by reverse sequences, site-specific sequences, or by less than 2 unique peptides were also removed. Mahalanobis distance with a p-value threshold of 0.001 (**Fig. 3.6A**) and standardised connectivity of less than -2.5 (**Fig. 3.6B**) were used to classify sample outliers. This procedure removed 9 samples (2 control and 7 MS). The R package NormalyzerDE was subsequently used to ascertain the best normalisation method. Cyclic loess was chosen as it best reduced intragroup variation (**Fig. 3.6C**). Missing values were deemed missing not at random as they were biased toward lower intensity values and were, therefore, imputed by the quantile regression imputation of left-censored data (QRILC) method (**Fig. 3.6D**) (Wei *et al.* 2018). Covariates, including age, sex, and post-mortem interval, were then regressed from the normalised and imputed dataset using the Empirical Bayes-moderated adjustment found within the WGCNA R package. Before performing weighted protein correlation network analysis (WPCNA), multiple soft threshold (power) values were tested to assess scale free topology. 8 was chosen as it was the lowest threshold to approximate scale-free topology with a fit of 0.9 (**Figure 3.6E**).

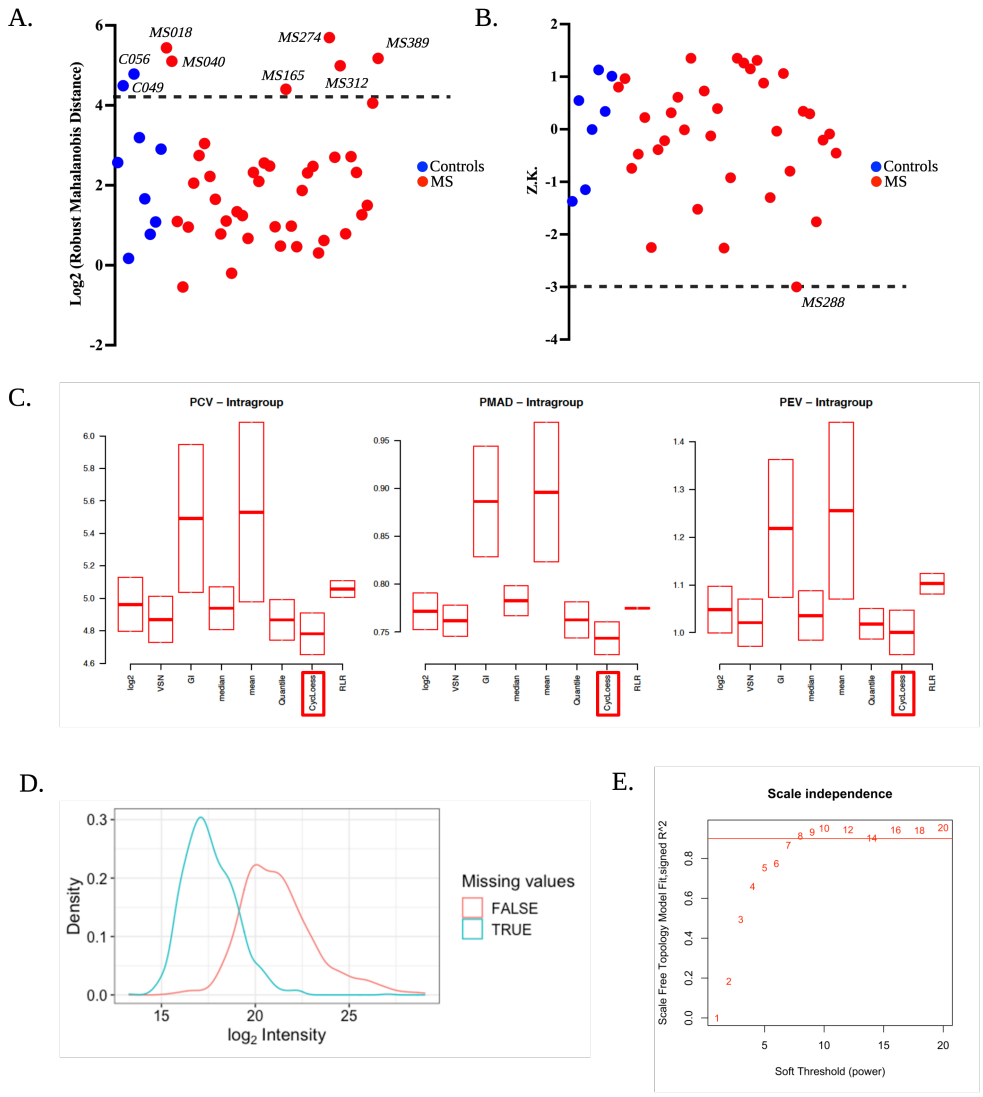


Figure 3.6. CSF Proteomic Data Pre-Processing Pipeline. (**A**) Outliers were first identified with a p-value threshold of 0.001 using a robust Mahalanobis distance tabulated with the following metrics: intragroup correlation, proportion missing, mean absolute deviation, and skewness. (**B**) An additional outlier was identified by a standardised connectivity (KZ) threshold less than -2.5. (**C**) Log2 normalisation, variance stabilization normalisation (VSN), global intensity normalisation (GI), median normalisation, mean normalisation, quantile normalisation, cyclic loess, and robust linear regression (RLR) were all compared by intragroup coefficient of variation, pooled median absolute deviation, and pooled intragroup estimate of variance. Cyclic loess (denoted with a red box) was deemed to perform best as it limited intragroup variation. (**D**) The density of missing values in the proteomic dataset was biased toward lower intensities, indicating these values were missing not at random and should be imputed by the quantile regression imputation of left-censored data (QRILC) method. (**E**) A soft threshold of 8 was chosen for WGCNA analysis as it was the lowest threshold to approximate scale-free topology with a fit of 0.9.

The WPCNA blockwiseModules function was run with the following parameters: power=8, deepSplit=4, minModuleSize=15, mergeCutHeight=0.07, TOMdenom=mean, bicor correlation (robustY=FALSE), axPOutliers=0.05, signed hybrid network type, PAM staging and PAM respects dendro as TRUE, minKMEtoStay = 0.3 and a maxBlockSize larger than the total number proteins in the pre-processed dataset. Total motor axonal number was the primary endpoint of this study. Modules that were found to relate to this pathological trait were subsequently tested for their relationship with MS status and other pathological markers that differed between MS and control cases in our cohort (demyelination presence and PGM1 inflammation) to control the false discovery rate (FDR).

Over-representation analysis (ORA) was performed for modules that displayed significant relationships with total motor axon number using the clusterProfiler R package. ORA aims to identify enrichment of ontology terms and pathways among a list of differentially expressed genes/proteins in comparison to a background distribution. Proteins found within modules that displayed significant relationships with total motor axon number were used as input with the background distribution including all annotated proteins identified by 2 unique peptides or more. A hypergeometric test was used to identify significantly enriched gene ontology terms (biological process). P-values were FDR adjusted for multiple comparisons. Ontology terms and pathways with an FDR<0.05 were reported as significant.

3.3 Results

3.3.1 Cohort Demographics

For the quantitative neuropathology study, MS and control cases contributed an equal proportion of spinal cord levels to the analyses (p=0.92). The distribution of sex (p =0.36) and post-mortem

interval (U=219, p=0.13) did not differ amongst the groups. However, as is common in post-mortem studies, the control cases were significantly older than the MS cases (U=118, p=0.0004).

For the CSF proteomics study, a different control cohort was used as paired control spinal cord tissue and CSF was unavailable from the tissue bank. The distribution of sex (p=0.072) was not different between MS and control cases though control cases were older (U=68.5 p=0.0028) and had a longer post-mortem interval (U=55, p=0.0006).

3.3.2 Quantitative Neuropathology

3.3.2.1 MS vs. Controls

When assessing spinal cord atrophy and axonal loss between MS and controls, MS cases displayed a reduction in CSA, motor tract area, motor axon density, and total motor axon number. CSA was reduced by 13.6% (p=0.042) (**Figure 3.7A**) while motor tract area was reduced 21.4% (p=0.0094) (**Figure 3.7B**). Axonal density was reduced by 27.4% (p=0.0005) (**Figure 3.7C**) with total motor axon number exhibiting a reduction of 34.6% (p=0.0084) (**Figure 3.7D**).

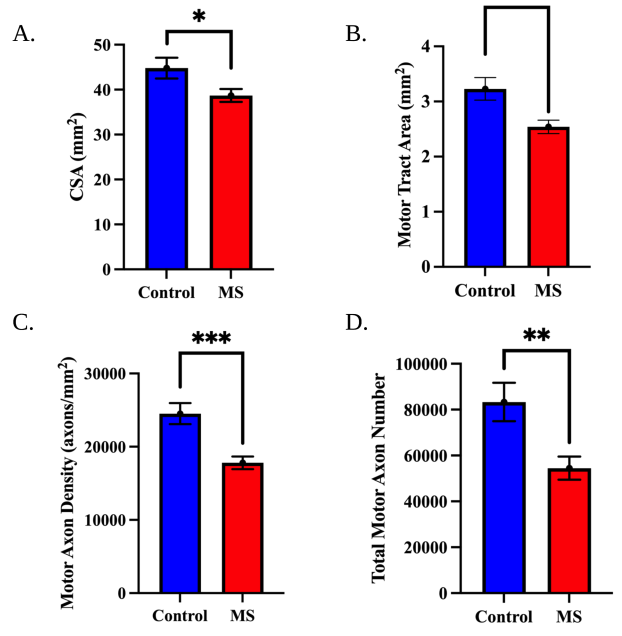


Figure 3.7. Neurodegenerative Differences Between the Control and MS Spinal Cord. Bar charts depicting the spinal cord cross-sectional area (**A**), motor tract (LCST and ACST) cross-sectional area (**B**), motor axon density (**C**), and total motor axon number (**D**) between control and MS cases. Values are pooled across all spinal cord levels available per case and represent estimated marginal means and standard errors derived from linear regression models controlling for age, sex, and post-mortem interval. P-values of comparisons not reaching significance are reported and asterisks indicate significant post-hoc pairwise comparisons (*p<0.05; **p<0.01; ***p<0.001; ****p<0.0001).

Differences in the expression of four myeloid cell markers between MS and control were also investigated. The area coverage of IBA1, a pan myeloid cell marker, was not different between MS and control cases (**Figure 3.8A**). The area coverage of CD68, an activated myeloid cell marker, demonstrated an increase in MS cases when compared to control (p=0.014) (**Figure 3.8B**). Area coverage of P2Y12, a supposed homeostatic myeloid cell marker, did not differ between MS and control (**Figure 3.8C**). Lastly, the area coverage of TMEM119, a resident microglial marker, did not exhibit differences amongst MS and control (**Figure 3.8D**).

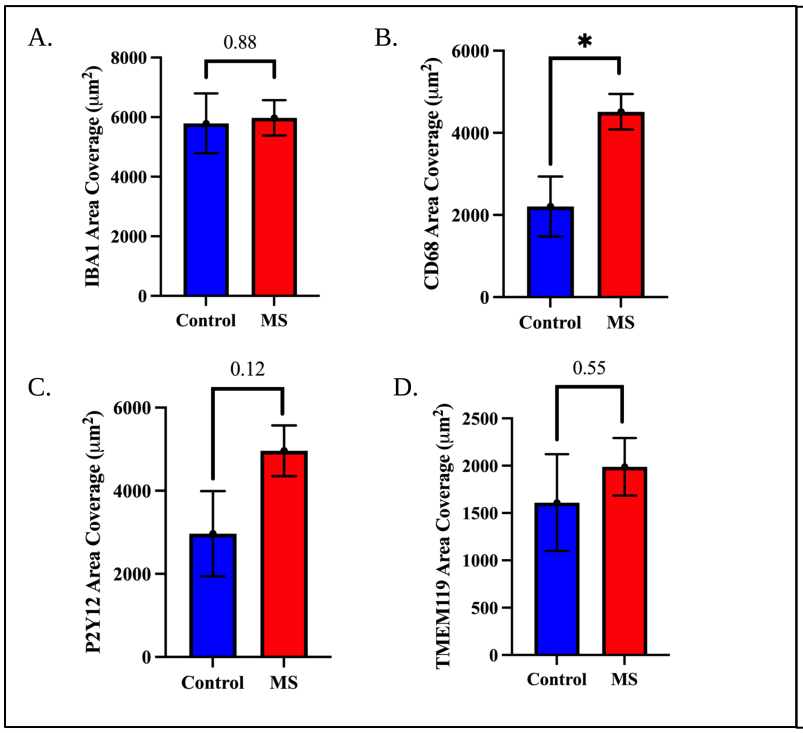


Figure 3.8. Myeloid Inflammatory Differences Between the Control and MS Spinal Cord. Bar charts depicting the motor tract area coverage by IBA1 (**A**), CD68 (**B**), P2Y12 (**C**), and TMEM119 (**D**) between control and MS cases. Values are pooled across all spinal cord levels available per case and represent estimated marginal means and standard errors derived from linear regression models controlling for age, sex, and post-mortem interval. P-values of comparisons not reaching significance are reported and asterisks indicate significant post-hoc pairwise comparisons (*p<0.05; **p<0.01; ***p<0.001; ****p<0.0001).

3.3.2.2 Relationships Between Features of MS Pathology

Within MS cases, the relationships between demyelination, atrophy, and axonal density were first explored. The presence of spinal cord lesions did not relate to CSA (**Figure 3.9A**). Motor axon density was also not associated with CSA (**Figure 3.9B**) nor with motor tract area (**Figure 3.9C**).

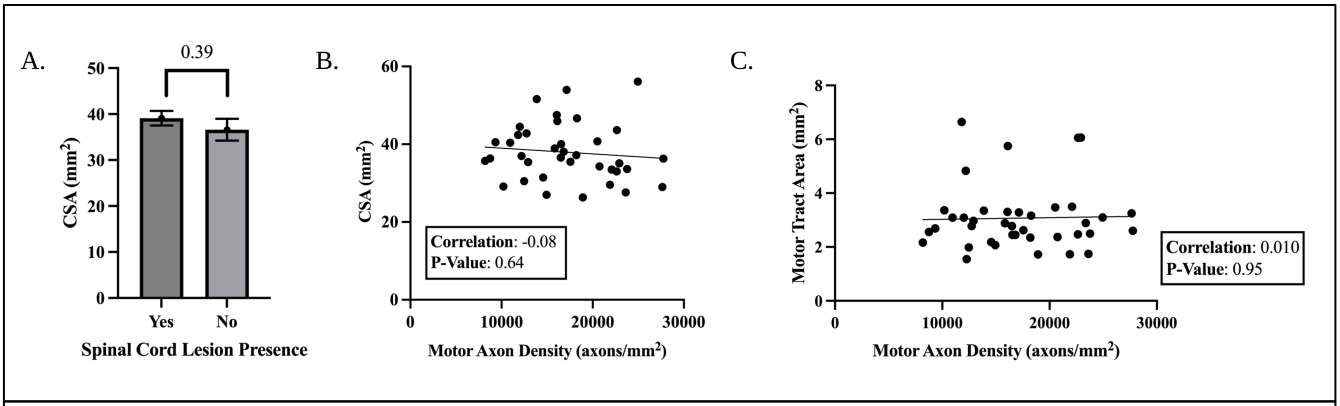


Figure 3.9. Relationship Between Demyelination, Atrophy, and Axonal loss in the MS Spinal Cord. (**A**) Bar chart depicting the spinal cord CSA of MS cases with and without spinal cord lesions. Values represent estimated marginal means and standard errors derived from linear regression models controlling for age, sex, and post-mortem interval. P-values of comparisons not reaching significance are reported and asterisks indicate significant post-hoc pairwise comparisons (*p<0.05; **p<0.01; ***p<0.001; ****p<0.0001). (**B-C**) Correlation plots and corresponding lines of best fit illustrating the relationships between spinal cord CSA and motor tract axon density (**B**) and spinal cord motor tract area and motor tract axon density (**C**). Spearman

To further probe the correlates of CSA, relationships with myeloid cell densities and measures of adaptive immunity were investigated. While area coverage of IBA1 (**Figure 3.10A**), P2Y12 (**Figure 3.10C**), and TMEM119 (**Figure 3.10D**) were all negatively correlated with CSA, these relationships did not reach statistical significance. On the other hand, CD68 (**Figure 3.10B**) negatively correlated with CSA (Spearman r=-0.34, p=0.041).

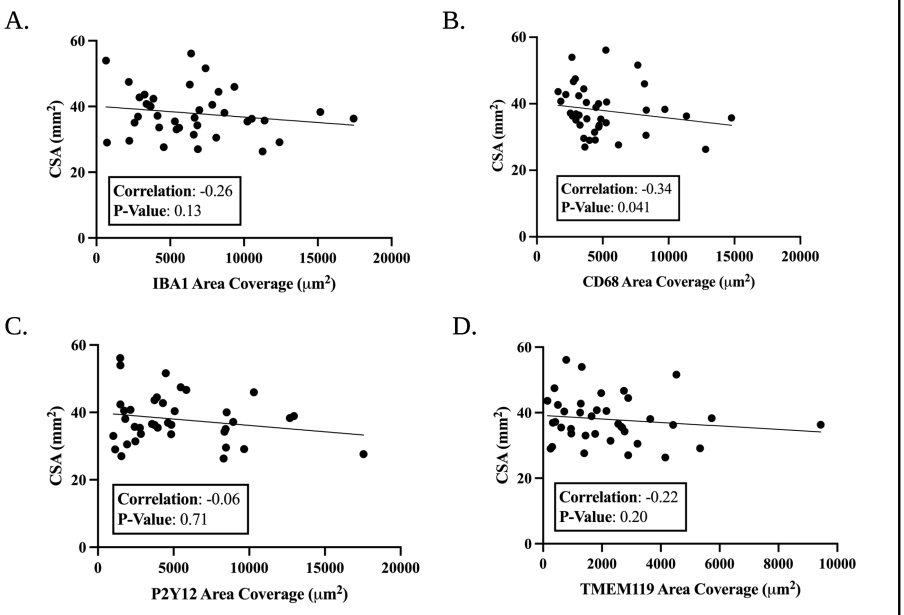


Figure 3.10. Relationship Between Myeloid Cell Inflammation and Spinal Cord CSA in MS. Correlation plots with accompanying lines of best fit highlighting the relationships between spinal cord cross-sectional area and (**A**) IBA1 motor tract area coverage, (**B**) CD68 motor tract area coverage, (**C**) P2Y12 motor tract area coverage, and (**D**) TMEM119 motor tract area coverage in MS cases. Spearman correlation coefficients and associated p-values are reported.

There was no relationship between either parenchymal (**Figure 3.11A**) or meningeal (**Figure 3.11C**) CD3 counts with CSA. In addition, discrete groups of CD20 parenchymal (**Figure 3.11B**) or meningeal inflammation (**Figure 3.11D**) did not exhibit differences in CSA.

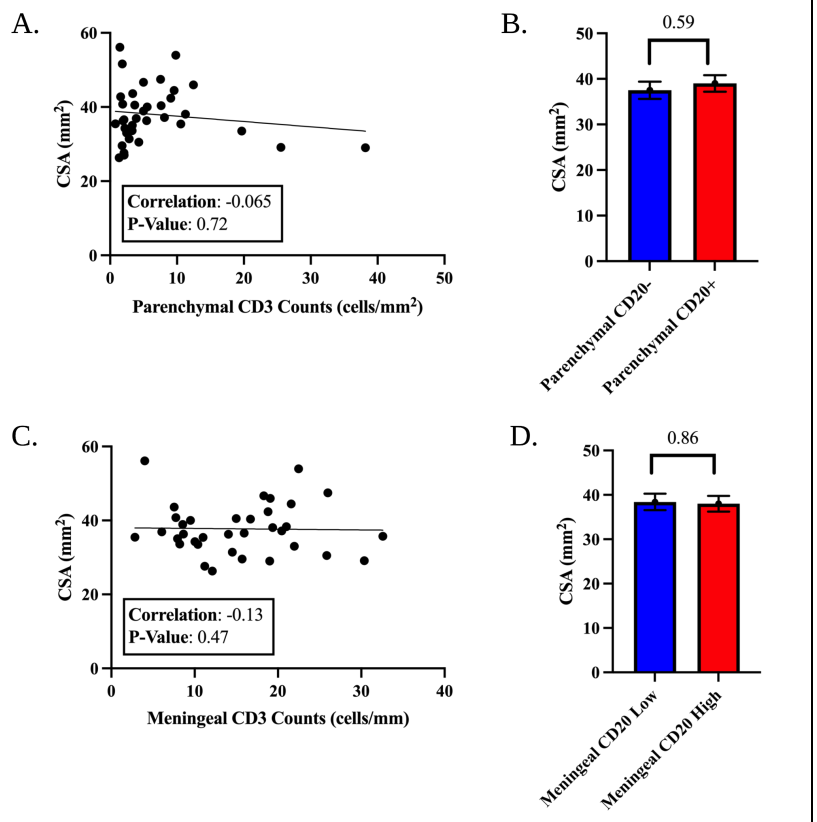


Figure 3.11. Relationship Between Adaptive Immune Cell Inflammation and Spinal Cord CSA in MS. Correlation plots with accompanying lines of best fit highlighting the relationships between spinal cord cross-sectional area and parenchymal (**A**) and meningeal (**C**) CD3 counts. Spearman correlation coefficients and associated p-values are reported. Bar charts depicting the spinal cord CSA of MS cases at the extremes of parenchymal (**B**) and meningeal (**D**) CD20 counts. Values represent estimated marginal means and standard errors derived from linear regression models controlling for age, sex, and post-mortem interval. P-values of comparisons not reaching significance are reported and asterisks indicate significant post-hoc pairwise comparisons (*p<0.05; **p<0.01; ***p<0.001; ****p<0.0001).

We next explored the determinants of total motor axon number. Cases with lesions in the motor tracts, where axonal number was measured, did not exhibit a reduction in total motor axon number compared to those without lesions (**Figure 3.12**).

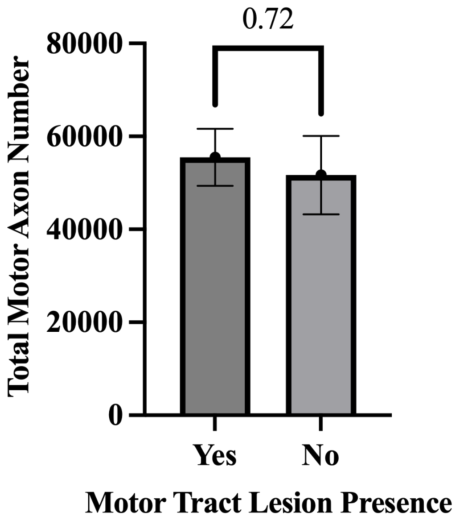


Figure 3.12. Relationship Between Demyelination and Total Motor Axon Number in the MS Spinal Cord. Bar chart depicting the spinal cord total motor axon number of MS cases with and without lesions in the spinal cord motor tracts. Values represent estimated marginal means and standard errors derived from linear regression models controlling for age, sex, and post-mortem interval. P-values of comparisons not reaching significance are reported and asterisks indicate significant post-hoc pairwise comparisons (*p<0.05; **p<0.01; ***p<0.001; ****p<0.0001).

IBA1 (**Figure 3.13A**), CD68 (**Figure 3.13B**), and TMEM119 (**Figure 3.13D**) area coverage all negatively correlated with total motor axon number (IBA: Spearman rho=-0.39, p=0.019; PGM1: Spearman rho=-0.38, p=0.022; TMEM119: Spearman rho=-0.37, p=0.029). Interestingly, P2Y12 did not display this relationship (**Figure 3.13C**).

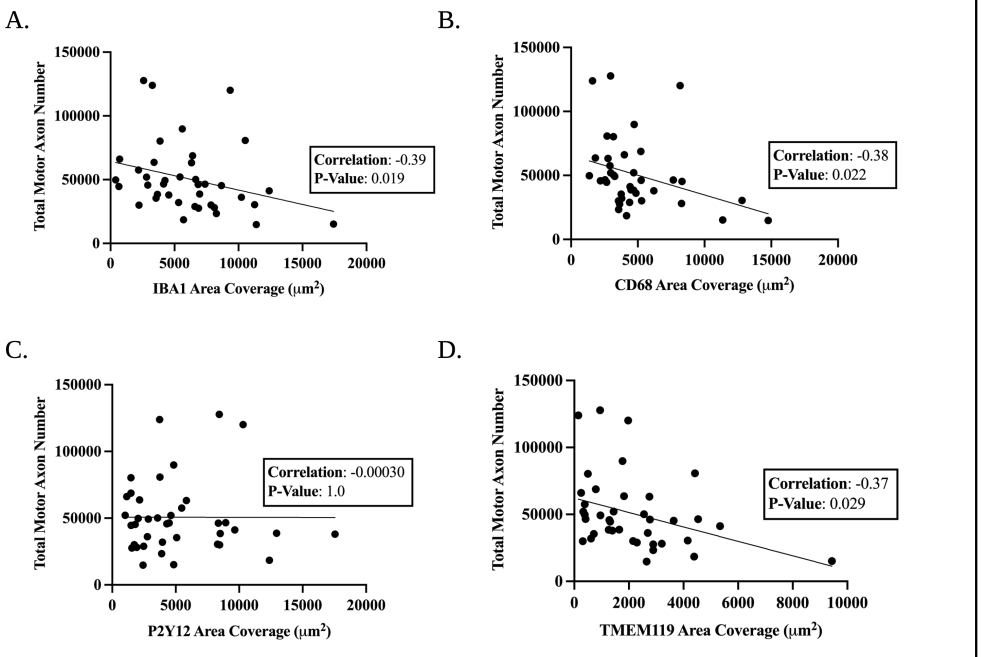


Figure 3.13. Relationship Between Myeloid Cell Inflammation and Spinal Cord Total Motor Axon Number in MS. Correlation plots with accompanying lines of best fit highlighting the relationships between spinal cord total motor axon number and (**A**) IBA1 motor tract area coverage, (**B**) CD68 motor tract area coverage, (**C**) P2Y12 motor tract area coverage, or (**D**) TMEM119 motor tract area coverage. Spearman correlation coefficients and associated p-values are reported.

Neither parenchymal (**Figure 3.14A**) nor meningeal (**Figure 3.14C**) CD3 related to total motor axon number. Discrete groups of CD20 parenchymal (**Figure 3.14B**) or meningeal CD20 (**Figure 3.14D**) also did not demonstrate differences in total motor axon number.

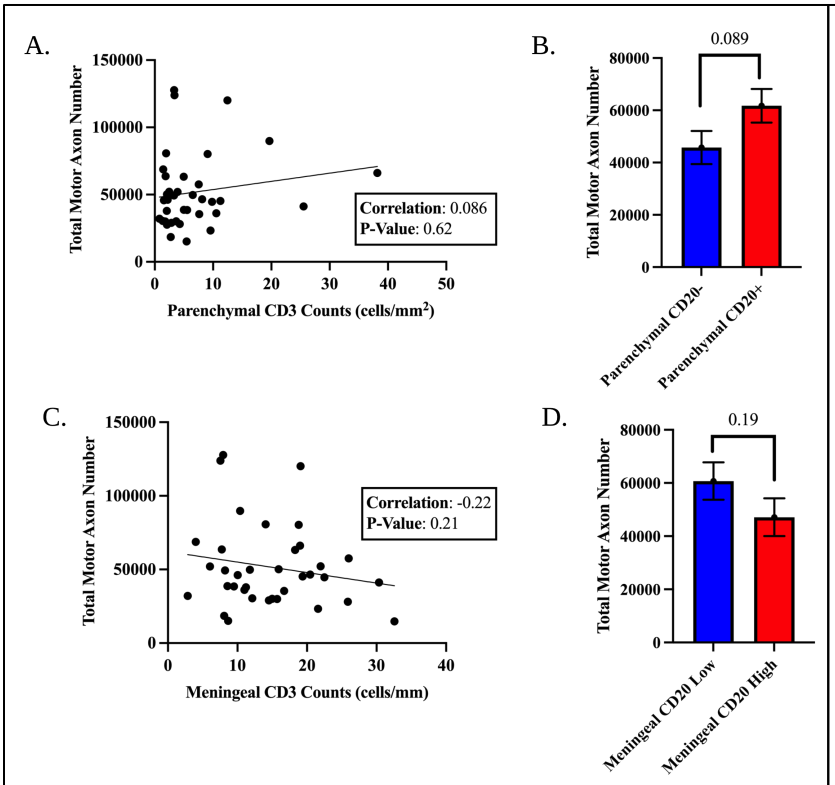


Figure 3.14. Relationship Between Adaptive Immune Cell Inflammation and Spinal Cord Total Motor Axon Number in MS. Correlation plots with accompanying lines of best fit highlighting the relationships between total motor axon number and parenchymal (**A**) and meningeal (**C**) CD3 counts. Spearman correlation coefficients and associated p-values are reported. Bar charts depicting the total motor axon number of MS cases at the extremes of parenchymal (**B**) and meningeal (**D**) CD20 counts. Values represent estimated marginal means and standard error derived from linear regression models controlling for age, sex, and post-mortem interval. P-values of comparisons not reaching significance are reported and asterisks indicate significant post-hoc pairwise comparisons (*p<0.05; **p<0.01; ***p<0.001; ****p<0.0001).

3.3.3 Cerebrospinal Fluid Weighted Protein Correlation Network Analysis

WPCNA clustered CSF proteins into 17 modules. 1 module, termed grey, represents the proteins that are not well correlated with any of the other modules and can be used as a negative control for subsequent analyses. Module-trait correlation analysis with our primary endpoint, total motor axon number, identified two modules, termed purple (**Figure 3.15A**) and light cyan (**Figure 3.15B**), with significant associations. Both modules were negatively associated with total motor axon number (purple: bivariate midweight correlation=-0.35, p=0.025; light cyan: bivariate midweight

correlation=-0.32, p=0.048) while the grey module was not significantly associated (**Figure 3.15C**).

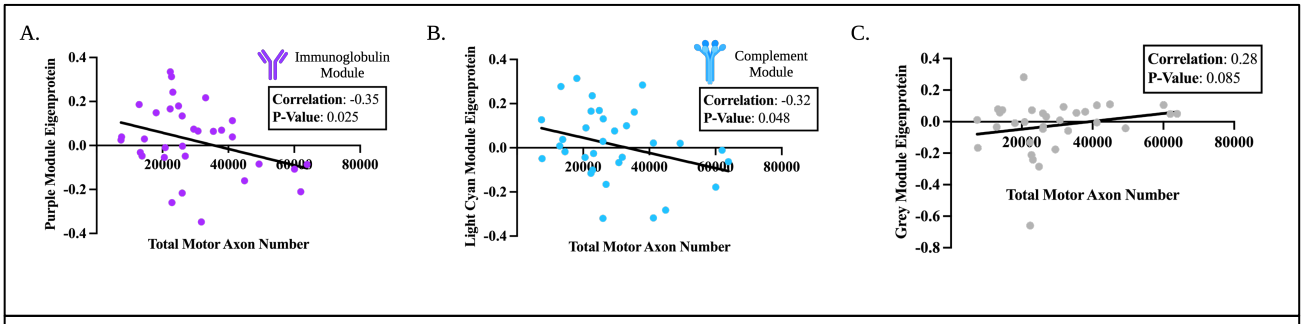


Figure 3.15. Weighted Protein Correlation Network Relationships with Total Motor Axon Number. Correlation plots with accompanying lines of best fit highlighting the relationships of the eigenprotein values (measure of multivariate expression) between the purple (immunoglobin module: **A**), light cyan (complement module: **B**), and grey (negative control module: **C**) modules with spinal cord total motor axon number. Bivariate midweight correlation coefficients and associated p-values are reported.

Gene ontogeny (GO) overrepresentation analysis was performed to understand the biological meaning of the proteins clustered into the purple and light cyan modules. The purple module (**Table 3.4**) was enriched for immunoglobulin proteins. GO terms (**Table 3.5**) included GO:0050853 B cell receptor signaling pathway ($p=4.40 \times 10^{-17}$) and GO:0002455 humoral immune response initated by circulting immunolglobulin ($p=5.18 \times 10^{-12}$).

Table 3.4. Purple Module Proteins and Module Membership (kME) Scores

Uniprot ID	Gene Name	kME
P80748	IGLV3-21	0.92259242
P01613	IGKV1D-33	0.84847088
A0A075B6L0	IGLC3	0.82740515
P01834	IGKC	0.82145359
B9A064	IGLL5	0.82051385
P01610	IGKV1-17	0.8105181
P01717	IGLV3-25	0.80940044
A0A075B6I9	IGLV7-46	0.78636153
D6RD17	JCHAIN	0.78180845
A0A075B6N9	IGHM	0.75755001
P01859	IGHG2	0.74913432

Uniprot ID	Gene Name	kME
P01876	IGHA1	0.74575858
P01714	IGLV3-19	0.73713087
A0A075B6R9	IGKV2D-24	0.72058965
P01861	IGHG4	0.71995158
P23083	IGHV1-2	0.70127247
P01857	IGHG1	0.69774968
A0A075B6N8	IGHG3	0.68034884
P01597	IGKV1-39	0.66741009
P01608	IGKV1D-33	0.65525929
P01824	IGHV4-39	0.65047314
D6RBP0	Sodium Channel and Clathrin Linker 1	0.62118821
P01708	IGLV2-11	0.61857553
P01743	IGHV1-46	0.57586645
A0A075B6R2	IGHV4-4	0.55695324
P01612	IGKV1-39	0.53774212

Table 3.5. Purple Module Gene Ontogeny Biological Process Analysis

GO Term ID	Description	Gene Ratio	Background Ratio	FDR
GO:0002250	adaptive immune response	21/22	68/1355	5.17E-26
GO:0050853	B cell receptor signaling pathway	11/22	15/1355	4.40E-17
GO:0050864	regulation of B cell activation	11/22	15/1355	4.40E-17
GO:0050871	positive regulation of B cell activation	11/22	15/1355	4.40E-17
GO:0006910	phagocytosis, recognition	11/22	20/1355	3.47E-15
GO:0006911	phagocytosis, engulfment	11/22	21/1355	6.20E-15
GO:0042113	B cell activation	11/22	23/1355	1.64E-14
GO:0050851	antigen receptor-mediated signaling pathway	11/22	26/1355	8.33E-14
GO:0002429	immune response-activating cell surface receptor signaling pathway	11/22	30/1355	4.83E-13
GO:0002757	immune response-activating signal transduction	11/22	30/1355	4.83E-13
GO:0042742	defense response to bacterium	11/22	41/1355	5.01E-13
GO:0002768	immune response-regulating cell surface receptor signaling pathway	11/22	31/1355	6.39E-13
GO:0006958	complement activation, classical pathway	11/22	35/1355	2.72E-12
GO:0002455	humoral immune response mediated by circulating immunoglobulin	11/22	37/1355	5.18E-12
GO:0016064	immunoglobulin mediated immune response	11/22	40/1355	1.23E-11

The light cyan module (**Table 3.6**) was enriched for complement-related proteins and GO terms (**Table 3.7**) included GO:0006956 complement activation ($p=4.68 \times 10^{-7}$) and GO:0006959 humoral immune response ($p=3.76 \times 10^{-7}$).

Table 3.6. Light Cyan Module Proteins and Module Membership (kME) Scores

Uniprot ID	Gene Name	kME
D6R934	C1qB	0.89178446
P23142	Fibulin-1	0.87900831
P08571	CD14	0.81643254
P02747	C1qC	0.80068718
P09871	C1s	0.79560242
P00736	C1r	0.79555542
D6RBV2	LMAN2	0.77231299
P55058	Phospholipid Transfer Protein	0.7606089
K7ERG9	Complement Factor D	0.74470678
P10643	C7	0.73187467
E9PEK4	CSF1R	0.72898115
H0Y755	Fc gamma receptor IIIa	0.70465416
P0C0L5	C4B	0.6527829
Q9Y6R7	IgGFc-binding protein	0.64512042
F5GZZ9	CD163	0.59545784
P18428	LBP	0.55746401
P04433	IGKV3-11	0.55280345
P02745	C1QA	0.51789886
Q9Y279	V-set and immunoglobulin domain-containing protein	0.36769628

Table 3.7. Light Cyan Module Gene Ontogeny Biological Process Analysis

GO Term ID	Description	Gene Ratio	Background Ratio	FDR
GO:0045087	innate immune response	13/17	119/1355	9.46E-09
GO:0006956	complement activation	9/17	44/1355	4.68E-08
GO:0002684	positive regulation of immune system process	12/17	118/1355	5.16E-08
GO:0002252	immune effector process	11/17	99/1355	1.07E-07
GO:0006952	defense response	14/17	212/1355	1.07E-07
GO:0016064	immunoglobulin mediated immune response	8/17	40/1355	2.71E-07
GO:0019724	B cell mediated immunity	8/17	40/1355	2.71E-07

GO Term ID	Description	Gene Ratio	Background Ratio	FDR
GO:0006959	humoral immune response	9/17	63/1355	3.76E-07
GO:0002253	activation of immune response	9/17	64/1355	4.04E-07
GO:0006958	complement activation, classical pathway	7/17	35/1355	1.80E-06
GO:0002274	myeloid leukocyte activation	4/17	23/1355	0.00214041
GO:0006957	complement activation, alternative pathway	3/17	11/1355	0.00406926
GO:0032760	positive regulation of tumor necrosis factor production	3/17	15/1355	0.01027228
GO:0032640	tumor necrosis factor production	3/17	20/1355	0.02227712
GO:0001816	cytokine production	5/17	77/1355	0.02430018
GO:0006909	phagocytosis	4/17	50/1355	0.03382491
GO:0070663	regulation of leukocyte proliferation	3/17	26/1355	0.04309612

We investigated the relationship between individual protein correlation and module membership. Strong positive correlations demonstrate that there are certain hub proteins that drive the module-trait relationship. Positive correlations were observed between protein-trait and module membership values for the purple (**Figure 3.16A**) and light cyan modules (**Figure 3.16B**). Therefore, the proteins with the highest kME module membership values were considered hub proteins and taken further for validation in the next chapter (c.f. Chapter 4). These included IgG (purple) and C1q (light cyan).

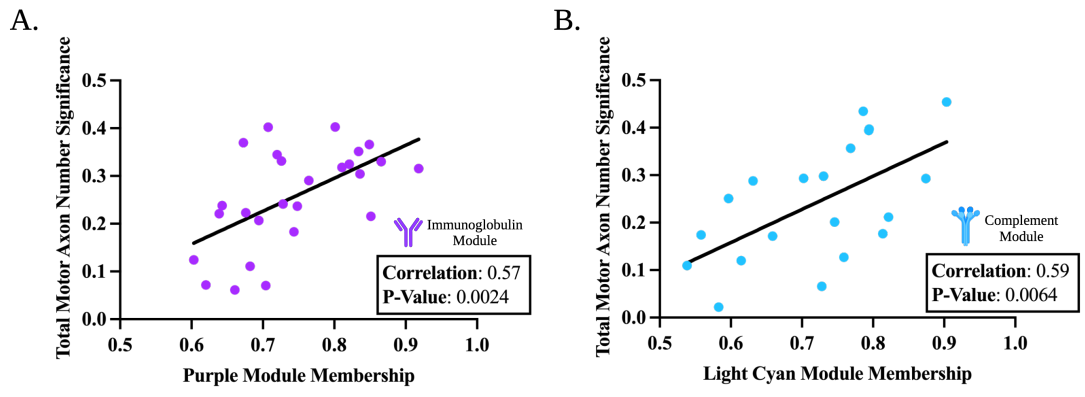


Figure 3.16. Protein-Trait Significance and Module Membership Relationships. Correlation plots with accompanying lines of best fit highlighting the relationship between individual proteins in the purple (**A**) and light cyan (**B**) modules and module membership values. Bivariate midweight correlation coefficients and associated p-values are reported.

We next performed targeted analyses to investigate the relationship between the purple and light cyan modules with MS status, demyelination, and PGM1 inflammation. Expression of the purple module was increased in MS cases compared to control with borderline significance (p=0.059) (**Figure 3.17A**). The light cyan module did not differ between MS and control cases (**Figure 3.17B**).

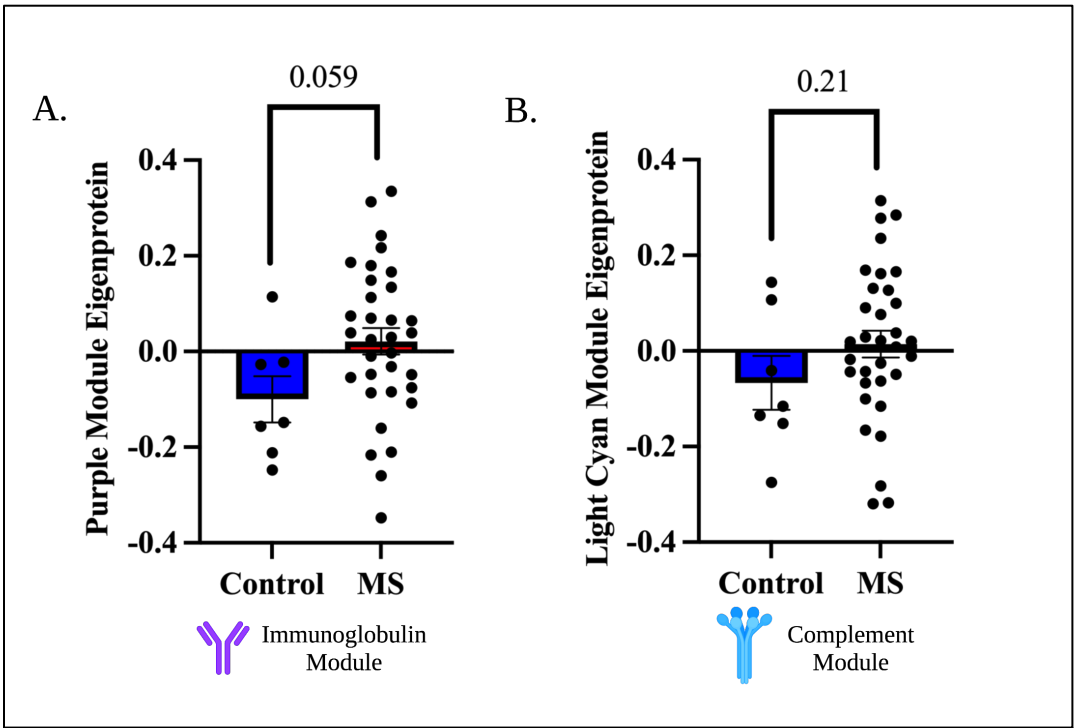


Figure 3.17. Weighted Protein Correlation Network Relationships with MS Status. Bar charts depicting the expression of the purple (**A**) and light cyan (**B**) modules between control and MS cases. P-values of comparisons not reaching significance are reported and asterisks indicate significant post-hoc pairwise comparisons (*p<0.05; **p<0.01; ***p<0.001; ****p<0.0001).

Expression of the purple module was higher in cases that harboured spinal cord lesions compared to those without lesions (p=0.0014) (**Figure 3.18A**). This relationship was not observed with the light cyan module (**Figure 3.18B**).

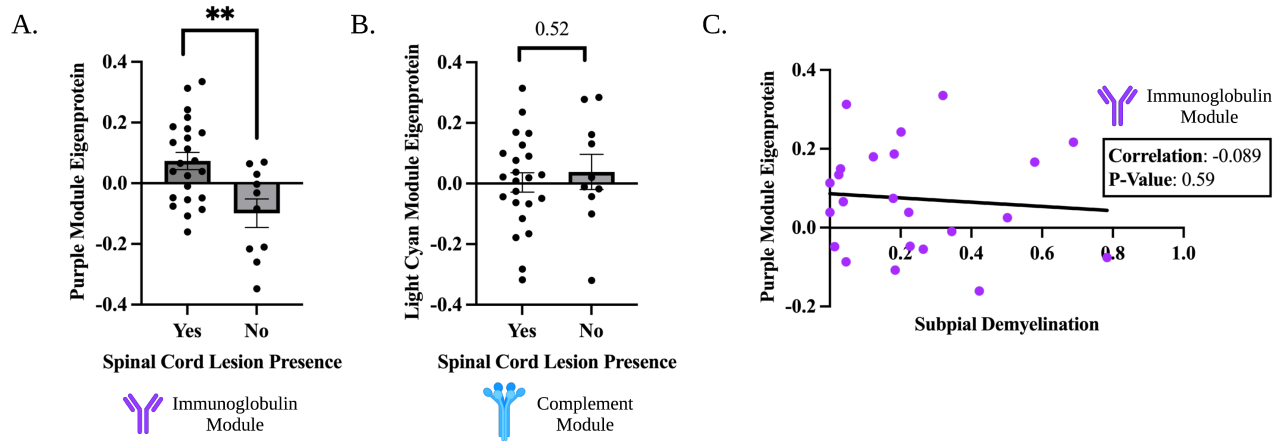


Figure 3.18. Weighted Protein Correlation Network Relationships with Demyelination. Bar charts depicting the expression of the purple (**A**) and light cyan (**B**) modules between MS cases with and without spinal cord lesions. P-values of comparisons not reaching significance are reported and asterisks indicate significant post-hoc pairwise comparisons (*p<0.05; **p<0.01; ***p<0.001; ****p<0.0001). (**C**) Correlation plot with the accompanying line of best fit highlighting the relationship between purple module expression and the extent of subpial demyelination. The bivariate midweight correlation coefficient and associated p-value is reported.

Interestingly, expression of the purple module did not correlate with the extent of subpial demyelination in the cases that harboured lesions (Figure 3.19C). Lastly, neither the purple (**Figure 3.19A**) nor light cyan (**Figure 3.19B**) module correlated with PGM1 area coverage.

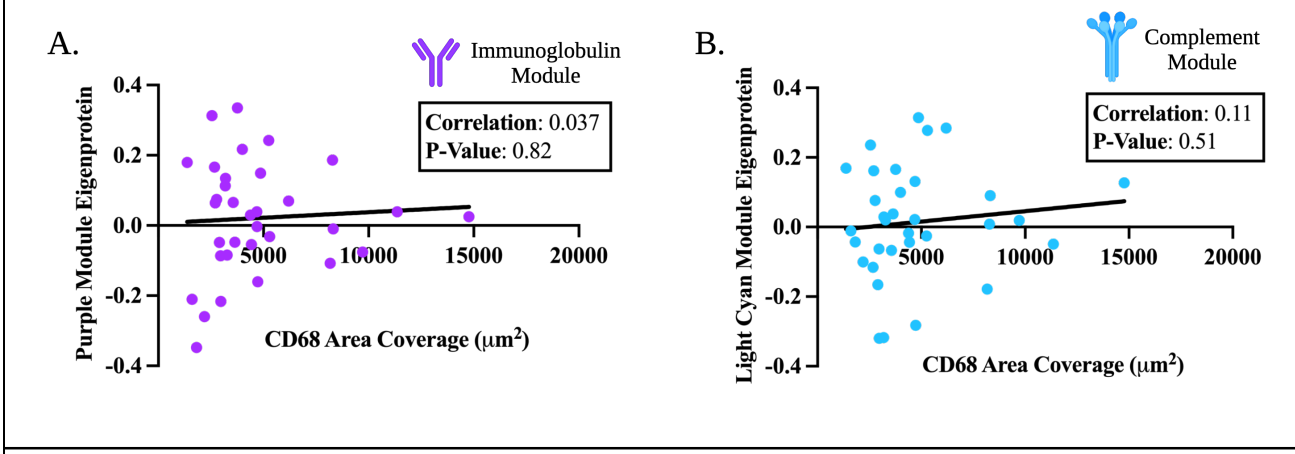


Figure 3.19. Weighted Protein Correlation Network Relationships with Myeloid Cell Inflammation. Correlation plots with the accompanying lines of best fit highlighting the relationship between purple (**A**) and light cyan (**B**) module expression and spinal cord CD68 area coverage. Bivariate midweight correlation coefficients and associated p-values are reported.

3.4 Discussion

Spinal cord axonal loss in motor tracts is an important contributor to irreversible disability in MS. However, our understanding of the determinants of this essential process and biomarkers of its development is incomplete. Therefore, we characterised the neuropathological features associated with spinal cord axonal loss in the motor tracts and profiled the deep proteome of paired post-mortem CSF to identify potential biomarkers of this pathological hallmark of progression. We demonstrate that MS cases demonstrate more severe atrophy, axonal loss, and activated myeloid cells compared to control cases. Within MS cases, measures of spinal cord atrophy do not relate to the extent of demyelination and axonal loss. However, activated myeloid cells negatively correlated with spinal cord CSA and total motor axonal counts. Lastly, CSF proteomic profiling identified two modules, enriched in immunoglobulins and complement, that displayed a relationship with axonal loss. These findings nominate a complex interplay between CSF opsonins and activated myeloid cells in the pathogenesis of spinal cord axonal loss.

CSA and motor tract axonal counts were decreased in the MS spinal cord when compared to control as reported by other studies. However, the magnitude of change was found to differ. The global decrease in spinal cord cross-sectional area (13.6%) we observed was less than the CSA decrease reported by Petrova *et al.* 2018. This is likely due to the different sampling strategies employed between studies. We chose to sample more cases less comprehensively given the strong correlations observed amongst individual pathological measures within cases. This allowed us to better capture between-subject heterogeneity that characterises the MS disease process. Motor axonal density and total motor axon number was reduced by 27.4% and 34.6%, respectively. The extent of axonal loss is most similar in magnitude to work by Ganter *et al.* 1999 and De Luca *et al.* 2004 while studies by Lovas *et al.* 2000, Tallantyre *et al.* 2009, Petrova *et al.* 2018 reported

nearly double the extent of axonal loss. Methodological differences likely underlie these discrepancies. Palmgren silver staining was used in our study and by Ganter *et al.* 1999 and De Luca *et al.* 2004, while immunohistochemical antibodies of neurofilament were used by other groups. Tallantyre *et al.* 2009 and Petrova *et al.* 2018 used a phosphorylated neurofilament antibody while the work by Lovas *et al.* 2000 used a phosphorylation agnostic neurofilament heavy chain antibody. Changes in the phosphorylation status of neurofilaments is a known feature of MS (Petzold *et al.* 2008, Schirmer *et al.* 2011) and neurofilament expression more broadly is known to be dysregulated following injury. In fact, neurofilament proteins are released into the CSF and blood following axonal damage. Therefore, immunohistochemical techniques, as compared to traditional histochemical methods, may blur the lines between damaged and degenerated axons leading to overestimation of axonal loss. However, taken together, our work complements previous studies that have demonstrated decreases in CSA and axonal counts to represent salient features of MS spinal cord pathology.

Myeloid pathological features also segregated with MS status in our cohort. An analysis of four myeloid markers indicated that the expression of CD68 was the only marker increased in MS normal-appearing white matter (NAWM) compared to control tissue. This indicates that proliferation of a specific population of activated myeloid cells, rather than more broad classes characterised by expression of IBA1 (pan-myeloid) or TMEM119 (resident microglia), drive the myeloid inflammatory process in the spinal cord NAWM. These findings contrast work studying brain white matter tissue that demonstrated a decrease in TMEM119 and P2Y12 immunoreactivity in MS NAWM compared to controls and did not identify a difference in CD68 expression (Zrzavy *et al.* 2017). Regional heterogeneity is likely to underly these differences as recent single-nucleus RNA sequencing studies have identified remarkable regional diversity in glial cell populations

between brain and spinal cord white matter (Seeker *et al.* 2022). Further work must probe the molecular underpinnings of these differences and how they may contribute to the heterogeneity observed in MS.

We next evaluated the impact of spinal cord lesions on both atrophy and axonal loss. Interestingly, cases with spinal cord lesions did not display more profound atrophy compared to their non-lesioned counterparts. Pathological and clinicoradiographic evidence support a dissociation between spinal cord lesions and global atrophy (Evangelou *et al.* 2005, Kearney *et al.* 2015, Bussas *et al.* 2022). While fibrosis within lesions may exhibit a "space filling" effect and contribute to a lack of correlation being detected, the hypothesis that lesions are not strong contributors to atrophy cannot be ignored. With respect to axonal loss, it has been hypothesised that focal lesions lead to intralesional axonal loss and distal Wallerian degeneration of connected pathways. However, previous neuropathological studies have demonstrated heterogeneity in the extent of axonal injury and subsequent loss within focal lesions (Ferguson *et al.* 1997, Trapp *et al.* 1998, Ganter *et al.* 1999, Lovas *et al.* 2000, Tallantyre *et al.* 2009, Tallantyre *et al.* 2010, Petrova *et al.* 2018). This heterogeneity is likely modified by the inflammatory milieu, functional reserve, disease duration, demographic features, environmental factors, and underlying genetic susceptibilities. The impact of lesions on axonal pathology distally has also been variable. White matter lesion burden in the cerebral hemispheres has consistently demonstrated a strong relationship with axonal loss in the corpus callosum (Evangelou *et al.* 2000, Ciccarelli *et al.* 2003), suggesting a role for Wallerian degeneration in the MS pathological cascade. However, evidence of Wallerian degeneration in the cortex and spinal cord has been debated, indicating that regional heterogeneity may be at play (DeLuca *et al.* 2006, Klaver *et al.* 2015, Petrova *et al.* 2018, Kiljan *et al.* 2021). In fact, perturbation

of Wallerian degeneration in mice subjected to experimental autoimmune encephalomyelitis, a spinal cord predominant model of inflammatory demyelination, did not lead to a significant reduction in acute axonal injury or ultimate axonal loss (Singh *et al.* 2017). The recent discovery of myelocortical MS, a new MS variant in which pathology is localised to the cortex and spinal cord, also furthers our understanding of regional heterogeneity in MS (Trapp *et al.* 2018). The lack of cerebral white matter pathology in these cases in the setting of profound neurodegeneration of connected anatomical sites also demonstrates that a dissociation between demyelination and degeneration is not only plausible, but likely. In our work, cases with spinal cord demyelination in the lateral or anterior funiculi did not display more profound axonal loss in NAWM of the motor tracts found within these funiculi (LCST and ACST) when compared to their non-lesioned counterparts. These findings are in line with work by De Luca *et al.* 2006 in which lesion burden that was sampled more comprehensively did not significantly relate to axonal loss when controlling for clinical covariates. Taken together, our work suggests that primary neurodegenerative mechanisms may be at play in driving the propagation of spinal cord axonal loss in the NAWM. However, a primary axonopathy in the spinal cord may still act in concert with Wallerian degeneration. A study of Wallerian degeneration and its relationships with pathology in the human MS spinal cord must be undertaken to assess the plausibility of this hypothesis.

We then evaluated the relationships between inflammation and both CSA and axonal loss. Interestingly, myeloid cell inflammation, as measured by CD68 immunoreactivity in the NAWM, was negatively correlated with CSA. However, CD3 and CD20 inflammation in the parenchymal and meningeal spaces did not demonstrate significant correlations. Similar to the relationship observed with CSA, myeloid cell inflammation was demonstrated to be negatively correlated with total axon number. Previous work did not identify a relationship with CD68 and spinal cord axonal

loss but rather with MHC Class II+ cells (Androdias *et al.* 2010). This discrepancy is likely because the KP1 clone of CD68 was used in this work and is not optimised for use in fixed tissue as compared to the PGM1 clone we employed (Falini *et al.* 1993). We did observe a negative correlation between meningeal CD3 cell counts and axonal loss though this failed to reach statistical significance as in the study by Androdias *et al.* 2010. Differences in tissue preparation may underlie these differences. Our spinal cord specimens were embedded in paraffin wax which may disrupt inflammatory structures in the meninges (Aloisi *et al.* 2010). Overall, these findings suggests that an inflammatory process driven by myeloid cells outside the lesion contributes to axonal loss and tissue loss more broadly in MS.

When investigating relationships between neurodegenerative features, CSA and axonal loss, no correlations emerged. Previous histopathological studies have also reported a dissociation between these two features of spinal cord pathology (Bjartmar *et al.* 2000, Petrova *et al.* 2018). These findings demonstrate that cross-sectional measures of atrophy lack the appropriate sensitivity to estimate axonal loss. These findings have implications for radiographic monitoring of patients and prognostication and suggest spinal cord atrophy measured at one time point is likely to fail at the prediction of future disability accumulation. However, data suggests that longitudinal assessments of spinal cord atrophy may have better predictive potential, and this will be further explored in the next chapter.

We next performed unbiased proteomic profiling of post-mortem CSF. WPCNA identified two modules, enriched in opsonins, that related to axonal loss. Hub protein analysis of these two modules identified IgG and C1q as drivers of the module-trait relationship. From a biological perspective, while complement can be synthesised and act independently of antibodies, the fact

that IgG and C1q driven modules relate to axonal loss suggest that these factors are likely acting in concert. In fact, while IgG deposition and complement activation is a known feature of MS white and grey matter lesional pathology throughout its life cycle, (Compston *et al.* 1989, Gay *et al.* 1997, Storch *et al.* 1998, Lucchinetti *et al.* 2000, Barnett *et al.* 2004, Breij *et al.* 2008, Barnett *et al.* 2009, Lucchinetti *et al.* 2011, Sádaba *et al.* 2012, Ingram *et al.* 2014, Watkins *et al.* 2016, Loveless *et al.* 2018, Absinta *et al.* 2021, Cooze *et al.* 2022, Muñoz *et al.* 2022), studies of normal-appearing tissue have also begun to observe opsonin activity, albeit to a lesser degree (Sádaba *et al.* 2012, Ingram *et al.* 2014, Watkins *et al.* 2016, Loveless *et al.* 2018, Cooze *et al.* 2022, Muñoz *et al.* 2022). Therefore, the extent and distribution of IgG and complement deposition in our spinal cord pathological specimen is the subject of current work. We also observed a relationship between the purple (immunoglobulin-enriched) module and the presence of spinal cord demyelination. However, this relationship was not driven by the extent of subpial disease which further supports the argument against an outside-in pathological mechanism of demyelination described in Chapter 2. Taken together, these findings suggest that the perivascular space, where CSF flows, rather than the contiguous subpial surface is an important site for the development of demyelinating and neurodegenerative pathology in the spinal cord.

The nature of IgG production could not be sourced in this study as we lacked paired blood samples. Our findings suggest that immunoglobulin concentration in CSF, regardless of whether it is the intrathecal fraction, relates to an objective measure of neurodegeneration. Interestingly, in contrast to other work, we did not identify a relationship between B cell inflammation and axonal loss in our cohort (Reali *et al.* 2020). This may indicate that the immunoglobulin fraction of relevance to axonal pathology accesses the intrathecal compartment from the blood through a breached vascular barrier. In fact, a recent clinical study demonstrated that patients with a breached blood-brain-

barrier, as measured by the albumin quotient, had increased levels of IgG in the CSF and more pronounced axonal damage, as measured by CSF NfL (Marco *et al.* 2021).

Similarly, the source of complement identified in the CSF could not be ascertained. Complement may be produced locally within the CNS, mainly by activated myeloid cells. However, we did not observe a correlation between myeloid cell density and light cyan (complement module) eigenprotein expression, indicating that intra-CNS production may not be the major source. Complement is also synthesised by the liver and found in circulating plasma. Given that barrier disruption is commonplace in progressive MS patients, the complement found in the CSF relevant to axonal damage may originate from circulating blood.

We were unable to identify a significant difference in the expression of these modules between MS and control post-mortem CSF. This may be a result of the small sample size of our heterogeneous control set. However, these findings may also highlight that disparate mechanisms are involved in MS susceptibility and progression as has been suggested by genetic studies (George *et al.* 2016). For example, the environment in which opsonins are circulating is likely of critical importance. In fact, activated myeloid cells, which we observed to be increased in MS, may set the stage for opsonin pathogenicity in MS.

Overall, two important relationships with axonal loss have emerged. Activated myeloid cells and intrathecal opsonins independently segregate with more severe spinal cord axonal loss (**Figure 3.20**). However, we understand that our work solely provides a static end-stage view of a dynamic process and does not have the ability to disentangle whether the CSF factors identified are involved in the pathogenetic cascade or represent an epiphenomenon that is just a consequence of inflammatory tissue damage. To address these limitations, we have assessed the relationship

between our CSF biomarkers and clinicoradiographic disability using a well-characterised living MS cohort which is the subject of the next chapter.

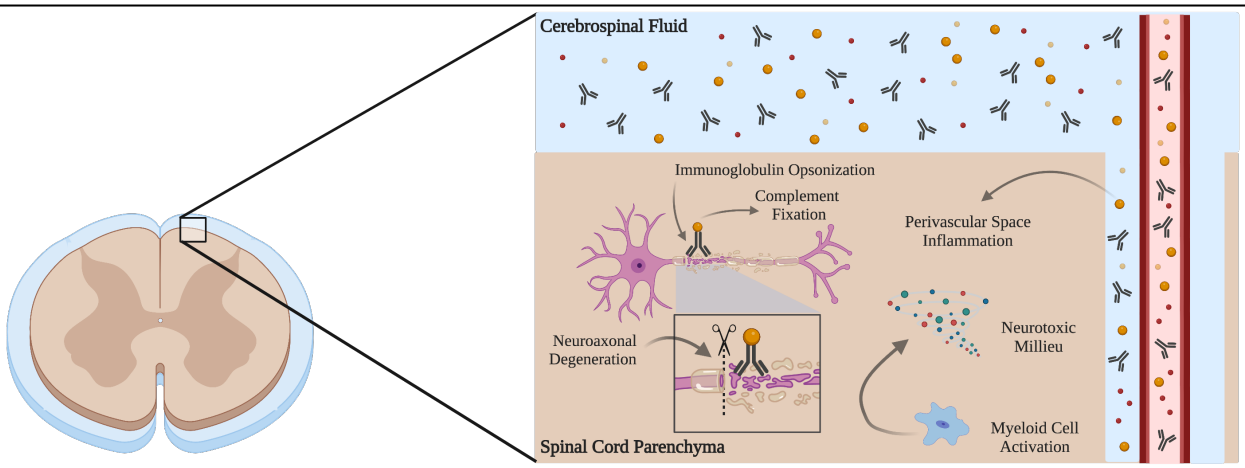


Figure 3.20. Working Hypothesis Detailing the Potential Determinants of Axonal Loss in MS. Myeloid cell activation promotes abrogation of neurotoxic molecules that prime axons to degenerate. Immunoglobulins and complement found within the subarachnoid and perivascular spaces and detectable via CSF profiling, diffuse into the MS spinal cord parenchyma through breached barriers. Immunoglobulins (IgG) opsonise axonal elements and fix complement (C1q) which promotes damage and degeneration.

4. Clinicoradiographic Exploration of Pathologically-Identified Cerebrospinal Fluid Biomarkers of Spinal Cord Pathology

4.1 Introduction

The greatest determinant of disability in MS is entry into the progressive phase, which in most patients, is characterised by a relentless myelopathy. Clinical measures of disability progression, including EDSS and PIRA, are biased towards the capture of motor disability, which is tightly linked to spinal cord pathology. In fact, longitudinal measures of spinal cord atrophy associate strongly with clinical outcome (Lukas *et al.* 2015, Rocca *et al.* 2017, Bischof *et al.* 2022), though molecular biomarkers of these processes have remained elusive.

Proteomics has revealed itself as a key tool used to identify molecular biomarkers of disease. However, shotgun proteomic studies of patient samples have been unable to reproducibly identify specific biomarkers of progression in MS (Farias *et al.* 2014, Kroksveen *et al.* 2015). This untargeted approach is marred with limitations stemming from clinicopathologic heterogeneity. Misdiagnosis and poor stratification of patients by insensitive clinical and radiographic surrogates of disability limit the ability to detect relevant candidates. Therefore, targeted investigations of pre-defined candidates have improved statistical power to combat these limitations. In fact, targeted quantification of CSF NfL has been shown to rise and fall with disease activity and predict clinicoradiographic progression (Salzer *et al.* 2010, Teunissen *et al.* 2012). Interestingly, levels in the serum seem to exhibit an improved predictive value (Kosa *et al.* 2022b). However, neurofilament light chains are not specific to underlying pathophysiology but rather a proxy marker of injury. Platforms for the identification of new pathologically-relevant candidates are lacking. In the previous chapter, we leveraged a robust pipeline integrating quantitative spinal cord

neuropathology with post-mortem CSF proteomics and network analyses. We demonstrated that the concentration of opsonins (IgG and C1q) in the CSF associated with more severe spinal cord axonal loss. In this chapter, we took our candidate molecules for targeted validation in a well-characterised clinical cohort with longitudinal imaging available for study. We hypothesised that the expression of our candidate proteins in the CSF of living patients would predict MS status and the rate of clinically and radiographically measured disease progression.

4.2 Materials and Methods

4.3.1 Study Population

A deeply endophenotyped *in vivo* MS (n=171) and control (n=75) cohort with indexed CSF was available for study. All patients were recruited from the University of Basel under an approved research ethics board protocol (Project-ID 2019-01873) for CSF collection. The control patients were chosen to exhibit a wide range of non-MS diagnoses which mimic those observed in a general neurology practice. A comprehensive intake was performed for all MS and control patients at the CSF collection timepoint. Information available for all patients included age, sex, clinical diagnoses, and medication history. MS-specific information included disease duration, relapse history, and index EDSS. A subset of MS patients (n=109) were enrolled in the Swiss MS Cohort Study (Disanto *et al.* 2016) and underwent longitudinal clinical and radiographic assessment every 6-12 months. A graphical representation of all assessments and the associated timelines is outlined in section 4.3.2 and summarised in **Figure 4.1**.

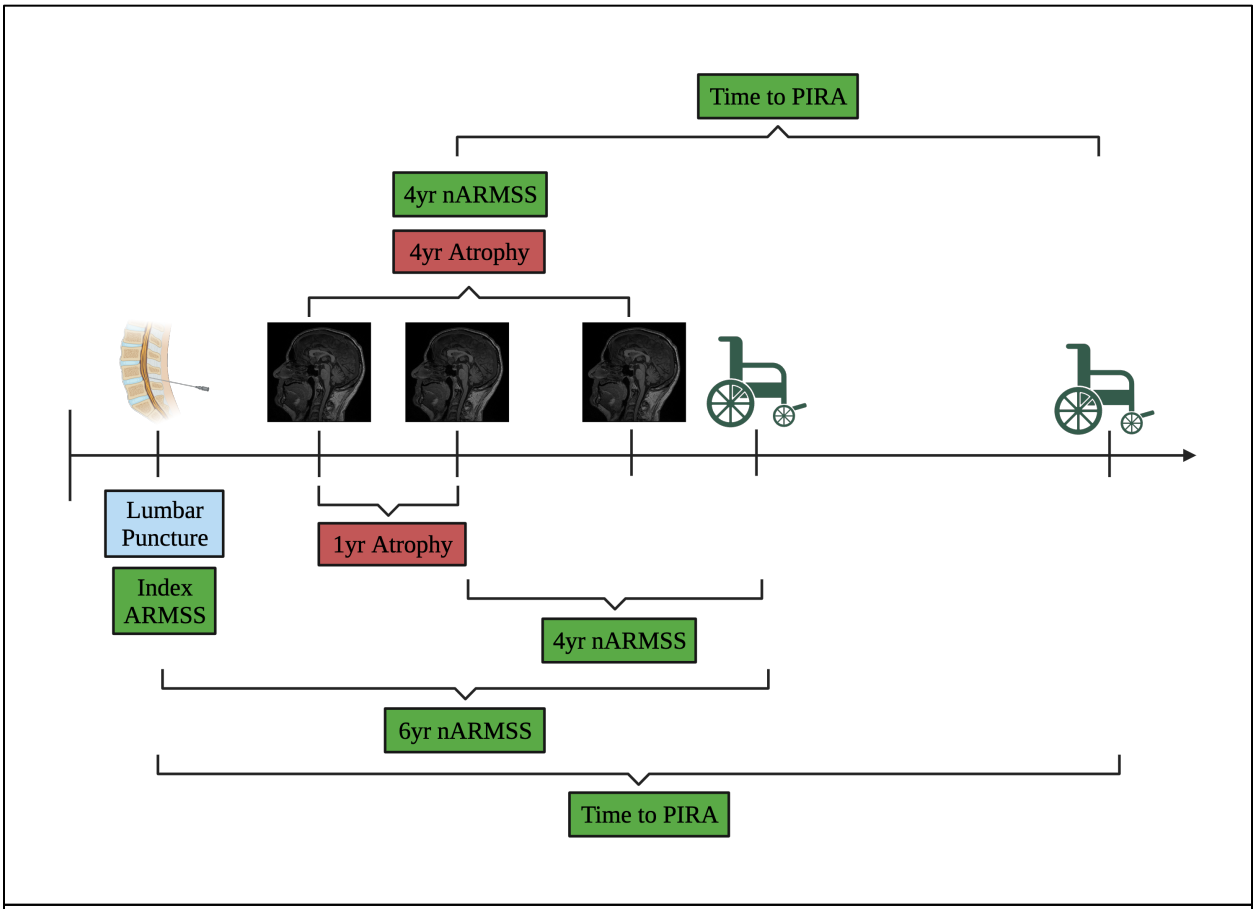


Figure 4.1. Patient Assessment Summary. Timeline for the biochemical, clinical, and radiographic assessments performed in the MS cohort.

4.3.2 Clinical Disability Assessment and Calculation

At the time of CSF collection, all enrolled MS patients had index EDSS values that were scaled by age and converted into the ARMSS for cross-sectional disability analyses (Manouchehrinia *et al.* 2017). The normalised ARMSS (nARMSS) scale was calculated using three epochs: 1) 6-years following the CSF collection visit; 2) 4-years following the 1-year atrophy assessment; and 3) the period during the 4-year atrophy assessment (Manouchehrinia *et al.* 2021). Patients were grouped into two distinct categories, those with positive nARMSS values and those with negative nARMSS values. Patients with a positive nARMSS score have spent most of their follow-up above the median expected for patients of the same age while those with a negative nARMSS score have

spent the majority of their follow-up period below the median expected. Analysis epochs were chosen that struck a balance between patient follow-up and patient inclusion.

Confirmed disability worsening (CDW) events over the length of patient follow-up were recorded using the same epochs described above. CDW events were classified as either a ≥1.5 point increase in EDSS for patients with a baseline EDSS of 0, ≥1.0 point for patients with a baseline EDSS of 1–5, and ≥0.5 point increase for patients with a baseline EDSS of ≥5.5. The increase in EDSS must have occurred at least 6 months from baseline and confirmed at least 6 months from the recorded increase. A roving baseline was used due to its increased sensitivity for detecting disability worsening (Kappos *et al.* 2018, Lepore *et al.* 2021). All CDW events were classified as either PIRA or relapse-associated worsening (RAW). To qualify as PIRA, no clinical relapse or gadolinium-enhancing brain lesion could be recorded beginning from 3 months prior to the reference event to 3 months after the confirmation.

4.2.3 Radiographic Assessment of Spinal Cord Atrophy

3D volumetric T1-weighted isotropic (1 x 1 x 1 mm^3) magnetisation-prepared rapid gradient echo (MPRAGE) MRI brain sequences were used as input to measure spinal cord atrophy, a radiographic measure of disability (Kearney *et al.* 2015, Lukas *et al.* 2015, Moccia *et al.* 2019b). The C1-C2 spinal cord level is visible on this brain MRI sequence and volumetric data correlates strongly with total spinal cord volume measured using dedicated spinal cord imaging that is not typically obtained for routine MS monitoring. MRI scans were acquired using the same vendor (Siemens). No software or hardware upgrades were performed between baseline and follow-up scans. Baseline and follow-up scans were all performed using the same field strength (1.5T or 3T)

and baseline scans all occurred post-lumbar puncture (LP). We chose two epochs, 1-year follow-up after LP and 4-year follow-up after LP.

A well-validated registration-based method, generalised boundary shift integral (GBSI), was employed to assess longitudinal spinal cord atrophy between baseline and 1-year and 4-year follow-up scans. Compared to segmentation-based methods in which individual cross-sectional area measures are obtained at each time point and then subtracted to assess change in volume, GBSI is not subject to the same variability across scans because it co-registers images into the same space and directly measures changes in atrophy (Moccia *et al.* 2019a, Moccia *et al.* 2020). This significantly reduces error and increases statistical power. In the GBSI pipeline (**Figure 4.2**), the C1 and C2 levels were first identified manually. The spinal cord was then segmented using the DeepSeg, a convolutional neural network, found within the Spinal Cord Toolbox (SCT) (De Leener *et al.* 2017, Gros *et al.* 2019). The MRI image then underwent denoising and bias field correction. The spinal cord was straightened and a 3D symmetric and inverse-consistent affine registration was performed to the space half-way between the baseline and follow-up scan to limit bias. 9 degrees of freedom were used, which included translation, rotation, and skew in three directions. The spinal cord segmentation masks were transposed to the halfway space using linear interpolation. The probabilistic boundary shift mask (pXOR) between baseline and follow-up scans was estimated. On a voxel-to-voxel basis, the intensity differences between baseline and follow-up scans were tabulated and weighted by the pXOR probability mask to compute the GBSI. Percent spinal cord volume change was calculated by dividing the GBSI by the spinal cord mask volume of the baseline scan and subsequently annualised. Patients were segregated into discrete groups based on whether they experienced atrophy over the two follow-up periods.

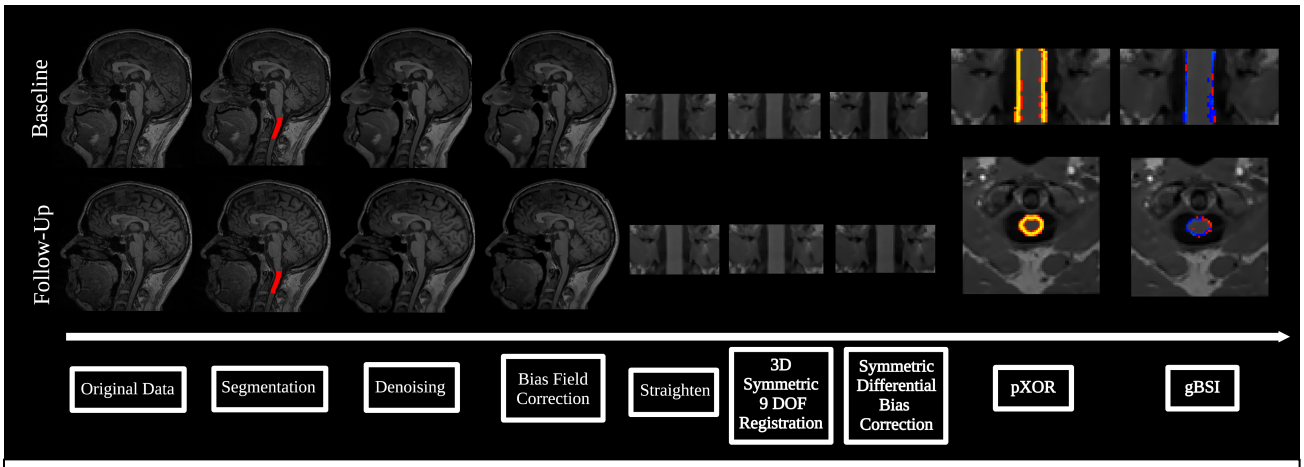


Figure 4.2. GBSI MRI Analysis Pipeline. The C1-C2 region of the spinal cord was first manually defined on 3D T1-weighted MPRAGE brain scans before automatic segmentation of the spinal cord. The resulting image underwent denoising and bias field correction. The spinal cord was straightened before 3D symmetric registration of baseline and follow-up scans into the half-way space and symmetric differential bias correction. The probabilistic pXOR mask was generated and used to tabulate the generalised boundary shift integral.

4.2.4 Cerebrospinal Fluid SomaScan® Proteomics

CSF samples were stored at −80°C and shipped to SomaLogic (Boulder, CO) on dry ice for SomaScan® analysis. SomaScan® proteomic data was collected using the Novartis custom 5k SomaScan® assay which contains 5,080 single-stranded slow off-rate modified aptamers (SOMAmers) generated from chemically-modified nucleotides. 4,785 SOMAmers target 4,137 unique human genes and 249 SOMAmers bind non-human proteins. SOMAmers bind proteins in their native conformation found within complex matrices. All SOMAmers 1) are biotinylated to allow for streptavidin capture of SOMAmer-protein complexes, 2) possess a photocleavable linker for repetitive capture and release, and 3) have a fluorescent tag that allows for quantification of protein abundance. Polyanionic competitors are spiked into the assay and used to promote dissociation of weak protein-SOMAmer interactions and improve specificity. 46 specific SOMAmers encompass various aspects of assay quality control and normalisation. These include non-specific spuriomers, non-biotinylated SOMAmers, non-cleavable SOMAmers, and

hybridisation control SOMAmers. Given the curse of dimensionality, relatively small sample sizes, and limitations associated with untargeted analyses in clinical cohorts, we solely performed a targeted assessment of the relationships between our biomarkers of interest identified in the previous chapter, IgG and C1q, and clinicoradiographic parameters.

4.2.5 Statistical Analysis

4.2.5.1 Clinicoradiographic Relationships

Atrophy rate measurements of ±5% were defined as outliers given that previous work has deemed these to lie more than two standard deviations away from controls (Moccia *et al.* 2019a, Moccia *et al.* 2020, Prados *et al.* 2020). Differences in ARMSS values between patients that displayed spinal cord atrophy and those that did not were assessed using student T-tests. The fisher exact test was used to assess the relationship between atrophy and PIRA during the 4-year MRI scan interval. Cox proportional hazards models were used to assess the time to PIRA following measurement of 1-year atrophy. Graphical representations of all results were created in Prism 9 and imported into BioRender to create figure panels. Statistical analyses was performed in RStudio Version 1.4.1717. A p-value of 0.05 was used to define statistically significant comparisons in all analyses.

4.2.5.2 Cerebrospinal Fluid SomaScan® Proteomics

171 MS patients and 75 control patients underwent CSF SomaScan® analysis. 39 MS and 9 control patients were excluded because they were taking corticosteroids within 1 month prior to LP. Details of the remaining patients are described in **Table 4.1**.

Table 4.1. MS and Control Clinical Cohort Demographics

		Multiple Sclerosis (*n*=132)	Control (*n*=66)	Difference
Age (Mean ± SD)		39.9 ± 13.3	54.4 ± 16.3	****(p<0.0001)
Sex (M:F)		34:98	29:37	*(p=0.0147)
Disease Type	*Primary Progressive*	9		
	Secondary Progressive	5		
	Relapsing-Remitting	42		
	Clinically Isolated Syndrome	75		
Index ARMSS (Mean ± SD)		4.3 ± 2.4		

The remaining SomaScan® data was pre-processed using the Somalogic recommended pipeline. The normalisation procedure included hybridisation control normalisation, intraplate median signal normalisation, plate scaling and calibration, and median signal normalisation to a pooled reference sample. The estimated lower limit of detection was extrapolated for each SOMAmer using corresponding buffer samples (Candia *et al.* 2022). Zeros were imputed for sample-SOMAmer combinations below the lower limit of detection. SOMAmer proteins (N=342) were removed that were not quantified in more than 75% of samples. Signal-to-noise ratios (SNR) were tabulated for each SOMAmer using the corresponding buffer sample and proteins with an SNR less than 0.45 (N=44) were also removed (Dammer *et al.* 2022). One deprecated protein was also removed. This procedure resulted in 4,398 SOMAmers available for quantification. The genes encoding the removed SOMAmers were randomly distributed across the genome and the resulting proteins available for downstream analysis demonstrated an unbiased spread across the genome. Age and sex were regressed out of the entire dataset using an Empirical Bayes-moderated adjustment with the WGCNA R package whilst protecting the relationship between MS and control. Differences in CSF candidate protein expression between 1) MS and control, 2) atrophy

groups, and 3) nARMSS groups was determined using student T-tests. Relationships between candidate CSF protein expression and cross-sectional ARMSS were assessed using the non-parametric Spearman correlation. Univariate cox-proporational hazards models assessed the impact of CSF protein expression on the time to PIRA. Graphical representations of all results were created in Prism 9 and imported into BioRender to create figure panels. Statistical analyses was performed in RStudio Version 1.4.1717. A p-value of 0.05 was used to define statistically significant comparisons in all analyses.

4.2.5.3 Cerebrospinal Fluid Proteomics Modelling of Age

Given the biggest risk factor for entrance into the progressive phase of MS is age (Koch *et al.* 2010), we tested the hypothesis that CSF composition could be used to predict biological age and understand whether MS is associated with accelerated ageing. To accomplish this, the nestedCV package in R was used to build elastic net models predicting age. All SOMAmers measured in the CSF entered the model and regularisation built into the elastic net model paradigm performed feature selection. Models were built using the control cohort only and fit was assessed using a nested cross-validation scheme (**Figure 4.3**). The control model was used to predict age in the MS cohort. The non-parametric Spearman correlation was used to assess the relationships between chronological and predicted ages in the control and MS cohorts separately. Model residuals for the control and MS cohort were calculated by extracting the difference between chronological and predicted ages. The external cross-validation loop generated the predicated ages that entered the calculations for control patients to eliminate bias from the optimisation of model parameters in this cohort. An unpaired T-test was used to determine whether the residuals differed between controls and MS patients. Graphical representations of all results were created in Prism 9 and imported into BioRender to create figure panels. Statistical analyses was performed in RStudio

Version 1.4.1717. A p-value of 0.05 was used to define statistically significant comparisons in all analyses.

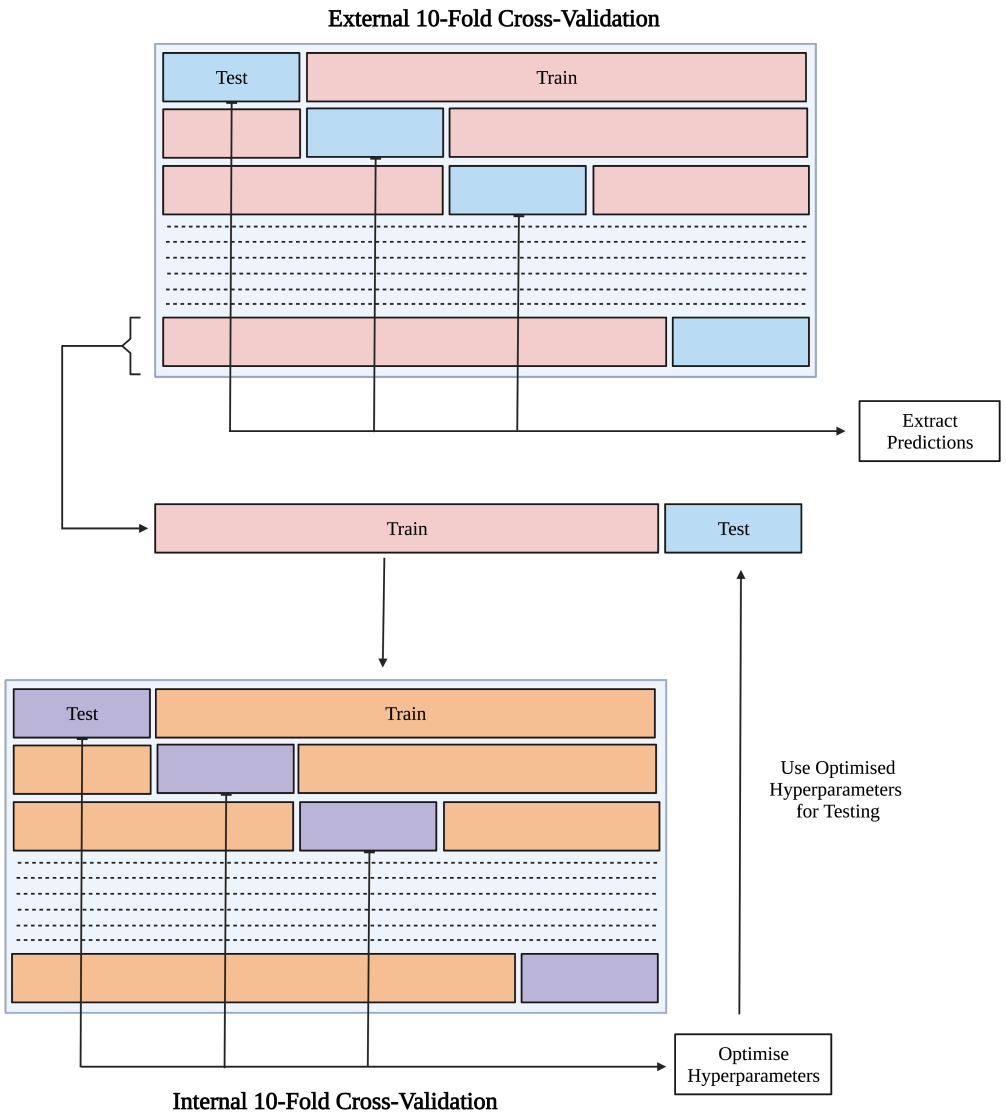


Figure 4.3. Nested Cross-Validation Workflow. The external loop consists of samples split into 10 test and train folds. The internal loop consists of splitting each train fold into an additional 10 test and train folds. Model hyperparameters (alpha and lambda) are optimised in the internal validation loop. Optimised hyperparameters are then applied to the test set from the external loop and unbiased predictions and estimates of model performance are extracted for downstream analyses.

4.3 Results

4.3.1 Cohort Demographics

For the GBSI analyses, 90 MS patients underwent a 1-year atrophy assessment, and 70 MS patients were followed over a 4-year period. Outlier detection led to exclusion of 33 (out of 90) patients for the 1-year epoch and 0 (out of 70) patients for the 4-year epoch. These outlier rates are in line with previous work from our collaborators (Moccia *et al.* 2020). In fact, increased follow-up time decreases the variation observed due to inherent noise in the MRI-based tabulation of atrophy, especially in the measurement of small structures, and reduces the number of outliers generated (**Figure 4.4**).[3]

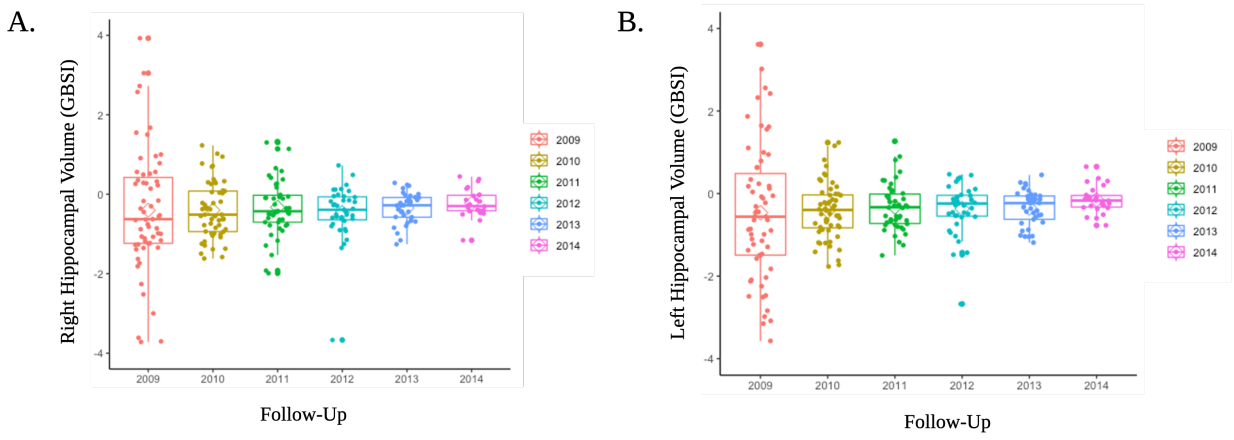


Figure 4.4. Impact of Increased Follow-Up on Hippocampal GBSI. Summary boxplots displaying atrophy data of the right (**A**) and left (**B**) hippocampus derived from GBSI analysis of patients using 1, 2, 3, 4, and 5-year follow-up (baseline scan in 2008).

For the SomaScan analyses, 132 MS and 66 control cases had CSF proteomics data available for study. Control cases were significantly older than MS ($U=2175$, $p<0.0001$) and displayed a female bias ($p=0.015$).

[3] Data for figure 4.2 was kindly provided by Ferran Prados (UCL).

4.3.2 Relationships Between Clinical Disability and Spinal Cord Atrophy

The relationship between clinical disability and atrophy over the 1-year and 4-year epoch was assessed. On segregating patients who experienced atrophy versus those who did not over the 1-year and 4-year follow-up periods, ARMSS values at either the index or follow-up scan did not differ between groups (**Figure 4.5**)

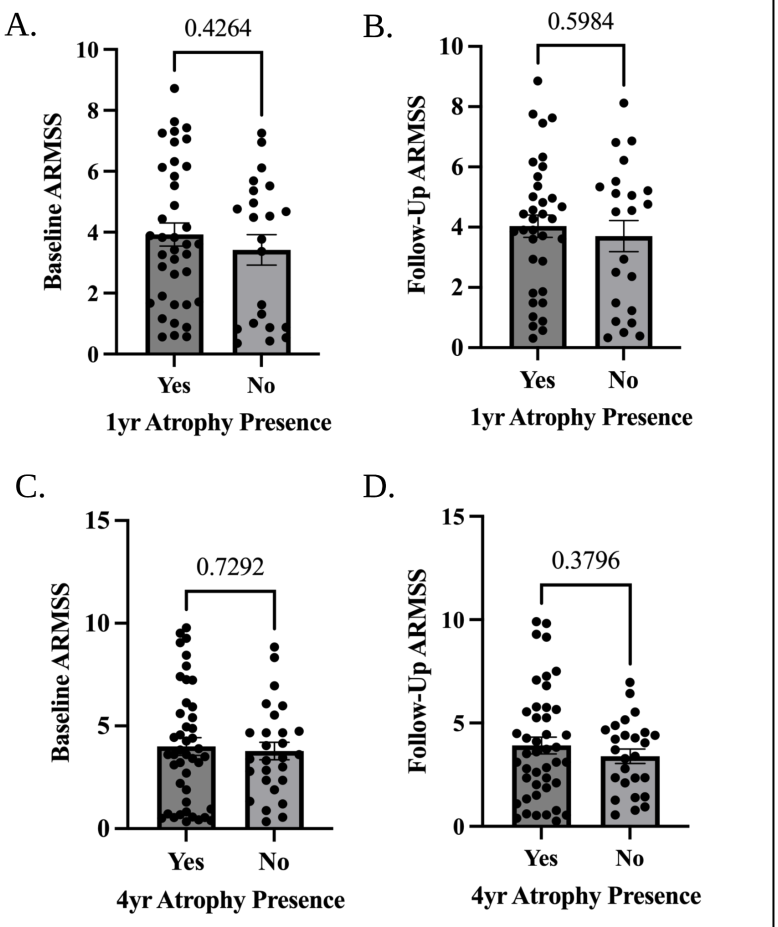


Figure 4.5. Relationship Between Atrophy and Cross-Sectional MS Disability (ARMSS). Bar charts depicting the ARMSS values at baseline (**A,C**) and follow-up (**B,D**) between patients with and without atrophy over 1 year (**A,B**) and 4 years (**C,D**). Values represent observed means and standard errors. P-values of comparisons not reaching significance are reported and asterisks indicate significant post-hoc pairwise comparisons (*p<0.05; **p<0.01; ***p<0.001; ****p<0.0001).

The relationship between the presence of atrophy and longitudinal disability accumulation was also evaluated. Patients were categorised as having a positive or negative nARMSS value four years after 1-year MRI follow-up and during the 4-year atrophy follow-up period. The proportion of patients with positive and negative nARMSS 4 years after the 1-year atrophy assessment did not differ between patients with and without atrophy (**Figure 4.6A**). In addition, the proportion of patients with positive and negative nARMSS values, measured during the 4-year atrophy follow-up period, did not differ between patients with and without atrophy (**Figure 4.6B**).

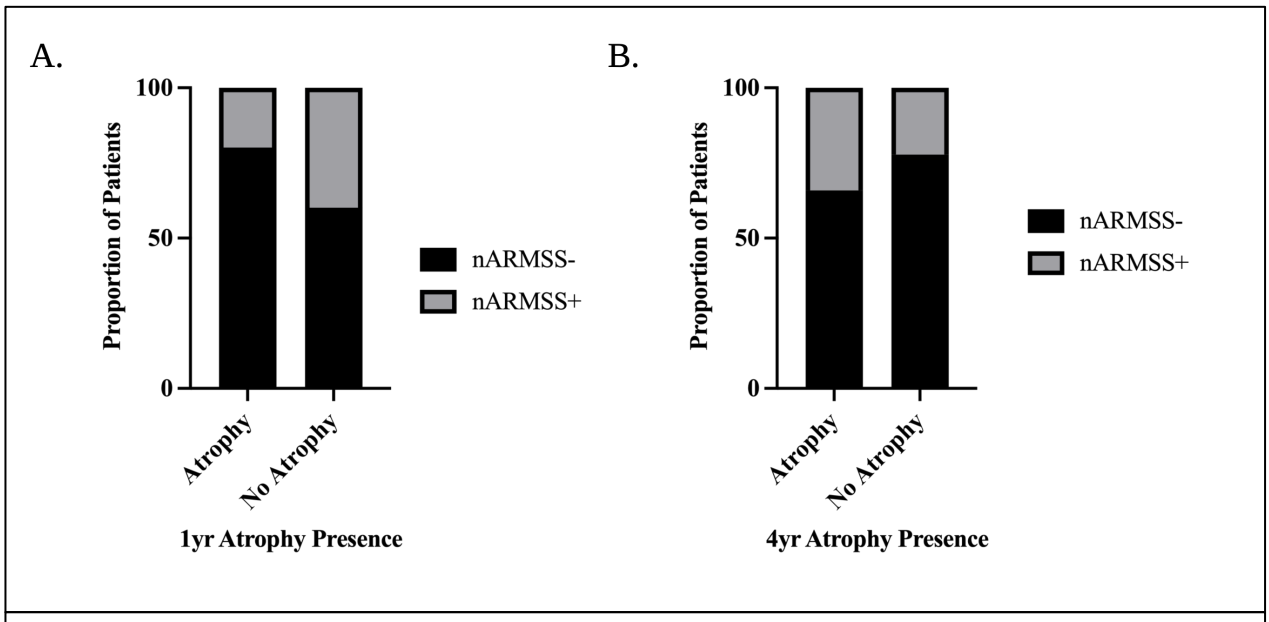


Figure 4.6. Relationship Between Atrophy and Longitudinal MS Disability (nARMSS). Stacked bar charts displaying the proportion of patients with and without atrophy over 1 year (**A**) and 4-year follow-up (**B**) that exhibited a negative or positive nARMSS longitudinal disability value in the 4 years following MRI (**A**) or during the MRI follow-up period (**B**).

The proportion of patients that displayed PIRA during the 4-year atrophy follow-up period did not differ between those with and without atrophy (**Figure 4.7A**). In a time-to-event analysis, the presence of atrophy over 1-year did not hasten the time to PIRA development afterwards (**Figure 4.7B**).

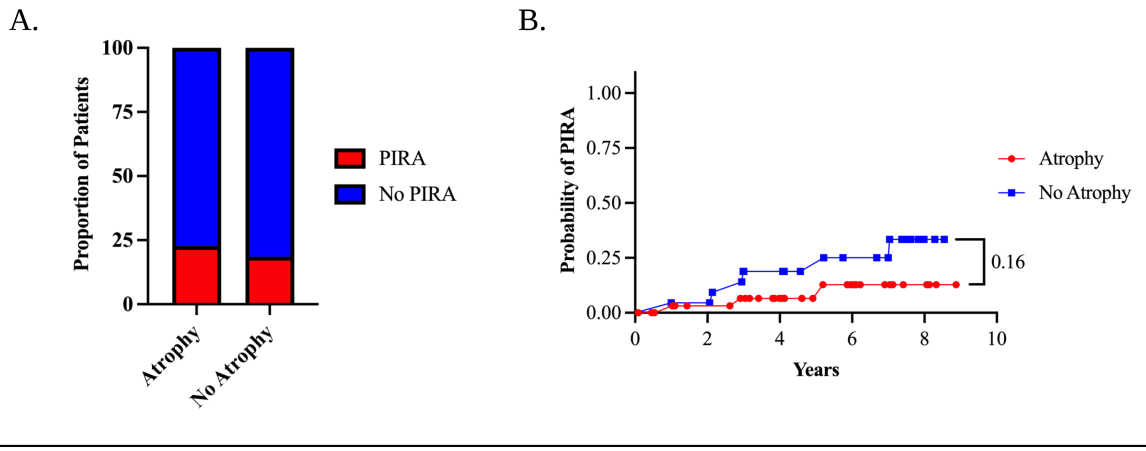


Figure 4.7. Relationship Between Atrophy over 4 years and MS Disease Progression (Presence of PIRA). (**A**) Stacked bar chart displaying the proportion of patients with and without atrophy that experienced PIRA over the 4-year follow-up period. (**B**) Kaplan Meier curves highlighting the probability of PIRA in the follow-up period of cases with and without atrophy over 1-year.

4.3.3 Targeted Analysis of CSF Proteomic Relationships

In the previous results chapter, the hub proteins (IgG and C1q) associated with axonal loss. Given the relevance of axonal loss to clinical disability, the CSF expression of IgG and C1q was estimated from the SomaScan® data and related MS status, cross-sectional disability (ARMSS), longitudinal disability (nARMSS), and progression (PIRA).

Expression of all 6 SOMAmers mapping to IgG was found to be elevated in the CSF of MS patients compared to controls ($p<0.0001$ for all SOMAmers) (**Figure 4.8A-F**). The expression of the SOMAmer mapping to C1q more broadly did not differ between MS and control patients (**Figure 4.9A**) while the SOMAmer characterising the C1qC subunit was elevated in MS compared to control CSF ($p=0.034$) (**Figure 4.9B**).

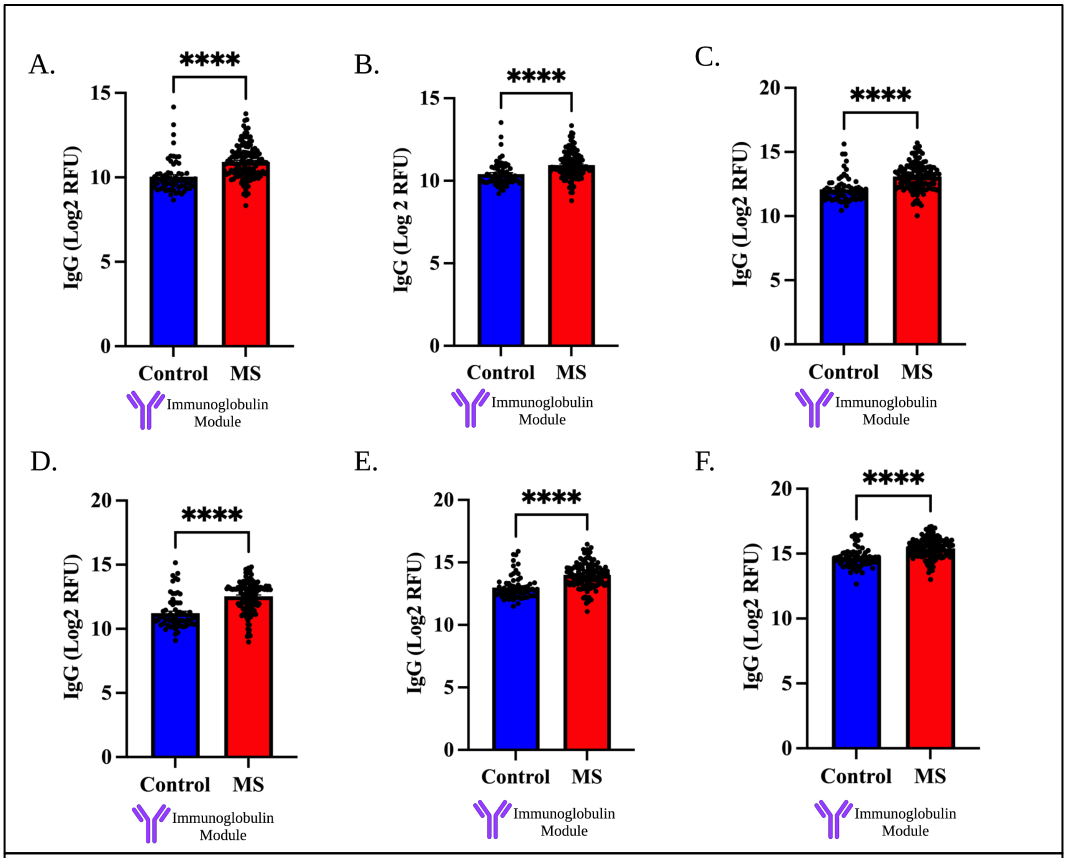
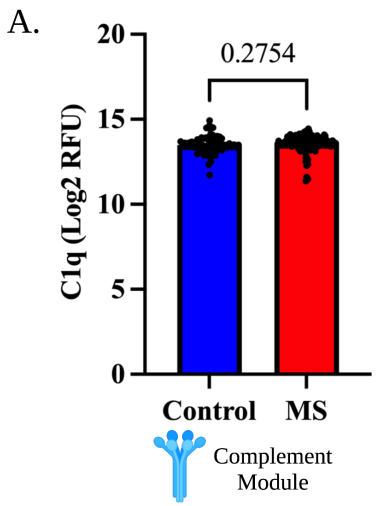


Figure 4.8. CSF IgG in Control and MS Patients. (**A-F**) Bar charts displaying relative fluorescent units of 6 SOMAmers mapping to IgG in control and MS CSF. Values represent observed means and standard errors. P-values of comparisons not reaching significance are reported and asterisks indicate significant post-hoc pairwise comparisons (*p<0.05; **p<0.01; ***p<0.001; ****p<0.0001).



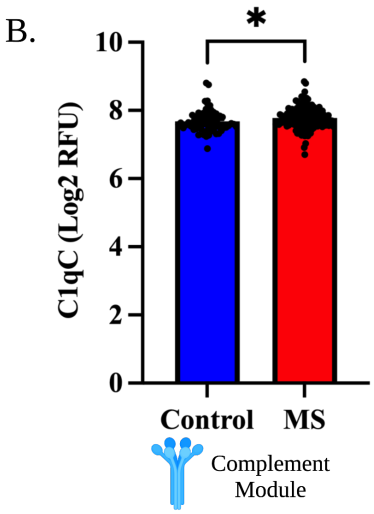


Figure 4.9. CSF Complement in Control and MS Patients. Bar charts displaying relative fluorescent units of SOMAmers mapping to C1q (**A**) and C1qC (**B**) in control and MS CSF. Values represent observed means and standard errors. P-values of comparisons not reaching significance are reported and asterisks indicate significant post-hoc pairwise comparisons (*p<0.05; **p<0.01; ***p<0.001; ****p<0.0001).

The expression of 4 out of 6 SOMAmers mapping to IgG correlated with ARMSS at the time of CSF sampling (p=0.033; p=0.025; p=0.042; p=0.016) (**Figure 4.10A-F**). In contrast to the relationships observed with MS and control patients, C1q correlated with ARMSS (p=0.0044) (**Figure 4.11A**) while the C1qC subunit did not (**Figure 4.11B**).

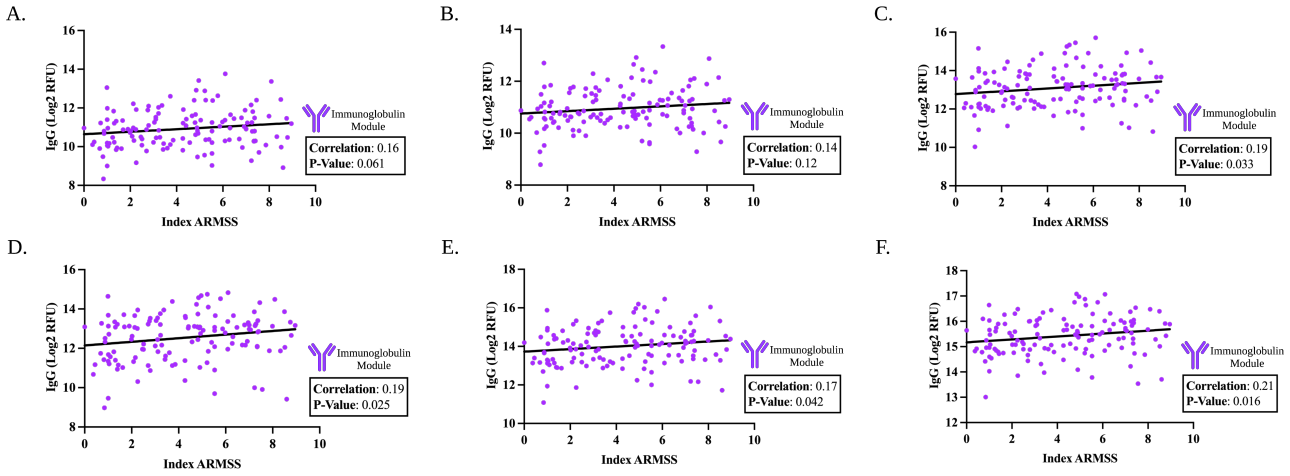


Figure 4.10. Relationships Between CSF IgG and Cross-Sectional MS Disability (ARMSS). (**A-F**) Correlation plots displaying relative fluorescent units of 6 SOMAmers mapping to IgG in MS CSF and the relationship with ARMSS at the time of CSF sampling. Spearman correlation coefficients, the line of best fit, and associated p-values are reported.

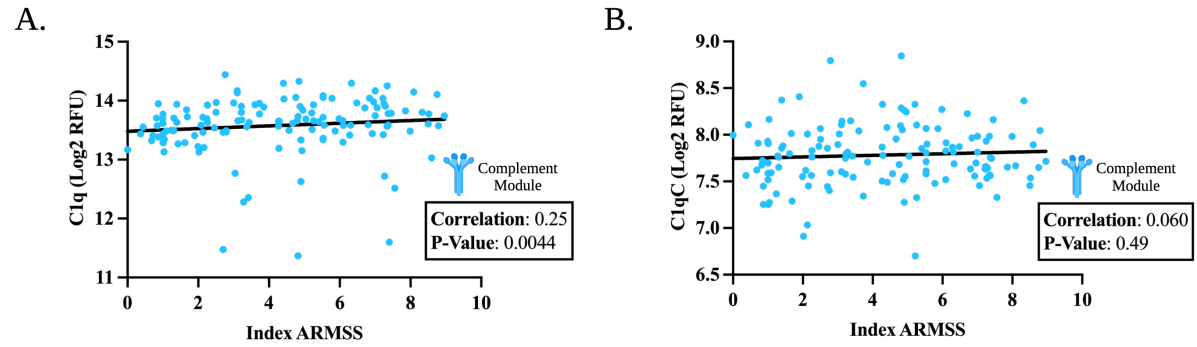


Figure 4.11. Relationships Between CSF Complement and Cross-Sectional MS Disability (ARMSS). (**A-F**) Correlation plots displaying relative fluorescent units of SOMAmers mapping to C1q (**A**) and C1qC (**B**) and the relationship with ARMSS at the time of CSF sampling. Spearman correlation coefficients, the line of best fit, and associated p-values are reported.

The expression of IgG did not differ between patients that exhibited a positive nARMSS (more severe disease course over 6 years post-LP) and negative nARMSS (less severe disease course over 6 years post-LP) (**Figure 4.12A-F**).

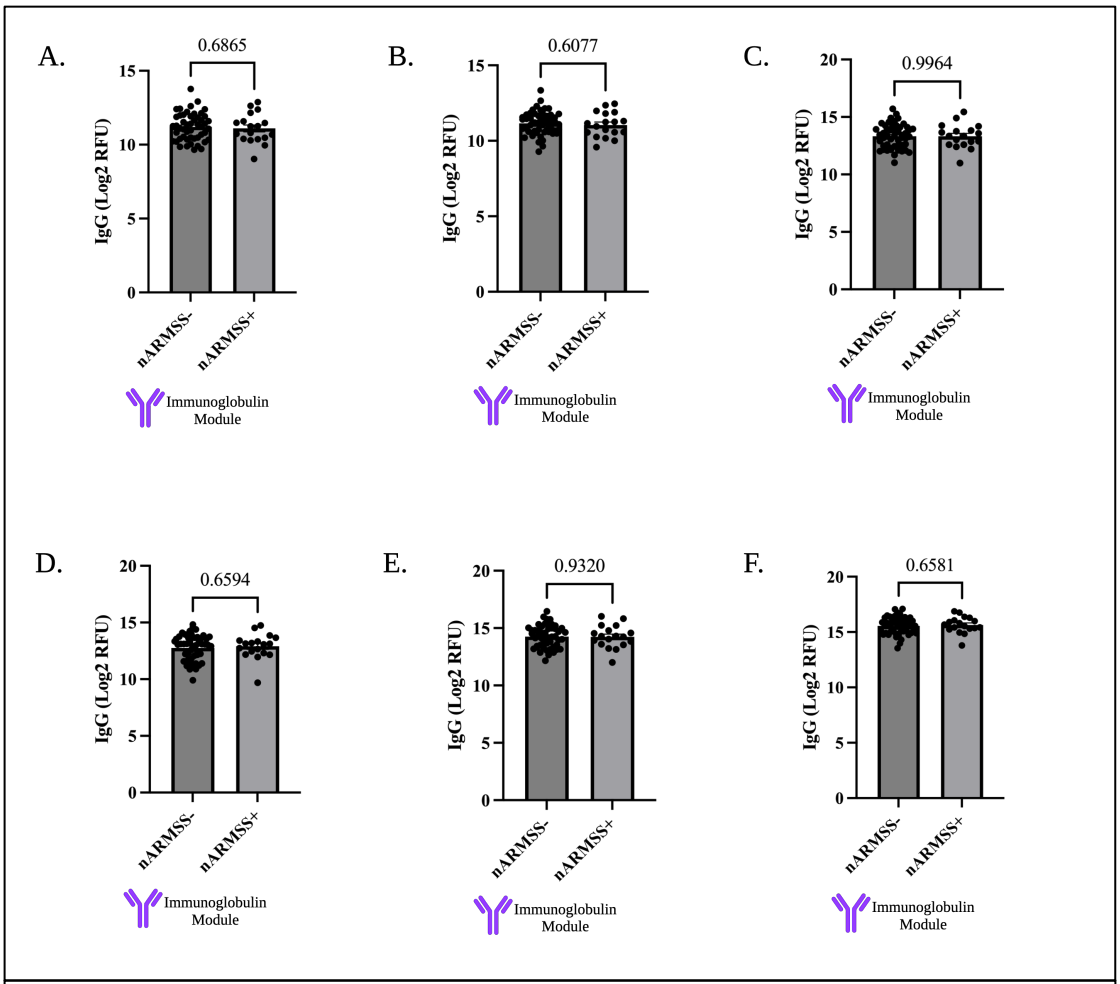


Figure 4.12. Relationships Between CSF IgG and Longitudinal MS Disability (nARMSS). (**A-F**) Bar charts displaying relative fluorescent units of 6 SOMAmers mapping to IgG in the CSF of MS patients with negative and positive nARMSS values 6 years post-LP. Values represent observed means and standard errors. P-values of comparisons not reaching significance are reported and asterisks indicate significant post-hoc pairwise comparisons (*p<0.05; **p<0.01; ***p<0.001; ****p<0.0001).

In addition, expression of C1q (**Figure 4.13A**) and the C1qC subunit (**Figure 4.13B**) did not differ between nARMSS discrete groups.

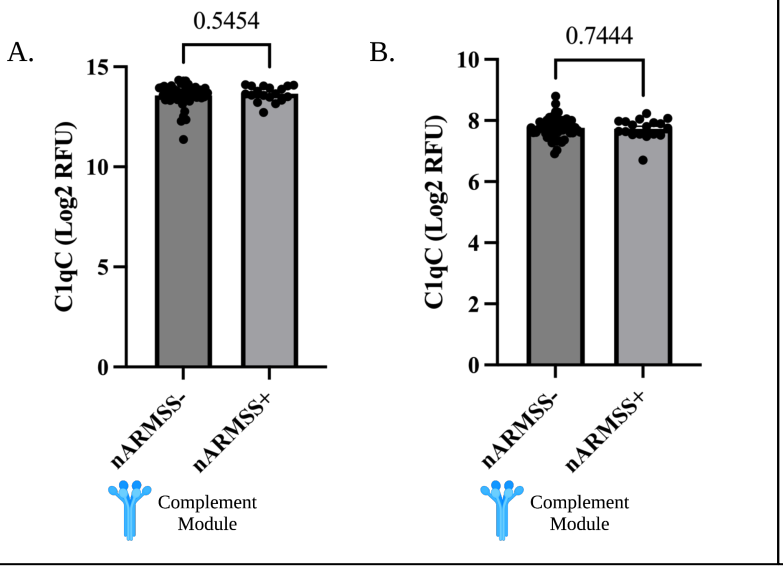


Figure 4.13. Relationships Between CSF Complement and Longitudinal MS Disability (nARMSS). Bar charts displaying Relative fluorescent units of SOMAmers mapping to C1q (**A**) and C1qC (**B**) in the CSF of MS patients with negative and positive nARMSS values 6 years post-LP. Values represent observed means and standard errors. P-values of comparisons not reaching significance are reported and asterisks indicate significant post-hoc pairwise comparisons (*p<0.05; **p<0.01; ***p<0.001; ****p<0.0001).

Also, CSF expression of IgG, C1q, or the C1qC subunit did not predict a faster time to PIRA (**Figure 4.14**).

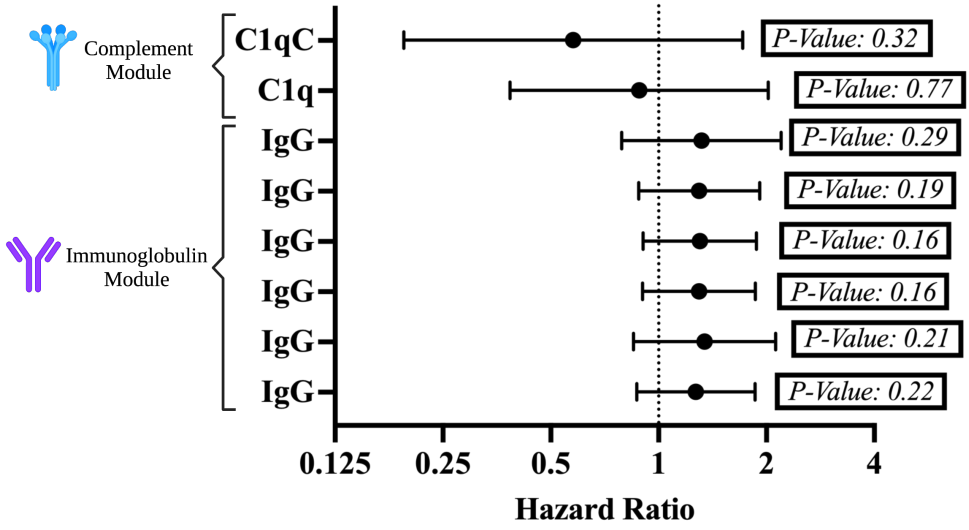


Figure 4.14. CSF Biomarkers and MS Disease Progression (time to PIRA). Forest plot displaying the hazard ratio of PIRA associated with the relative fluorescent units of SOMAmers mapping to IgG, C1q, and C1qC. P-values from each univariate cox proportional hazard model are reported.

The expression of IgG did not differ between MS patients with and without atrophy over 1-year (**Figure 4.15A-F**) or 4-year follow-up (**Figure 4.16A-F**).

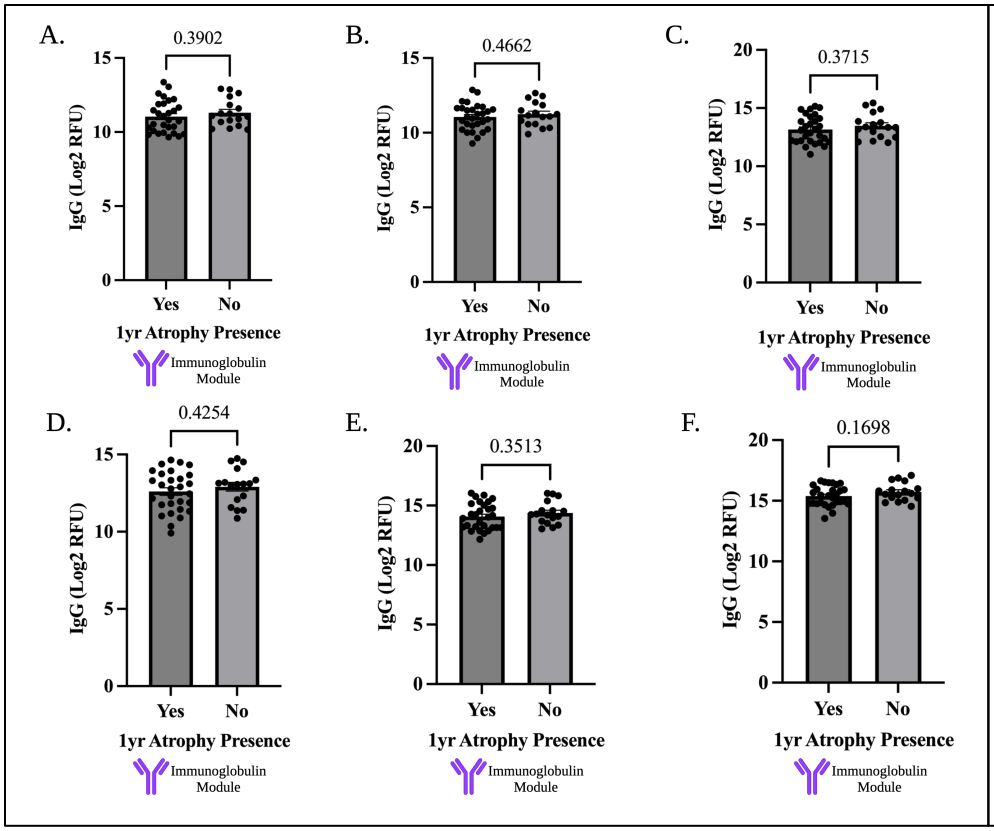


Figure 4.15. CSF IgG and Spinal Cord Atrophy over 1 year in MS Patients. (**A-F**) Bar charts displaying relative fluorescent units of 6 SOMAmers mapping to IgG in the CSF of MS patients with and without atrophy over 1 year. Values represent observed means and standard errors. P-values of comparisons not reaching significance are reported and asterisks indicate significant post-hoc pairwise comparisons (*p<0.05; **p<0.01; ***p<0.001; ****p<0.0001).

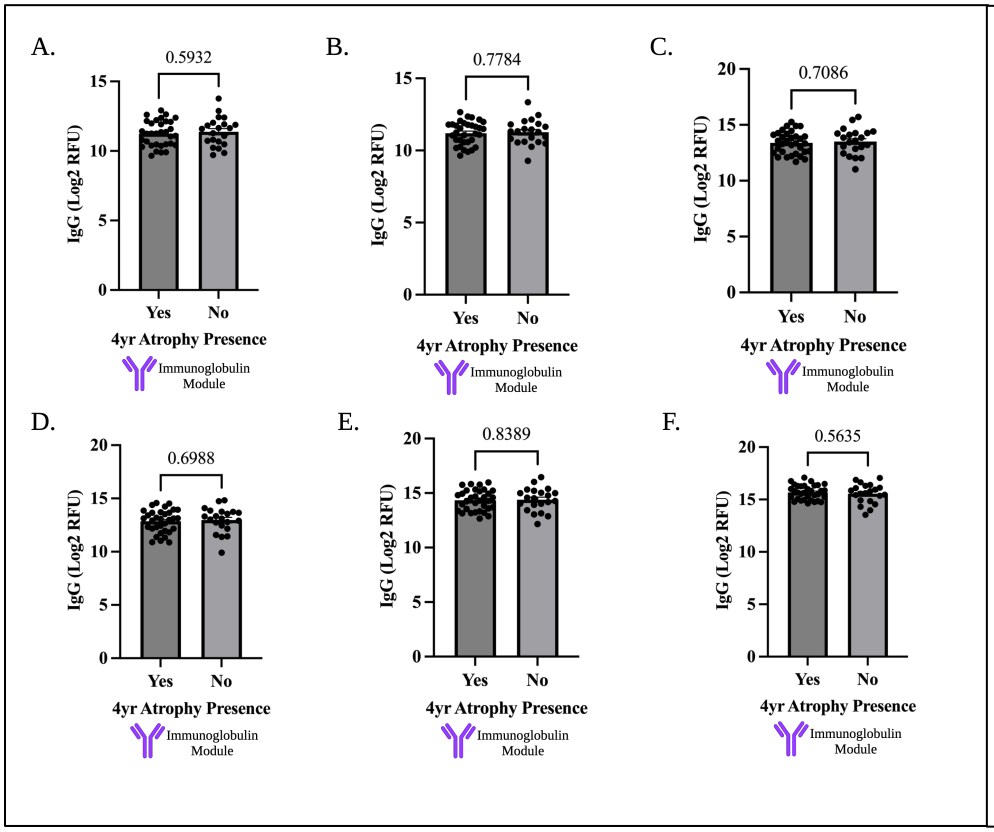


Figure 4.16. CSF IgG and Spinal Cord Atrophy over 4 years in MS Patients. (**A-F**) Bar charts displaying relative fluorescent units of 6 SOMAmers mapping to IgG in the CSF of MS patients with and without atrophy over 4 years. Values represent observed means and standard errors. P-values of comparisons not reaching significance are reported and asterisks indicate significant post-hoc pairwise comparisons (*p<0.05; **p<0.01; ***p<0.001; ****p<0.0001).

Similarly, C1q and the C1qC subunit did not differ between 1-year (**Figure 4.17A-B**) or 4-year atrophy groups (**Figure 4.18A-B**).

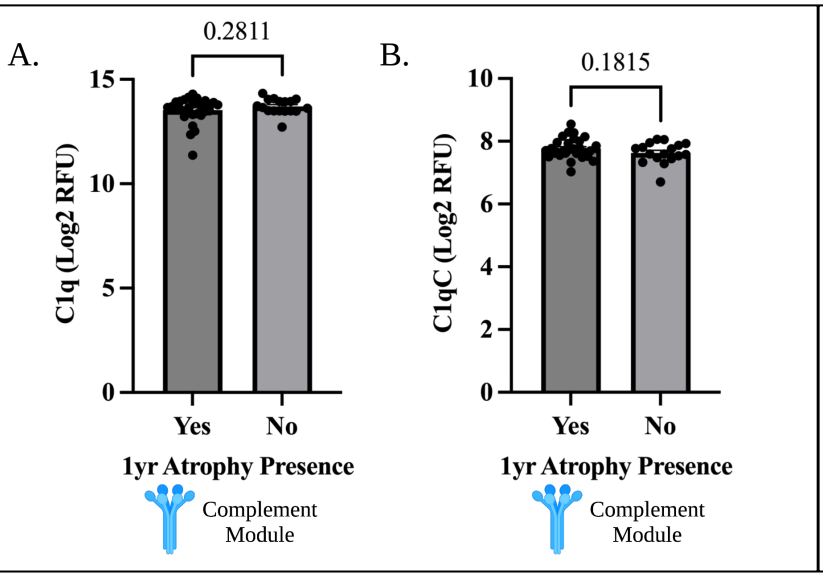


Figure 4.17. CSF Complement and Spinal Cord Atrophy over 1 year in MS Patients. Bar charts displaying relative fluorescent units of SOMAmers mapping to C1q (**A**) and C1qC (**B**) in the CSF of MS patients with and without atrophy over 1 year. Values represent observed means and standard errors. P-values of comparisons not reaching significance are reported and asterisks indicate significant post-hoc pairwise comparisons (*p<0.05; **p<0.01; ***p<0.001; ****p<0.0001).

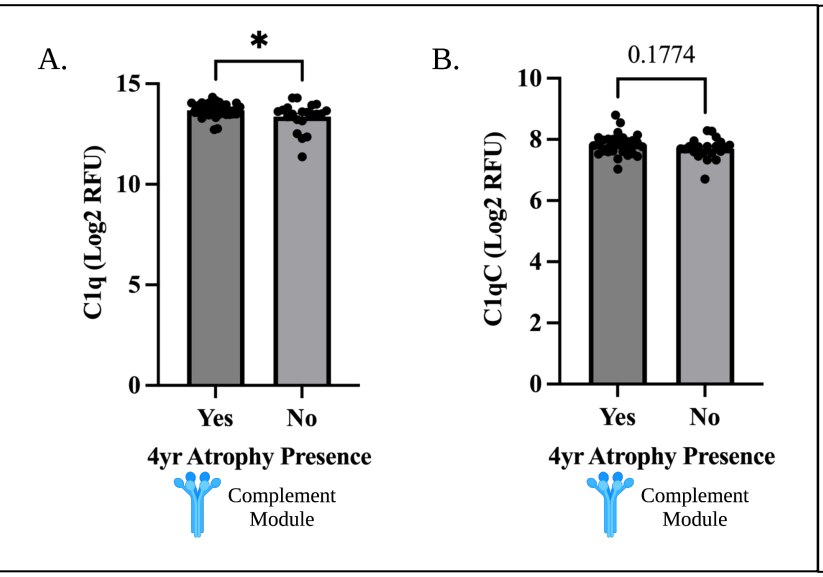


Figure 4.18. CSF Complement and Spinal Cord Atrophy over 4 years in MS Patients. Bar charts displaying relative fluorescent units of SOMAmers mapping to C1q (**A**) and C1qC (**B**) in the CSF of MS patients with and without atrophy over 4 years. Values represent observed means and standard errors. P-values of comparisons not reaching significance are reported and asterisks indicate significant post-hoc pairwise comparisons (*p<0.05; **p<0.01; ***p<0.001; ****p<0.0001).

4.3.4 Cerebrospinal Fluid Determined Age in Multiple Sclerosis

A cross-validated elastic net model built in the control cohort demonstrated strong performance as evidenced by significant correlations between chronological and predicted age (r=0.87, p<0.0001) (**Figure 4.19A**). The model was deployed on the MS cohort to generate predictions and there was

also a significant correlation between chronological and predicted age (r=0.79, p<0.0001) (**Figure 4.19B**). The model residuals for the MS cohort were increased when compared to controls, indicating that the model built using control CSF proteomic data overestimates age in MS cases (**Figure 4.19C**). The top 10 proteins that positively (highlighted in yellow) and negatively (highlighted in orange) associated with age in the model are listed in **Table 4.2**.

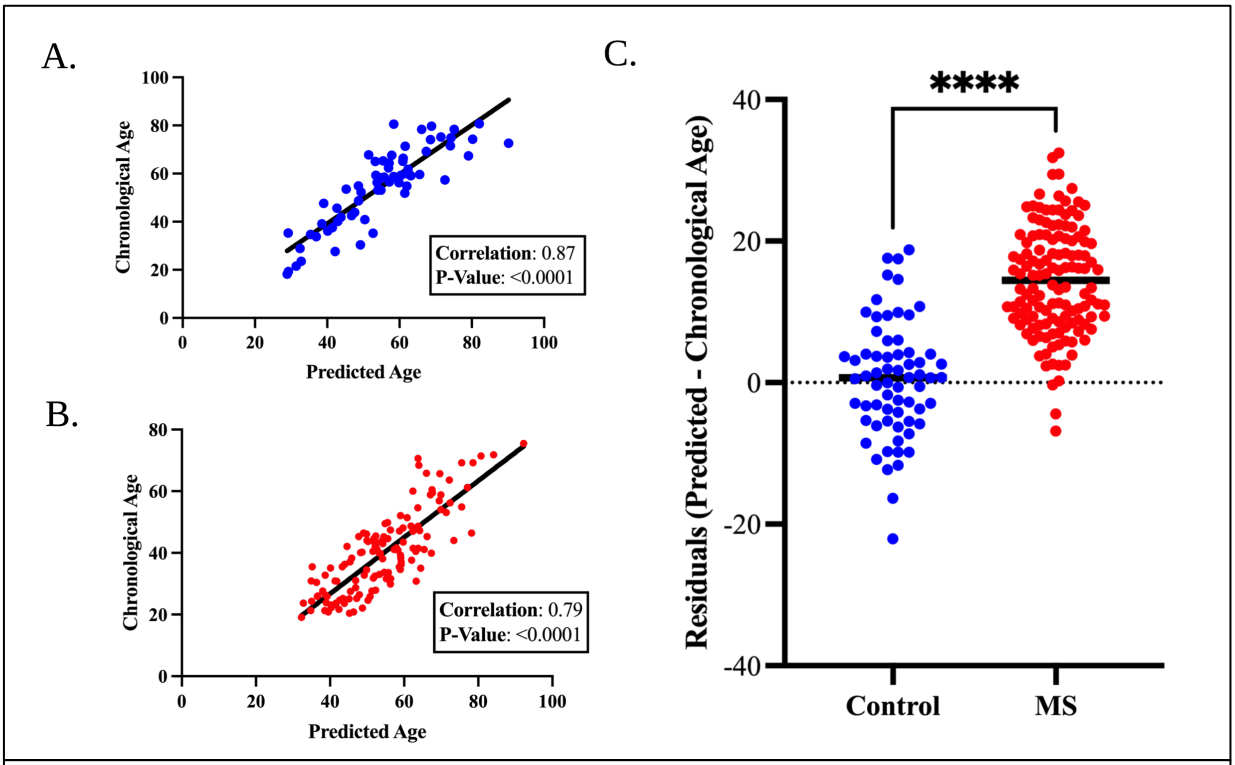


Figure 4.19. CSF Elastic Net Models of Age. An elastic net model trained on all CSF SOMAmers to predict age in a control cohort was applied to both control and MS cases. Correlation plots displaying the relationship between actual and predicted ages of control (**B**) and MS (**C**) patients. To eliminate bias from the elastic net model being trained using the control cohort, predicted age values are derived from a nested cross-validation scheme for these subjects. Spearman correlation coefficients, lines of best fit, and associated p-values are reported. **(C)** Dot plot displaying the residuals from the elastic net model when applied to control subjects and MS patients. Asterisks indicate a significant student T-test (*p<0.05; **p<0.01; ***p<0.001; ****p<0.0001).

Table 4.2. CSF Proteomics Elastic Net Model Coefficients

Protein Names	Coefficients
Netrin 1	2.044730659
Major Histocompatibility Complex, Class II, DQ Alpha 2	1.837533418
Secretory Leukocyte Peptidase Inhibitor	1.670527215
ATP Binding Cassette Subfamily C Member 6	1.396138192
Ribonuclease A Family Member 4	1.396024637
von Willebrand Factor	0.974569113
Serpin Family A Member 3	0.836225966
Integrin Subunit Alpha 1, Beta 1	0.789131101
Glycolipid Transfer Protein	0.671946485
p21 (RAC1) Activated Kinase 6	0.640818243
Tenascin X	-0.704307178
Interleukin 27 Receptor Subunit Alpha	-0.755063202
Hyaluronan and Proteoglycan Link Protein 1	-0.856647979
Zeta Chain of T Cell Receptor Associated Protein Kinase 70	-0.867564774
ADP Ribosylation Factor Like GTPase 3	-0.975811014
Collagen Type I Alpha 1 Chain	-1.140741124
Alpha-2, 8-Sialyltransferase 8B	-1.158658084
Leucine Rich Repeat Containing 37 Member A2	-1.275419056
C1q/TNF-Related Protein-3	-1.512431808
Legumain	-1.906254335

4.4 Discussion

Molecular biomarkers of disease progression in MS have yet to be clinically deployed. We leveraged a unique well-characterised clinical cohort to better understand the relationship between spinal cord atrophy and clinical disability and explore the relationship between pathologically-relevant biomarker candidates identified in the previous chapter and clinicoradiographic disability accumulation. In our cohort, we did not identify a relationship between spinal cord atrophy and clinically-measured disability. While we did observe an increase in CSF opsonin expression in MS compard to control individuals, we did we identify a relationship between CSF opsonins and clinicoradiographic disability. However, leveraging the full proteomics dataset, we demonstrated

that MS was associated with accelerated ageing. These findings underscore the nuances of studying living MS cohorts for molecular biomarker discovery of disease progression and highlight the power and sensitivity of pathologically-derived outcomes.

We first assessed the relationship between clinical disability and estimated spinal cord atrophy measured using legacy brain scans and the highly sensitive GBSI pipeline. While previous studies have been able to identify a strong link between spinal cord atrophy and clinical disability across the disease course (Valsasina *et al.* 2015, Moccia *et al.* 2020), we did not observe such a relationship. The over-representation of patients with CIS in our cohort is a likely confound as many remained clinically stable during this early stage of their disease. In fact, 21/57 and 20/70 patients were still classified as CIS in the 1-year and 4-year atrophy analyeses, respectively. Previous work has demonstrated minimal longitudinal spinal cord volume changes in this patient population, especially in those who remained CIS after follow-up (Casserly *et al.* 2018). In fact, on the whole, our cohort was also quite stable clinically with less than 30 CDW events reported. Therefore, we will continue to follow these MS patients to better ascertain their clinical trajectory and see how relationships may emerge. From a technical perspective, the measurement of atrophy in such a small structure like the spinal cord, even with the most robust methods, is hampered by many technical challenges (Moccia *et al.* 2019b). These limitations are amplified when trying to measure the small effect sizes that would be expected in our CIS-enriched cohort based on previous work (Brex *et al.* 2001, Rashid *et al.* 2006, Brownlee *et al.* 2017).

Our findings from Chapter 2 also implicated the presence of lesions anywhere in the spinal cord neuraxis as a factor that influences disability progression. Given that lesion presence did not relate to CSA in our post-mortem analysis discussed in Chapter 3, spinal cord lesions would have served

as a precision variable in our analysis rather than a confounding covariate. Therefore, our inability to measure spinal cord lesion burden in this study may have contributed to the lack of relationship detected between atrophy and disability.

In addition, spinal cord atrophy measures were not corrected for any potential covariates in this study as there is not consensus on the factors of relevance and our sample size did not provide adequate degrees of freedom for the correction of multiple variables (Bédard *et al.* 2022). Further work investigating the determinants of spinal cord atrophy in healthy populations will be required to limit variability that may mask the biological signal of interest. Overall, new clinical research must also be performed to identify more sensitive clinical measuremetns of progression as currently available tools based on the EDSS are subject to fluctuations, especially in the short-term, which limits the ability to disintangle meaningful signal from noise (Kalincik *et al.* 2015).

In this chapter, we demonstrated that CSF expression of all SOMAmers mapping to IgG were significantly elevated in MS patients compared to controls. This finding is concordant with the diagnostic potential of oligoclonal bands which are used clinically (Thompson *et al.* 2018). However, oligoclonal bands measure intrathecal synthesis of IgG. Therefore, it is interesting that a measurement of IgG agnostic to its source (intrathecal vs peripheral) also demonstrates discriminative potential, especially when the compartor cohort has other neurological diseases. The SOMAmer mapping to the C1qC subunit also displayed a slight, but significant, increase in MS compared to control CSF while the SOMAmer more broadly binding to C1q did not. Elevations of C1q in MS compared to control CSF have been reported in two previous studies (Lindblom *et al.* 2016, Håkansson *et al.* 2020). However, our findings suggest that selection of a

target epitope for protein immunoassays, like SomaScan® or ELISA, is critical and must be considered when developing diagnostic tests.

Disability at the time of LP, as measured by ARMSS, correlated with the majority of SOMAmers mapping to IgG. A correlation was also observed with C1q but not the C1qC subunit. Further analyses did not observe relationships with IgG or C1q and longitudinal measures of disability or atrophy measured over 1-year or 4-years. Previous work has demonstrated that intrathecal IgG synthesis, as measured by oligoclonal bands or IgG index, is associated with faster disability worsening (Izquierdo *et al.* 2002, Tintore *et al.* 2015, Gasperi *et al.* 2019). However, cohort sizes were much larger in these studies compared to our work. Measurements of intrathecal IgG have also demonstrated correlations with serum NfL, a marker of axonal damage (Sinah *et al.* 2020), but no relationships with spinal cord atrophy have ever been investigated. We unfortunatley did not have paired proteomic measurements in blood and therefore the IgG measured does not specifically represent that of intrathecal origin. However, given the results of the previous chapter, we hypothesised that IgG levels more broadly may have a predictive role clinically. These findings suggest that an indiscrimant measure of IgG may not have the required sensitivity as a prognostic biomarker during life. However, we also must consider that molecular biomarkers may not correlate well with currently used clinicoradiographic tools because the biomarkers themselves are more sensitive to underlying pathological processes than the surrogate measures (Bielekova *et al.* 2004). This is underscored by our work in the previous chapter that demonstrated a lack of correlation between axonal loss and CSA whilst CSF IgG was correlated with axonal loss.

Through analysis of the broader anylates measured in the CSF, our data suggests that MS patients exhibit accelerated ageing. Our findings indicate that the use of chronological age in modeling MS

disability clinicoradiographically may be fundamentally flawed. Studies based on orthaganol experimental paradigms, namely MRI and epigenomic assessment, have also reported accelerated ageing in MS (Theodoropoulou *et al.* 2019, Cole *et al.* 2020, Kular *et al.* 2022). While our work does contrast the finidngs of a recent similar CSF-based analysis, we measured more proteins and used a larger control set with a broader age range (Kosa *et al.* 2022a). In fact, only 39% of the proteins found in the final elastic net model were measured in the previous study. Therefore, these findings suggest that the use of biologically-measured age in future studies may represent a more appropriate covariate in analysis workflows and tool used when tabulating novel disability assessments.

Overall, this chapter provides us with important insights into the difficulties of identifying molecular biomarkers of MS disease progression in living MS cohorts. Further research must be done to identify better metrics of disability progression that better reflect underlying pathological processes to be used for CSF biomarker modeling studies. However, we still believe that the approach we employed in the previous chapter has promise to develop pathologically-relevant biomarkers which can be validated in clinical cohorts with sufficient follow-up and characterisation.

5. Conclusions and Future Perspectives

5.1 Thesis Summary

In summary, this thesis has furthered our understanding of the determinants of spinal cord pathology in MS. Leveraging a large cohort of post-mortem specimen, we observed that demyelination was commonly inflammatory at end-stage disease and predicted a more aggressive clinical course. The topography of demyelination was shown to follow patterns of venous drainage and impact a limited circumference of the subpial surface. We also observed that axonal loss and myeloid inflammation were salient features of MS spinal cord pathology that were interrelated. Interestingly, lesion load was not a strong correlate of axonal loss. Post-mortem cerebrospinal fluid proteomics identified a signature, enriched in immunoglobulins and complement, that segregated with the degree of spinal cord axonal loss and demyelination. However, the relationship with demyelination was not driven by subpial disease. We investigated the ability of this signature to predict clinicoradiographic disease progression in living MS patients. We were unable to identify relationships with CSF opsonin expression and clinically measured disease progression nor spinal cord atrophy. In fact, spinal cord atrophy did not reliably predict a more aggressive disease course. Taken together, our findings paint an interesting picture and nominate converging mechanisms for the pathogenesis of spinal cord demyelination and axonal loss. The vascular distribution of demyelination, subpial sparing, and pathological relationships with CSF opsonins and activated myeloid cells all point to the perivascular space. In fact, one could surmise that vascular dysfunction in tandem with CSF opsonins and myeloid cell activation may independently set the stage for demyelination and axonal loss in non-lesional areas. The lack of biomarker validation in our clinical cohort only underscores the fact that pathological outcomes go beyond the resolution of present *in vivo* assessments. In fact, accelerated ageing was a striking feature of the living MS

CSF which suggests new modelling approaches may be needed to characterise MS clinicoradiographic disease progression. Our work has left many interesting outstanding questions which we are currently pursuing through the studies detailed below.

5.2 Ongoing Work and Future Directions

5.2.1 Integrated Transcriptomics to Investigate Divergent Molecular Profiles of Grey and White Matter Spinal Cord Tissue

Our topographical study described in Chapter 2, coupled with previous pathological studies, has hinted that the inflammatory architecture differs between grey and white matter of the spinal cord (Gilmore *et al.* 2006, Gilmore *et al.* 2009a, Gilmore *et al.* 2009b, DeLuca *et al.* 2013). However, the molecular underpinnings of these differences have yet to be elucidated. With generous support from 10x Genomics and MS Treatment, Research, and Education, we will leverage next-generation transcriptomics approaches to understand the molecular differences between normal-appearing and lesional white and grey matter of the MS spinal cord. Tissue has already been analysed histopathologically to quantify the distribution of demyelination and its inflammatory activity as seen in Chapter 2. Cases that harbour distinct inflammatory and inactive lesions of the white and grey matter with paired normal-appearing regions will be analysed using the 10x Genomics FFPE spatial transcriptomics and single-cell RNA flex assays. The 10x Genomics Visium Spatial Transcriptomics platform for FFPE tissue is the most modern and cutting-edge approach to understanding gene regulation changes in the context of histopathology (Asp *et al.* 2020). In the Visium approach, tissue is sectioned onto capture areas and processed for light or fluorescence microscopy to generate a histological map. However, serial sections previously analysed microscopically can also be used as overlays for gene expression. In our study, we will leverage our previously stained sections for PLP and CD68. Each Visium slide contains four tissue

capture areas (6.5mm by 6.5mm) that consist of ~5,000 55µm diameter spots. Each spot is comprised of millions of capture oligonucleotides (**Figure 6.1**).

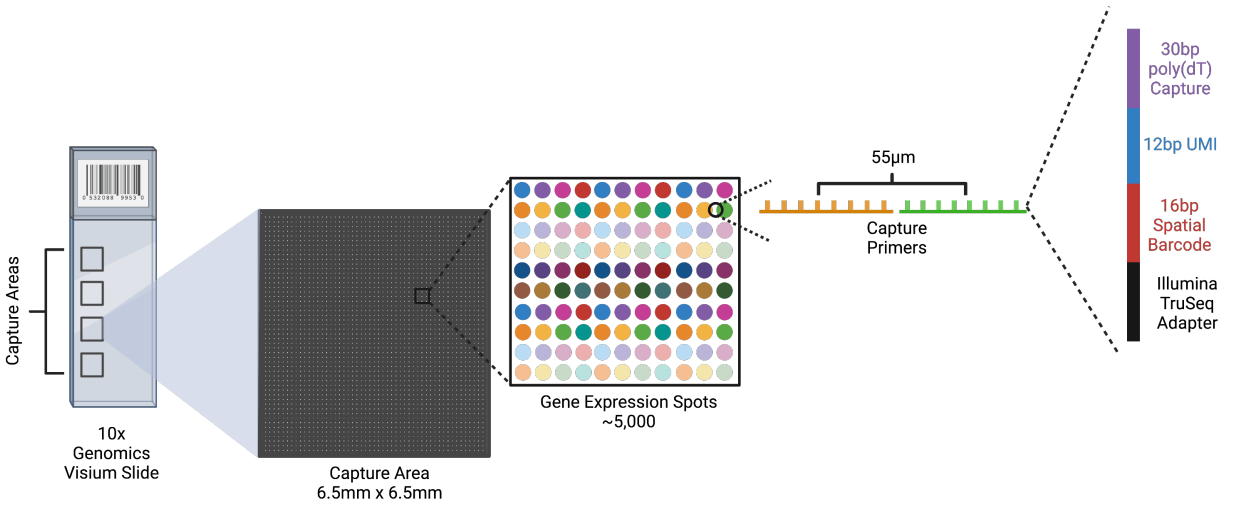


Figure 6.1. 10x Genomics Visium Spatial Transcriptomics Technology. Capture areas where tissue is mounted contain ~5,000 gene expression spots. Each gene expression spot consists of capture primers that span the whole transcriptome and every capture primer is comprised of a 30bp poly(dT) capture sequence, 12bp unique molecular identifier, 16bp spatial barcode, and Illumina TruSeq adapter.

The workflow we are employing for our study has proven reproducibility and is described in detail in **Figure 6.2**. Integrating this approach with the single-cell RNA flex assay improves resolution down to the single-cell level. Overall, combining these two innovative approaches with a pathologically-informed case selection paradigm will allow us to map single-cell profiles onto spatial regions of interest. Paired statistical approaches will provide adequate power to understand the differences between normal-appearing and lesional white and grey matter spinal cord tissue in MS. This molecular data provides us with the opportunity to better characterise MS heterogeneity and narrow in on the mediators that distinguish white and grey matter pathology within an anatomical region important for disease outcome.

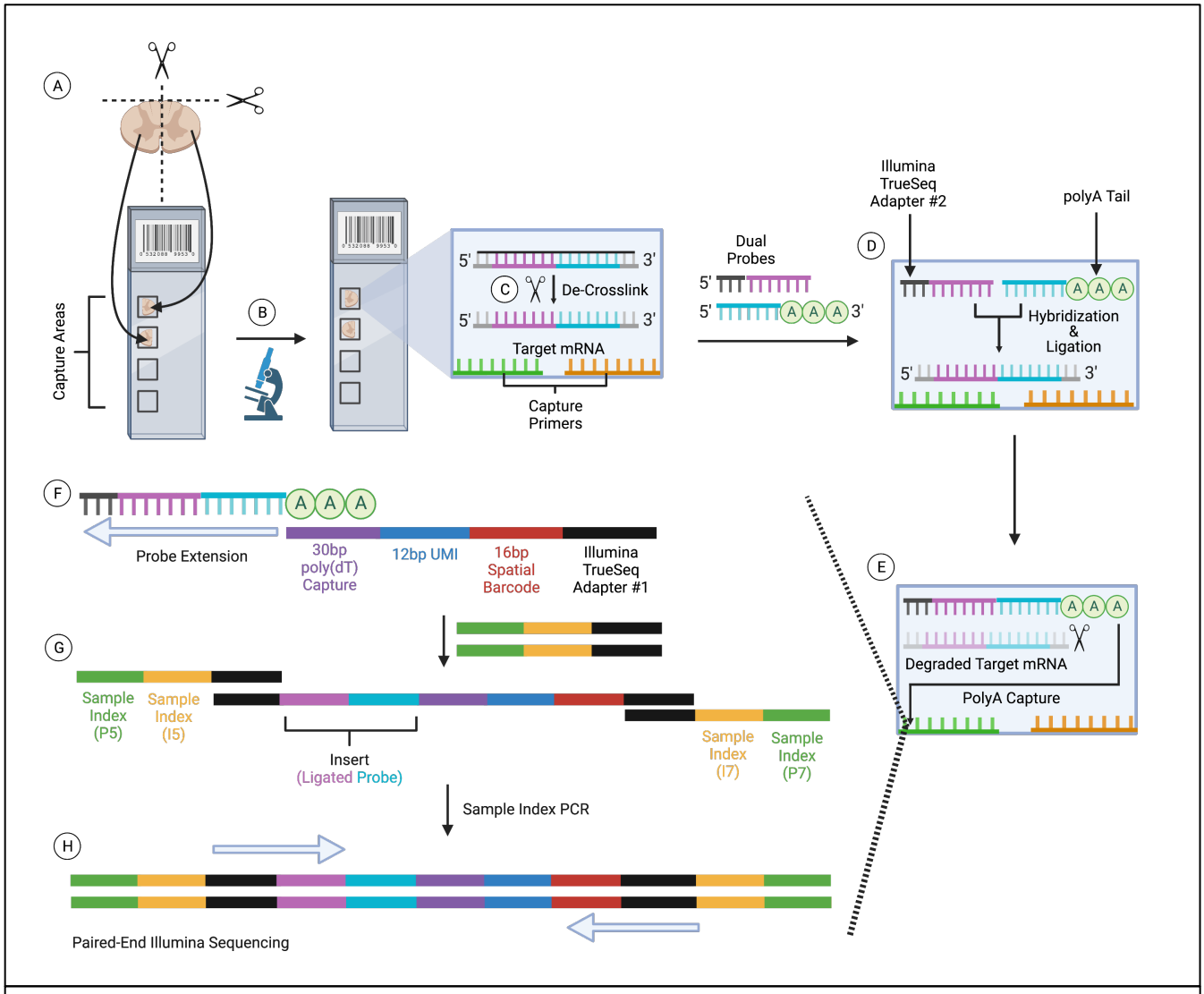


Figure 6.2. 10x Genomics Visium Spatial Transcriptomics Workflow. Tissue is cut and mounted onto capture areas (**A**) before being processed for microscopy (**B**). Target mRNA is de-crosslinked (**C**) before being hybridized and ligated with dual probes (**D**). Target mRNA is degraded with RNAse and the hybridized strand is captured through the polyA tail (**E**). Probes are extended (**F**) and dual indices are added by polymerase chain reaction (PCR) (**G**) before Illumina paired-end sequencing (**H**).

5.2.2 Assessment of Wallerian Degeneration in the Multiple Sclerosis Spinal Cord

In Chapter 3, we did not observe a tight connection between lesions and axonal loss, indicating that Wallerian degeneration may not be a strong driver of spinal cord axonal pathology. However, Wallerian degeneration in the human MS spinal cord has never been explored in detail. We have access to a unique autopsy cohort to study the relationship between lesions, Wallerian

degeneration, and axonal loss in the MS spinal cord. 10 MS cases have already been analysed post-mortem using advanced myelin water imaging techniques. This method provides detailed resolution to assess lesional pathology throughout the length of the spinal cord. Lesions of the motor tracts will be defined in order to target immunohistochemical analyses of interconnected non-lesional areas. Sections will be stained using Palmgren silver to quantify axonal loss and NPY-Y1R (Dziedzic *et al.* 2010) to assess Wallerian degeneration. Overall, this combined MRI-histology strategy leverages the power of both methods to answer a long-standing unanswered question about the pathogenesis of MS spinal cord neurodegeneration.

5.2.3 Tissue-Derived Immunohistochemical and Proteomic Relationships with Opsonins

Our findings in Chapter 3 have implicated circulating opsonins in the pathology of spinal cord axonal loss. However, a unified understanding of the mechanisms by which the CSF and parenchymal environments promote axonal loss has yet to be explored in detail. We have been fortunate to receive generous funding from the United States Department of Defense and European Charcot Foundation to 1) characterise the extent and distribution of opsonins within our well-characterised spinal cord post-mortem tissue and 2) extend our proteomic profiling to spinal cord tissue already assessed for axonal loss.

To accomplish the first aim, we will employ a robust multiplex staining approach to reconstruct the cellular architecture of the spinal cord with cell-specific markers so that we can better characterise the distribution of opsonin molecules. Semi-quantiative scoring and pixel quantitation algorithms using pre-defined trajectories from past studies will allow us to investigate the expression patterns of these markers in MS tissue and the relationship of these biomarkers with pre-collected robust pathological outcomes, notably axonal loss. The multiplex method will allow

us to directly visualise individual and combinatorial relationships between candidate biomarkers and pathologic outcomes within the same tissue slice. We will stratify cases by the extremes (top and bottom quartile) of staining patterns identified for each candidate protein to generate new comparison groups. Using our WPCNA pipeline, we will then identify new CSF biomarkers that differ between MS cases at the extremes of histochemical expression of IgG and C1q for further exploration.

To complete our second aim, we will isolate NAWM areas where axonal loss has been quantified through laser capture microdissection and perform downstream proteomics using the same LC-MS/MS methods already deployed on paired CSF samples. Parenchymal protein networks that correlate with the extent of spinal cord axonal loss and/or the opsonin-enriched CSF protein networks will be assessed in greater detail by gene ontology, cell type, and MS GWAS target gene enrichment analyses to identify pathways that mediate axonal loss. New hub proteins identified can then be explored using the multiplex immunohistochemistry workflow described above.

We believe that by leveraging this novel and iterative approach, we are uniquely positioned to begin the process of disentangling how the intrathecal and parenchymal compartments interact to promote axonal loss in the MS spinal cord with hopes of casting light onto novel pathogenic mechanisms of MS-related neurodegeneration that may be targeted therapeutically.

5.2.4 Immunoglobulin Specificity Profiling of Post-Mortem Cerebrospinal Fluid

There is a long history for the search for antigens involved in MS tissue damage. Our work aligns with previous clinical studies that have implicated immunoglobulins in the CSF as key players in the process of axonal damage (Farina *et al.* 2017, Sinah *et al.* 2020). However, the mechanism of

immunoglobulin-mediated damage has remained elusive. One hypothesis is that human autoantigens or molecular mimicry to pathogen-derived antigens promotes a CNS inflammatory reaction. In fact, epsilon-toxin, derived from *Clostridium perfringens*, has been shown to form pores in membranes, causes vascular damage, and promote demyelination (Rumah *et al.* 2013, Wagley *et al.* 2019, Ma *et al.* 2023). Therefore, opsonin reactions to pathogens or their products may explain the vascular-centred relationships we have observed. To test these hypotheses, we formed a new collaboration with the University of California San Francisco, a centre with renowned expertise in state-of-the-art antigen discovery technologies (O'Donovan *et al.* 2020, Zamecnik *et al.* 2020). We will probe the specificty of the antibodies found within our post-mortem CSF that associated with axonal loss. Phage immunoprecipitation sequencing of post-mortem CSF will be used to identify antibody targets that are associated with quantitative metrics of axonal loss (**Figure 6.3**). In short, a bacteriophage peptide library, spanning the whole human and viral/bacterial/fungal pathogen proteomes, will be incubated with antibody containing CSF and spinal cord homogenates. Bacteriophage-antibody complexes will be purified, and bacteriophage nucleic acid will be sequenced. Biocomputational mapping of these sequences will allow us to identify the peptides expressed by the antibody-captured bacteriophages. Candidates overlapping between CSF and spinal cord homogenates across cases will be studied further. This unique approach capitalises on deep endophenotyping of pathological samples to inform an innovative antigen discovery strategy aimed at understanding the contribution of antibodies to axonal loss in MS.

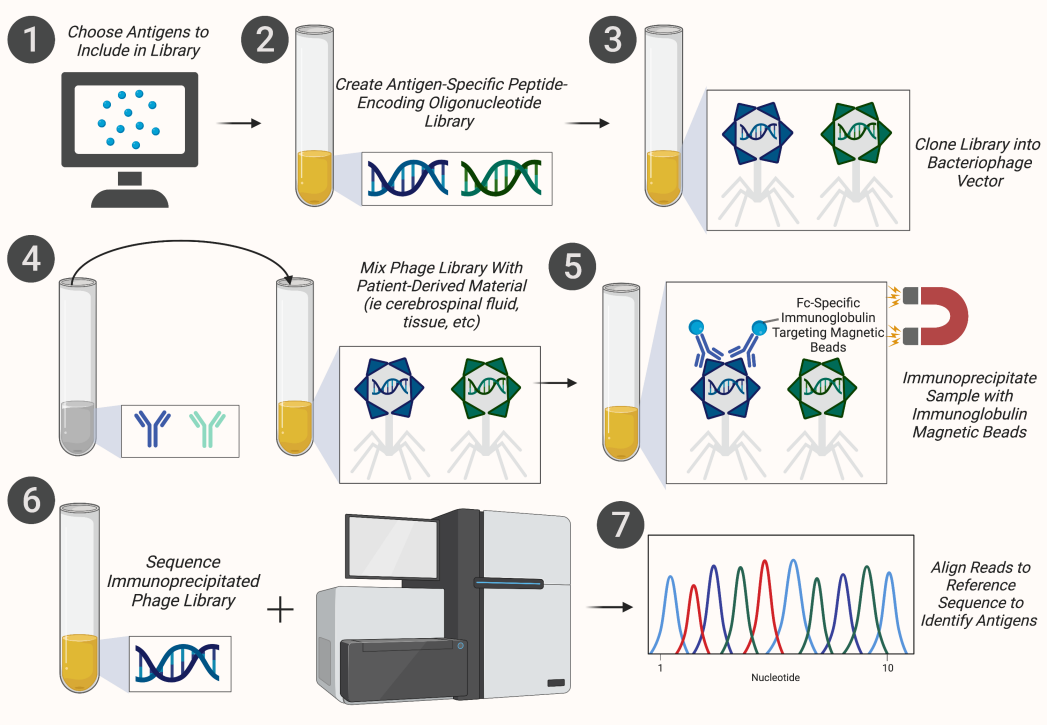


Figure 6.3. Phage Immunoprecipitation Sequencing Workflow. The process of phage immunoprecipitation sequencing begins by identifying antigens of interest (1) and creating an oligonucleotide library (2). This library is cloned into a bacteriophage vector (3) and mixed with patient material (4). Fc-specific magnetic beads immunoprecipitate antibody-bound phages (5). Nucleic acid is then sequenced from the recovered phages (6) and reads are aligned to the oligonucleotide library reference sequences to identify the antigens bound by patient antibodies (7).

5.2.5 Long-Term Follow-Up of Clinical Cohorts and Expansion of Phenotypic Characterisation for Biomarker Discovery

The approach to identify novel biomarkers of MS outcome by performing targeted validation of pathologically-relevant molecules in well-characterised living MS cohorts is extremely powerful. While our preliminary analysis did not cross-validate biomarkers of axonal loss, we will continue to monitor clinical and radiographic outcomes in our living cohort as their phenotype begins to differentiate. In addition, as part of our funding from the Department of Defense, we have the opportunity to generate CSF proteomic data from a new living MS cohort recruited from the Mandell MS Center. Patients at the Mandell MS Center undergo a battery of clinical tests beyond

EDSS assessment, including Timed 25 Foot Walk, 9-Hole Peg Test, and new sensitive rehabilitation tests. These clinical tests will allow for more sensitive phenotyping of patient trajectories. Overall, this cohort provides complementary clinical data that will facilitate validating pathologically-relevant biomarkers.

6. References

Absinta, M., D. Maric, M. Gharagozloo, T. Garton, M. D. Smith, J. Jin, K. C. Fitzgerald, A. Song, P. Liu, J. P. Lin, T. Wu, K. R. Johnson, D. B. McGavern, D. P. Schafer, P. A. Calabresi and D. S. Reich (2021). "A lymphocyte-microglia-astrocyte axis in chronic active multiple sclerosis." Nature **597**(7878): 709-714.

Absinta, M., L. Vuolo, A. Rao, G. Nair, P. Sati, I. C. Cortese, J. Ohayon, K. Fenton, M. I. Reyes-Mantilla, D. Maric, P. A. Calabresi, J. A. Butman, C. A. Pardo and D. S. Reich (2015). "Gadolinium-based MRI characterization of leptomeningeal inflammation in multiple sclerosis." Neurology **85**(1): 18-28.

Absinta, M., P. Sati, F. Masuzzo, G. Nair, V. Sethi, H. Kolb, J. Ohayon, T. Wu, I. C. M. Cortese and D. S. Reich (2019). "Association of Chronic Active Multiple Sclerosis Lesions With Disability In Vivo." JAMA Neurol **76**(12): 1474-1483.

Absinta, M., P. Sati, F. Masuzzo, G. Nair, V. Sethi, H. Kolb, J. Ohayon, T. Wu, I. C. M. Cortese and D. S. Reich (2019). "Association of Chronic Active Multiple Sclerosis Lesions With Disability In Vivo." JAMA Neurology **76**(12): 1474-1483.

Adams, C. W., Y. H. Abdulla, E. M. Torres and R. N. Poston (1987). "Periventricular lesions in multiple sclerosis: their perivenous origin and relationship to granular ependymitis." Neuropathol Appl Neurobiol **13**(2): 141-152.

Aloisi, F., B. Serafini, R. Magliozzi, O. W. Howell and R. Reynolds (2010). "Detection of Epstein-Barr virus and B-cell follicles in the multiple sclerosis brain: what you find depends on how and where you look." Brain **133**(Pt 12): e157.

Androdias, G., R. Reynolds, M. Chanal, C. Ritleng, C. Confavreux and S. Nataf (2010). "Meningeal T cells associate with diffuse axonal loss in multiple sclerosis spinal cords." Ann Neurol **68**(4): 465-476.

Arrambide, G., A. Rovira, J. Sastre-Garriga, C. Tur, J. Castilló, J. Río, A. Vidal-Jordana, I. Galán, B. Rodríguez-Acevedo, L. Midaglia, C. Nos, P. Mulero, M. J. Arévalo, M. Comabella, E. Huerga, C. Auger, X. Montalban and M. Tintore (2018). "Spinal cord lesions: A modest contributor to diagnosis in clinically isolated syndromes but a relevant prognostic factor." Mult Scler **24**(3): 301-312.

Asp, M., J. Bergenstråhle and J. Lundeberg (2020). "Spatially Resolved Transcriptomes—Next Generation Tools for Tissue Exploration." BioEssays **42**(10): 1900221.

Australia and C. New Zealand Multiple Sclerosis Genetics (2009). "Genome-wide association study identifies new multiple sclerosis susceptibility loci on chromosomes 12 and 20." Nat Genet **41**(7): 824-828.

Axelsson, M., C. Malmeström, S. Nilsson, S. Haghighi, L. Rosengren and J. Lycke (2011). "Glial fibrillary acidic protein: a potential biomarker for progression in multiple sclerosis." J Neurol **258**(5): 882-888.

Baranzini, S., S. Sawcer, C. International Multiple Sclerosis Genetics and M. S. C. Multiple (2022). Genetic analysis of multiple sclerosis severity identifies a novel locus and implicates CNS resilience as a major determinant of outcome, Research Square.

Barnett, M. H. and J. W. Prineas (2004). "Relapsing and remitting multiple sclerosis: Pathology of the newly forming lesion." Annals of Neurology **55**(4): 458-468.

Barnett, M. H., J. D. E. Parratt, E.-S. Cho and J. W. Prineas (2009). "Immunoglobulins and complement in postmortem multiple sclerosis tissue." Annals of Neurology **65**(1): 32-46.

Bartanusz, V., D. Jezova, B. Alajajian and M. Digicaylioglu (2011). "The blood-spinal cord barrier: morphology and clinical implications." Ann Neurol **70**(2): 194-206.

Bebo, B., I. Cintina, N. LaRocca, L. Ritter, B. Talente, D. Hartung, S. Ngorsuraches, M. Wallin and G. Yang (2022). "The Economic Burden of Multiple Sclerosis in the United States: Estimate of Direct and Indirect Costs." Neurology **98**(18): e1810-e1817.

Bédard, S. and J. Cohen-Adad (2022). "Automatic measure and normalization of spinal cord cross-sectional area using the pontomedullary junction." Frontiers in Neuroimaging **1**.

Bell, J. S., J. I. Spencer, R. L. Yates and G. C. DeLuca (2018). "The cortical blood-brain barrier in multiple sclerosis: a gateway to progression?" J Neurol **265**(4): 966-967.

Bevan, R. J., R. Evans, L. Griffiths, L. M. Watkins, M. I. Rees, R. Magliozzi, I. Allen, G. McDonnell, R. Kee, M. Naughton, D. C. Fitzgerald, R. Reynolds, J. W. Neal and O. W. Howell (2018). "Meningeal inflammation and cortical demyelination in acute multiple sclerosis." Ann Neurol **84**(6): 829-842.

Bhan, A., C. Jacobsen, I. Dalen, N. Bergsland, R. Zivadinov, G. Alves, K.-M. Myhr and E. Farbu (2021). "CSF neurofilament light chain predicts 10-year clinical and radiologic worsening in multiple sclerosis." Multiple Sclerosis Journal - Experimental, Translational and Clinical **7**(4): 20552173211060337.

Bielekova, B. and R. Martin (2004). "Development of biomarkers in multiple sclerosis." Brain **127**(7): 1463-1478.

Bischof, A., N. Papinutto, A. Keshavan, A. Rajesh, G. Kirkish, X. Zhang, J. M. Mallott, C. Asteggiano, S. Sacco, T. J. Gundel, C. Zhao, W. A. Stern, E. Caverzasi, Y. Zhou, R. Gomez, N. R. Ragan, A. Santaniello, A. H. Zhu, J. Juwono, C. J. Bevan, R. M. Bove, E. Crabtree, J. M. Gelfand, D. S. Goodin, J. S. Graves, A. J. Green, J. R. Oksenberg, E. Waubant, M. R. Wilson,

S. S. Zamvil, S. F. M.-E. T. University of California, B. A. C. Cree, S. L. Hauser and R. G. Henry (2022). "Spinal Cord Atrophy Predicts Progressive Disease in Relapsing Multiple Sclerosis." Annals of Neurology **91**(2): 268-281.

Bitsch, A., J. Schuchardt, S. Bunkowski, T. Kuhlmann and W. Brück (2000). "Acute axonal injury in multiple sclerosis. Correlation with demyelination and inflammation." Brain **123 (Pt 6)**: 1174-1183.

Bjartmar, C., G. Kidd, S. Mörk, R. Rudick and B. D. Trapp (2000). "Neurological disability correlates with spinal cord axonal loss and reduced N-acetyl aspartate in chronic multiple sclerosis patients." Ann Neurol **48**(6): 893-901.

Bjartmar, C., R. P. Kinkel, G. Kidd, R. A. Rudick and B. D. Trapp (2001). "Axonal loss in normal-appearing white matter in a patient with acute MS." Neurology **57**(7): 1248-1252.

Bjornevik, K., M. Cortese, B. C. Healy, J. Kuhle, M. J. Mina, Y. Leng, S. J. Elledge, D. W. Niebuhr, A. I. Scher, K. L. Munger and A. Ascherio (2022). "Longitudinal analysis reveals high prevalence of Epstein-Barr virus associated with multiple sclerosis." Science **375**(6578): 296-301.

Bø, L., C. A. Vedeler, H. I. Nyland, B. D. Trapp and S. J. Mørk (2003). "Subpial demyelination in the cerebral cortex of multiple sclerosis patients." J Neuropathol Exp Neurol **62**(7): 723-732.

Bodini, B., M. Veronese, D. García-Lorenzo, M. Battaglini, E. Poirion, A. Chardain, L. Freeman, C. Louapre, M. Tchikviladze, C. Papeix, F. Dollé, B. Zalc, C. Lubetzki, M. Bottlaender, F. Turkheimer and B. Stankoff (2016). "Dynamic Imaging of Individual Remyelination Profiles in Multiple Sclerosis." Ann Neurol **79**(5): 726-738.

Bot, J. C. J., F. Barkhof, C. H. Polman, G. J. L. à. Nijeholt, V. de Groot, E. Bergers, H. J. Ader and J. A. Castelijns (2004). "Spinal cord abnormalities in recently diagnosed MS patients." Neurology **62**(2): 226.

Breij, E. C., B. P. Brink, R. Veerhuis, C. van den Berg, R. Vloet, R. Yan, C. D. Dijkstra, P. van der Valk and L. Bö (2008). "Homogeneity of active demyelinating lesions in established multiple sclerosis." Ann Neurol **63**(1): 16-25.

Brex, P. A., S. M. Leary, J. I. O'Riordan, K. A. Miszkiel, G. T. Plant, A. J. Thompson and D. H. Miller (2001). "Measurement of spinal cord area in clinically isolated syndromes suggestive of multiple sclerosis." J Neurol Neurosurg Psychiatry **70**(4): 544-547.

Brown, J. W. L., A. Coles, D. Horakova, E. Havrdova, G. Izquierdo, A. Prat, M. Girard, P. Duquette, M. Trojano, A. Lugaresi, R. Bergamaschi, P. Grammond, R. Alroughani, R. Hupperts, P. McCombe, V. Van Pesch, P. Sola, D. Ferraro, F. Grand'Maison, M. Terzi, J. Lechner-Scott, S. Flechter, M. Slee, V. Shaygannejad, E. Pucci, F. Granella, V. Jokubaitis, M. Willis, C. Rice, N. Scolding, A. Wilkins, O. R. Pearson, T. Ziemssen, M. Hutchinson, K. Harding, J. Jones, C.

McGuigan, H. Butzkueven, T. Kalincik and N. Robertson (2019). "Association of Initial Disease-Modifying Therapy With Later Conversion to Secondary Progressive Multiple Sclerosis." Jama **321**(2): 175-187.

Brownlee, W. J., C. Tur, A. Manole, A. Eshaghi, F. Prados, K. A. Miszkiel, C. A. M. G. Wheeler-Kingshott, H. Houlden and O. Ciccarelli (2022). "HLA-DRB1*1501 influences long-term disability progression and tissue damage on MRI in relapse-onset multiple sclerosis." Multiple Sclerosis Journal: 13524585221130941.

Brownlee, W. J., D. R. Altmann, P. Alves Da Mota, J. K. Swanton, K. A. Miszkiel, C. G. Wheeler-Kingshott, O. Ciccarelli and D. H. Miller (2017). "Association of asymptomatic spinal cord lesions and atrophy with disability 5 years after a clinically isolated syndrome." Mult Scler **23**(5): 665-674.

Bruschi, N., G. Boffa and M. Inglese (2020). "Ultra-high-field 7-T MRI in multiple sclerosis and other demyelinating diseases: from pathology to clinical practice." European Radiology Experimental **4**(1): 59.

Bush, W. S., J. L. McCauley, P. L. DeJager, S. M. Dudek, D. A. Hafler, R. A. Gibson, P. M. Matthews, L. Kappos, Y. Naegelin, C. H. Polman, S. L. Hauser, J. Oksenberg, J. L. Haines, M. D. Ritchie and C. International Multiple Sclerosis Genetics (2011). "A knowledge-driven interaction analysis reveals potential neurodegenerative mechanism of multiple sclerosis susceptibility." Genes Immun **12**(5): 335-340.

Bussas, M., M. El Husseini, L. Harabacz, V. Pineker, S. Grahl, V. Pongratz, A. Berthele, I. Riederer, C. Zimmer, B. Hemmer, J. S. Kirschke and M. Mühlau (2022). "Multiple sclerosis lesions and atrophy in the spinal cord: Distribution across vertebral levels and correlation with disability." NeuroImage: Clinical **34**: 103006.

Callegari, I., T. Derfuss and E. Galli (2021). "Update on treatment in multiple sclerosis." La Presse Médicale **50**(2): 104068.

Calvi, A., M. A. Clarke, F. Prados, D. Chard, O. Ciccarelli, M. Alberich, D. Pareto, M. Rodríguez Barranco, J. Sastre-Garriga, C. Tur, A. Rovira and F. Barkhof (2023). "Relationship between paramagnetic rim lesions and slowly expanding lesions in multiple sclerosis." Mult Scler **29**(3): 352-362.

Candia, J., G. N. Daya, T. Tanaka, L. Ferrucci and K. A. Walker (2022). "Assessment of variability in the plasma 7k SomaScan proteomics assay." Scientific Reports **12**(1): 17147.

Casserly, C., E. E. Seyman, P. Alcaide-Leon, M. Guenette, C. Lyons, S. Sankar, A. Svendrovski, S. Baral and J. Oh (2018). "Spinal Cord Atrophy in Multiple Sclerosis: A Systematic Review and Meta-Analysis." J Neuroimaging **28**(6): 556-586.

Cendrowski, W. S. (1986). "Progression index and disability status in multiple sclerosis: a resurvey of 207 patients in central Poland." Schweiz Arch Neurol Psychiatr (1985) **137**(4): 5-13.

Chang, I., L. Kappos, G. Giovannoni, P. A. Calabresi, A. Sandrock, W. Cheng, S. Xiao, K. Riester, S. Belachew, A. Deykin and B. Zhu (2022). "Overall Disability Response Score: An integrated endpoint to assess disability improvement and worsening over time in patients with multiple sclerosis." Mult Scler **28**(14): 2263-2273.

Charcot, J. M. (1865). Sclrose des cordons latÈraux de la moelle ÈpiniËre chez une femme hystÈrique atteinte de contracture permanente des quatre membres. [Paris], [Typographie F. Malteste].

Chawade, A., E. Alexandersson and F. Levander (2014). "Normalyzer: a tool for rapid evaluation of normalization methods for omics data sets." Journal of proteome research **13**(6): 3114-3120.

Choi, S. R., O. W. Howell, D. Carassiti, R. Magliozzi, D. Gveric, P. A. Muraro, R. Nicholas, F. Roncaroli and R. Reynolds (2012). "Meningeal inflammation plays a role in the pathology of primary progressive multiple sclerosis." Brain **135**(Pt 10): 2925-2937.

Chu, A. B., J. L. Sever, D. L. Madden, M. Iivanainen, M. Leon, W. Wallen, B. R. Brooks, Y. J. Lee and S. Houff (1983). "Oligoclonal IgG bands in cerebrospinal fluid in various neurological diseases." Ann Neurol **13**(4): 434-439.

Ciccarelli, O., D. J. Werring, G. J. Barker, C. M. Griffin, C. A. Wheeler-Kingshott, D. H. Miller and A. J. Thompson (2003). "A study of the mechanisms of normal-appearing white matter damage in multiple sclerosis using diffusion tensor imaging--evidence of Wallerian degeneration." J Neurol **250**(3): 287-292.

Cole, J. H., J. Raffel, T. Friede, A. Eshaghi, W. J. Brownlee, D. Chard, N. De Stefano, C. Enzinger, L. Pirpamer, M. Filippi, C. Gasperini, M. A. Rocca, A. Rovira, S. Ruggieri, J. Sastre-Garriga, M. L. Stromillo, B. M. J. Uitdehaag, H. Vrenken, F. Barkhof, R. Nicholas, O. Ciccarelli and M. s. group (2020). "Longitudinal Assessment of Multiple Sclerosis with the Brain-Age Paradigm." Annals of Neurology **88**(1): 93-105.

Comabella, M., M. Fernández, R. Martin, S. Rivera-Vallvé, E. Borrás, C. Chiva, E. Julià, A. Rovira, E. Cantó, J. C. Alvarez-Cermeño, L. M. Villar, M. Tintoré and X. Montalban (2010). "Cerebrospinal fluid chitinase 3-like 1 levels are associated with conversion to multiple sclerosis." Brain **133**(Pt 4): 1082-1093.

Compston, D. A., B. P. Morgan, A. K. Campbell, P. Wilkins, G. Cole, N. D. Thomas and B. Jasani (1989). "Immunocytochemical localization of the terminal complement complex in multiple sclerosis." Neuropathol Appl Neurobiol **15**(4): 307-316.

Confavreux, C. and A. Compston (2006). "The natural history of multiple sclerosis." McAlpine's Multiple Sclerosis: 183-272.

Confavreux, C. and S. Vukusic (2006). "Age at disability milestones in multiple sclerosis." Brain **129**(Pt 3): 595-605.

Confavreux, C., S. Vukusic, T. Moreau and P. Adeleine (2000). "Relapses and Progression of Disability in Multiple Sclerosis." New England Journal of Medicine **343**(20): 1430-1438.

Consortium, I. M. S. G. (2019). "Multiple sclerosis genomic map implicates peripheral immune cells and microglia in susceptibility." Science **365**(6460): eaav7188.

Cooze, B. J., M. Dickerson, R. Loganathan, L. M. Watkins, E. Grounds, B. R. Pearson, R. J. Bevan, B. P. Morgan, R. Magliozzi, R. Reynolds, J. W. Neal and O. W. Howell (2022). "The association between neurodegeneration and local complement activation in the thalamus to progressive multiple sclerosis outcome." Brain Pathol **32**(5): e13054.

Correale, J., M. I. Gaitán, M. C. Ysrraelit and M. P. Fiol (2016). "Progressive multiple sclerosis: from pathogenic mechanisms to treatment." Brain **140**(3): 527-546.

Cotton, F., H. L. Weiner, F. A. Jolesz and C. R. Guttmann (2003). "MRI contrast uptake in new lesions in relapsing-remitting MS followed at weekly intervals." Neurology **60**(4): 640-646.

Dal-Bianco, A., G. Grabner, C. Kronnerwetter, M. Weber, R. Höftberger, T. Berger, E. Auff, F. Leutmezer, S. Trattnig, H. Lassmann, F. Bagnato and S. Hametner (2017). "Slow expansion of multiple sclerosis iron rim lesions: pathology and 7 T magnetic resonance imaging." Acta Neuropathol **133**(1): 25-42.

Dammer, E. B., L. Ping, D. M. Duong, E. S. Modeste, N. T. Seyfried, J. J. Lah, A. I. Levey and E. C. B. Johnson (2022). "Multi-Platform Proteomic Analysis of Alzheimer's Disease Cerebrospinal Fluid and Plasma Reveals Network Biomarkers Associated with Proteostasis and the Matrisome." bioRxiv: 2022.2006.2020.494087.

Damotte, V., L. Guillot-Noel, N. A. Patsopoulos, L. Madireddy, M. El Behi, C. International Multiple Sclerosis Genetics, C. Wellcome Trust Case Control, P. L. De Jager, S. E. Baranzini, I. Cournu-Rebeix and B. Fontaine (2014). "A gene pathway analysis highlights the role of cellular adhesion molecules in multiple sclerosis susceptibility." Genes Immun **15**(2): 126-132.

Dawson, J. W. (1916). "The Histology of Disseminated Sclerosis." Edinburgh Medical Journal **17**(4): 229-241.

De Leener, B., S. Lévy, S. M. Dupont, V. S. Fonov, N. Stikov, D. Louis Collins, V. Callot and J. Cohen-Adad (2017). "SCT: Spinal Cord Toolbox, an open-source software for processing spinal cord MRI data." Neuroimage **145**(Pt A): 24-43.

De Stefano, N., S. Narayanan, G. S. Francis, R. Arnaoutelis, M. C. Tartaglia, J. P. Antel, P. M. Matthews and D. L. Arnold (2001). "Evidence of axonal damage in the early stages of multiple sclerosis and its relevance to disability." Arch Neurol **58**(1): 65-70.

DeLuca, G. C., G. C. Ebers and M. M. Esiri (2004). "Axonal loss in multiple sclerosis: a pathological survey of the corticospinal and sensory tracts." Brain **127**(Pt 5): 1009-1018.

DeLuca, G. C., K. Williams, N. Evangelou, G. C. Ebers and M. M. Esiri (2006). "The contribution of demyelination to axonal loss in multiple sclerosis." Brain **129**(Pt 6): 1507-1516.

DeLuca, G. C., R. Alterman, J. L. Martin, A. Mittal, S. Blundell, S. Bird, H. Beale, L. S. Hong and M. M. Esiri (2013). "Casting light on multiple sclerosis heterogeneity: the role of HLA-DRB1 on spinal cord pathology." Brain **136**(Pt 4): 1025-1034.

Disanto, G., P. Benkert, J. Lorscheider, S. Mueller, J. Vehoff, C. Zecca, S. Ramseier, L. Achtnichts, O. Findling, K. Nedeltchev, E. W. Radue, T. Sprenger, C. Stippich, T. Derfuss, J. F. Louvion, C. P. Kamm, H. P. Mattle, C. Lotter, R. Du Pasquier, M. Schluep, C. Pot, P. H. Lalive, Ö. Yaldizli, C. Gobbi, L. Kappos and J. Kuhle (2016). "The Swiss Multiple Sclerosis Cohort-Study (SMSC): A Prospective Swiss Wide Investigation of Key Phases in Disease Evolution and New Treatment Options." PLoS One **11**(3): e0152347.

Doherty, D. and M. J. Bamshad (2012). "Exome sequencing to find rare variants causing neurologic diseases." Neurology **79**(5): 396-397.

Duell, F., B. Evertsson, F. A. Nimer, Å. Sandin, D. Olsson, T. Olsson, M. Khademi, M. A. Hietala, F. Piehl and M. Hansson (2020). "Diagnostic accuracy of intrathecal kappa free light chains compared with OCBs in MS." Neurology - Neuroimmunology Neuroinflammation **7**(4): e775.

Dyment, D. A., G. C. Ebers and A. Dessa Sadovnick (2004). "Genetics of multiple sclerosis." The Lancet Neurology **3**(2): 104-110.

Dyment, D. A., M. Z. Cader, M. J. Chao, M. R. Lincoln, K. M. Morrison, G. Disanto, J. M. Morahan, G. C. De Luca, A. D. Sadovnick, P. Lepage, A. Montpetit, G. C. Ebers and S. V. Ramagopalan (2012). "Exome sequencing identifies a novel multiple sclerosis susceptibility variant in the TYK2 gene." Neurology **79**(5): 406-411.

Dziedzic, T., I. Metz, T. Dallenga, F. B. König, S. Müller, C. Stadelmann and W. Brück (2010). "Wallerian degeneration: a major component of early axonal pathology in multiple sclerosis." Brain Pathol **20**(5): 976-985.

Eden, D., C. Gros, A. Badji, S. M. Dupont, B. De Leener, J. Maranzano, R. Zhuoquiong, Y. Liu, T. Granberg, R. Ouellette, L. Stawiarz, J. Hillert, J. Talbott, E. Bannier, A. Kerbrat, G. Edan, P. Labauge, V. Callot, J. Pelletier, B. Audoin, H. Rasoanandrianina, J. C. Brisset, P. Valsasina, M. A. Rocca, M. Filippi, R. Bakshi, S. Tauhid, F. Prados, M. Yiannakas, H. Kearney, O. Ciccarelli,

S. A. Smith, C. Andrada Treaba, C. Mainero, J. Lefeuvre, D. S. Reich, G. Nair, T. M. Shepherd, E. Charlson, Y. Tachibana, M. Hori, K. Kamiya, L. Chougar, S. Narayanan and J. Cohen-Adad (2019). "Spatial distribution of multiple sclerosis lesions in the cervical spinal cord." Brain **142**(3): 633-646.
Elliott, C., J. S. Wolinsky, S. L. Hauser, L. Kappos, F. Barkhof, C. Bernasconi, W. Wei, S. Belachew and D. L. Arnold (2019). "Slowly expanding/evolving lesions as a magnetic resonance imaging marker of chronic active multiple sclerosis lesions." Mult Scler **25**(14): 1915-1925.

Eshaghi, A., R. V. Marinescu, A. L. Young, N. C. Firth, F. Prados, M. Jorge Cardoso, C. Tur, F. De Angelis, N. Cawley, W. J. Brownlee, N. De Stefano, M. Laura Stromillo, M. Battaglini, S. Ruggieri, C. Gasperini, M. Filippi, M. A. Rocca, A. Rovira, J. Sastre-Garriga, J. J. G. Geurts, H. Vrenken, V. Wottschel, C. E. Leurs, B. Uitdehaag, L. Pirpamer, C. Enzinger, S. Ourselin, C. A. Gandini Wheeler-Kingshott, D. Chard, A. J. Thompson, F. Barkhof, D. C. Alexander and O. Ciccarelli (2018). "Progression of regional grey matter atrophy in multiple sclerosis." Brain **141**(6): 1665-1677.

Evangelou, N., D. Konz, M. M. Esiri, S. Smith, J. Palace and P. M. Matthews (2000). "Regional axonal loss in the corpus callosum correlates with cerebral white matter lesion volume and distribution in multiple sclerosis." Brain **123 (Pt 9)**: 1845-1849.

Evangelou, N., G. C. DeLuca, T. Owens and M. M. Esiri (2005). "Pathological study of spinal cord atrophy in multiple sclerosis suggests limited role of local lesions." Brain **128**(Pt 1): 29-34.

Falini, B., L. Flenghi, S. Pileri, M. Gambacorta, B. Bigerna, H. Durkop, F. Eitelbach, J. Thiele, R. Pacini, A. Cavaliere and et al. (1993). "PG-M1: a new monoclonal antibody directed against a fixative-resistant epitope on the macrophage-restricted form of the CD68 molecule." Am J Pathol **142**(5): 1359-1372.

Farias, A. S., F. Pradella, A. Schmitt, L. M. Santos and D. Martins-de-Souza (2014). "Ten years of proteomics in multiple sclerosis." Proteomics **14**(4-5): 467-480.

Farina, G., R. Magliozzi, M. Pitteri, R. Reynolds, S. Rossi, A. Gajofatto, M. D. Benedetti, F. Facchiano, S. Monaco and M. Calabrese (2017). "Increased cortical lesion load and intrathecal inflammation is associated with oligoclonal bands in multiple sclerosis patients: a combined CSF and MRI study." J Neuroinflammation **14**(1): 40.
Ferguson, B., M. K. Matyszak, M. M. Esiri and V. H. Perry (1997). "Axonal damage in acute multiple sclerosis lesions." Brain **120 (Pt 3)**: 393-399.

Filippi, M., M. A. Rocca, F. Barkhof, W. Brück, J. T. Chen, G. Comi, G. DeLuca, N. De Stefano, B. J. Erickson, N. Evangelou, F. Fazekas, J. J. G. Geurts, C. Lucchinetti, D. H. Miller, D. Pelletier, B. F. G. Popescu and H. Lassmann (2012). "Association between pathological and MRI findings in multiple sclerosis." The Lancet Neurology **11**(4): 349-360.

Filippi, M., M. Bozzali, M. Rovaris, O. Gonen, C. Kesavadas, A. Ghezzi, V. Martinelli, R. I. Grossman, G. Scotti, G. Comi and A. Falini (2003). "Evidence for widespread axonal damage at the earliest clinical stage of multiple sclerosis." Brain **126**(2): 433-437.

Filippi, M., P. Preziosa, A. Meani, G. D. Costa, S. Mesaros, J. Drulovic, J. Ivanovic, A. Rovira, M. Tintorè, X. Montalban, O. Ciccarelli, W. Brownlee, K. Miszkiel, C. Enzinger, M. Khalil, F. Barkhof, E. M. M. Strijbis, J. L. Frederiksen, S. P. Cramer, E. Fainardi, M. P. Amato, C. Gasperini, S. Ruggieri, V. Martinelli, G. Comi, M. A. Rocca and o. b. o. t. M. S. Group (2022). "Performance of the 2017 and 2010 Revised McDonald Criteria in Predicting MS Diagnosis After a Clinically Isolated Syndrome." A MAGNIMS Study **98**(1): e1-e14.

Filippi, M., W. Brück, D. Chard, F. Fazekas, J. J. G. Geurts, C. Enzinger, S. Hametner, T. Kuhlmann, P. Preziosa, À. Rovira, K. Schmierer, C. Stadelmann and M. A. Rocca (2019). "Association between pathological and MRI findings in multiple sclerosis." Lancet Neurol **18**(2): 198-210.

Fog, T. (1950). "Topographic distribution of plques in the spinal cord in multiple sclerosis." Archives of Neurology & Psychiatry **63**(3): 382-414.

Fog, T. (1965). "The topography of plaques in multiple sclerosis with special reference to cerebral plaques." Acta neurologica Scandinavica. Supplementum **15**: 1-161.

Fransen, N. L., C. C. Hsiao, M. van der Poel, H. J. Engelenburg, K. Verdaasdonk, M. C. J. Vincenten, E. B. M. Remmerswaal, T. Kuhlmann, M. R. J. Mason, J. Hamann, J. Smolders and I. Huitinga (2020). "Tissue-resident memory T cells invade the brain parenchyma in multiple sclerosis white matter lesions." Brain **143**(6): 1714-1730.

Frischer, J. M., S. Bramow, A. Dal-Bianco, C. F. Lucchinetti, H. Rauschka, M. Schmidbauer, H. Laursen, P. S. Sorensen and H. Lassmann (2009). "The relation between inflammation and neurodegeneration in multiple sclerosis brains." Brain **132**(Pt 5): 1175-1189.

Frischer, J. M., S. D. Weigand, Y. Guo, N. Kale, J. E. Parisi, I. Pirko, J. Mandrekar, S. Bramow, I. Metz, W. Brück, H. Lassmann and C. F. Lucchinetti (2015). "Clinical and pathological insights into the dynamic nature of the white matter multiple sclerosis plaque." Ann Neurol **78**(5): 710-721.

Ganter, P., C. Prince and M. M. Esiri (1999). "Spinal cord axonal loss in multiple sclerosis: a post-mortem study." Neuropathol Appl Neurobiol **25**(6): 459-467.

Gasperi, C., A. Salmen, G. Antony, A. Bayas, C. Heesen, T. Kümpfel, R. A. Linker, F. Paul, M. Stangel, B. Tackenberg, F. T. Bergh, C. Warnke, F. Weber, H. Wiendl, B. Wildemann, U. K. Zettl, U. Ziemann, F. Zipp, H. Tumani, R. Gold, B. Hemmer and f. t. G. C. N. o. M. Sclerosis (2019). "Association of Intrathecal Immunoglobulin G Synthesis With Disability Worsening in Multiple Sclerosis." JAMA Neurology **76**(7): 841-849.

Gatenbee, C. D., A.-M. Baker, S. Prabhakaran, R. J. C. Slebos, G. Mandal, E. Mulholland, S. Leedham, J. R. Conejo-Garcia, C. H. Chung, M. Robertson-Tessi, T. A. Graham and A. R. A. Anderson (2021). "VALIS: Virtual Alignment of pathoLogy Image Series." bioRxiv: 2021.2011.2009.467917.

Gay, F. W., T. J. Drye, G. W. Dick and M. M. Esiri (1997). "The application of multifactorial cluster analysis in the staging of plaques in early multiple sclerosis. Identification and characterization of the primary demyelinating lesion." Brain **120 (Pt 8)**: 1461-1483.

Gentleman, S. M., M. J. Nash, C. J. Sweeting, D. I. Graham and G. W. Roberts (1993). "β-Amyloid precursor protein (βAPP) as a marker for axonal injury after head injury." Neuroscience Letters **160**(2): 139-144.

George, M. F., F. B. Briggs, X. Shao, M. A. Gianfrancesco, I. Kockum, H. F. Harbo, E. G. Celius, S. D. Bos, A. Hedström, L. Shen, A. Bernstein, L. Alfredsson, J. Hillert, T. Olsson, N. A. Patsopoulos, P. L. De Jager, A. B. Oturai, H. B. Søndergaard, F. Sellebjerg, P. S. Sorensen, R. Gomez, S. J. Caillier, B. A. Cree, J. R. Oksenberg, S. L. Hauser, S. D'Alfonso, M. A. Leone, F. Martinelli Boneschi, M. Sorosina, I. van der Mei, B. V. Taylor, Y. Zhou, C. Schaefer and L. F. Barcellos (2016). "Multiple sclerosis risk loci and disease severity in 7,125 individuals from 10 studies." Neurol Genet **2**(4): e87.

Geraldes, R., M. M. Esiri, R. Perera, S. A. Yee, D. Jenkins, J. Palace and G. C. DeLuca (2020). "Vascular disease and multiple sclerosis: a post-mortem study exploring their relationships." Brain **143**(10): 2998-3012.

Geraldes, R., O. Ciccarelli, F. Barkhof, N. De Stefano, C. Enzinger, M. Filippi, M. Hofer, F. Paul, P. Preziosa, A. Rovira, G. C. DeLuca, L. Kappos, T. Yousry, F. Fazekas, J. Frederiksen, C. Gasperini, J. Sastre-Garriga, N. Evangelou, J. Palace and M. s. g. on behalf of the (2018). "The current role of MRI in differentiating multiple sclerosis from its imaging mimics." Nature Reviews Neurology **14**(4): 199-213.

Geurts, J. J. and F. Barkhof (2008). "Grey matter pathology in multiple sclerosis." Lancet Neurol **7**(9): 841-851.

Gilmore, C. P., I. Donaldson, L. Bö, T. Owens, J. Lowe and N. Evangelou (2009a). "Regional variations in the extent and pattern of grey matter demyelination in multiple sclerosis: a comparison between the cerebral cortex, cerebellar cortex, deep grey matter nuclei and the spinal cord." J Neurol Neurosurg Psychiatry **80**(2): 182-187.

Gilmore, C. P., J. J. Geurts, N. Evangelou, J. C. Bot, R. A. van Schijndel, P. J. Pouwels, F. Barkhof and L. Bö (2009b). "Spinal cord grey matter lesions in multiple sclerosis detected by post-mortem high field MR imaging." Mult Scler **15**(2): 180-188.

Gilmore, C. P., G. C. DeLuca, L. Bö, T. Owens, J. Lowe, M. M. Esiri and N. Evangelou (2009c). "Spinal Cord Neuronal Pathology in Multiple Sclerosis." Brain Pathology **19**(4): 642-649.

Gilmore, C. P., L. Bö, T. Owens, J. Lowe, M. M. Esiri and N. Evangelou (2006). "Spinal cord gray matter demyelination in multiple sclerosis-a novel pattern of residual plaque morphology." Brain Pathol **16**(3): 202-208.

Giovannoni, G., G. Cutter, M. P. Sormani, S. Belachew, R. Hyde, H. Koendgen, V. Knappertz, D. Tomic, D. Leppert, R. Herndon, C. A. M. Wheeler-Kingshott, O. Ciccarelli, D. Selwood, E. V. di Cantogno, A. F. Ben-Amor, P. Matthews, D. Carassiti, D. Baker and K. Schmierer (2017). "Is multiple sclerosis a length-dependent central axonopathy? The case for therapeutic lag and the asynchronous progressive MS hypotheses." Mult Scler Relat Disord **12**: 70-78.

Gregory, S. G., S. Schmidt, P. Seth, J. R. Oksenberg, J. Hart, A. Prokop, S. J. Caillier, M. Ban, A. Goris, L. F. Barcellos, R. Lincoln, J. L. McCauley, S. J. Sawcer, D. A. Compston, B. Dubois, S. L. Hauser, M. A. Garcia-Blanco, M. A. Pericak-Vance, J. L. Haines and G. Multiple Sclerosis Genetics (2007). "Interleukin 7 receptor alpha chain (IL7R) shows allelic and functional association with multiple sclerosis." Nat Genet **39**(9): 1083-1091.

Gros, C., B. De Leener, A. Badji, J. Maranzano, D. Eden, S. M. Dupont, J. Talbott, R. Zhuoquiong, Y. Liu, T. Granberg, R. Ouellette, Y. Tachibana, M. Hori, K. Kamiya, L. Chougar, L. Stawiarz, J. Hillert, E. Bannier, A. Kerbrat, G. Edan, P. Labauge, V. Callot, J. Pelletier, B. Audoin, H. Rasoanandrianina, J. C. Brisset, P. Valsasina, M. A. Rocca, M. Filippi, R. Bakshi, S. Tauhid, F. Prados, M. Yiannakas, H. Kearney, O. Ciccarelli, S. Smith, C. A. Treaba, C. Mainero, J. Lefeuvre, D. S. Reich, G. Nair, V. Auclair, D. G. McLaren, A. R. Martin, M. G. Fehlings, S. Vahdat, A. Khatibi, J. Doyon, T. Shepherd, E. Charlson, S. Narayanan and J. Cohen-Adad (2019). "Automatic segmentation of the spinal cord and intramedullary multiple sclerosis lesions with convolutional neural networks." Neuroimage **184**: 901-915.

Grussu, F., T. Schneider, C. Tur, R. L. Yates, M. Tachrount, A. Ianuş, M. C. Yiannakas, J. Newcombe, H. Zhang, D. C. Alexander, G. C. DeLuca and C. A. M. Gandini Wheeler-Kingshott (2017). "Neurite dispersion: a new marker of multiple sclerosis spinal cord pathology?" Ann Clin Transl Neurol **4**(9): 663-679.

Haider, L., C. Simeonidou, G. Steinberger, S. Hametner, N. Grigoriadis, G. Deretzi, G. G. Kovacs, A. Kutzelnigg, H. Lassmann and J. M. Frischer (2014). "Multiple sclerosis deep grey matter: the relation between demyelination, neurodegeneration, inflammation and iron." J Neurol Neurosurg Psychiatry **85**(12): 1386-1395.

Håkansson, I., J. Ernerudh, M. Vrethem, C. Dahle and K. N. Ekdahl (2020). "Complement activation in cerebrospinal fluid in clinically isolated syndrome and early stages of relapsing remitting multiple sclerosis." Journal of Neuroimmunology **340**: 577147.

Hamzaoui, M., J. Garcia, G. Boffa, A. Lazzarotto, M. Absinta, V. A. G. Ricigliano, T. Soulier, M. Tonietto, P. Gervais, A. Bissery, C. Louapre, M. Bottlaender, B. Bodini and B. Stankoff (2023). "Positron emission tomography with [(18) F]-DPA-714 unveils a smoldering component in most multiple sclerosis lesions which drives disease progression." Ann Neurol.

Harirchian, M. H., F. Fatehi, P. Sarraf, N. M. Honarvar and S. Bitarafan (2018). "Worldwide prevalence of familial multiple sclerosis: A systematic review and meta-analysis." Mult Scler Relat Disord **20**: 43-47.

Hendricks, R., D. Baker, J. Brumm, T. Davancaze, C. Harp, A. Herman, H. V. Büdingen, M. Townsend and S. K. Fischer (2019). "Establishment of neurofilament light chain Simoa assay in cerebrospinal fluid and blood." Bioanalysis **11**(15): 1405-1418.

Heß, K., L. Starost, N. W. Kieran, C. Thomas, M. C. J. Vincenten, J. Antel, G. Martino, I. Huitinga, L. Healy and T. Kuhlmann (2020). "Lesion stage-dependent causes for impaired remyelination in MS." Acta Neuropathol **140**(3): 359-375.

Howell, O. W., C. A. Reeves, R. Nicholas, D. Carassiti, B. Radotra, S. M. Gentleman, B. Serafini, F. Aloisi, F. Roncaroli, R. Magliozzi and R. Reynolds (2011). "Meningeal inflammation is widespread and linked to cortical pathology in multiple sclerosis." Brain **134**(Pt 9): 2755-2771.

Howell, O. W., J. L. Rundle, A. Garg, M. Komada, P. J. Brophy and R. Reynolds (2010). "Activated microglia mediate axoglial disruption that contributes to axonal injury in multiple sclerosis." J Neuropathol Exp Neurol **69**(10): 1017-1033.

Imrell, K., A.-M. Landtblom, J. Hillert and T. Masterman (2006). "Multiple sclerosis with and without CSF bands: Clinically indistinguishable but immunogenetically distinct." Neurology **67**(6): 1062-1064.

Ingram, G., S. Loveless, O. W. Howell, S. Hakobyan, B. Dancey, C. L. Harris, N. P. Robertson, J. W. Neal and B. P. Morgan (2014). "Complement activation in multiple sclerosis plaques: an immunohistochemical analysis." Acta Neuropathol Commun **2**: 53.

International Multiple Sclerosis Genetics, C. (2009). "The expanding genetic overlap between multiple sclerosis and type I diabetes." Genes Immun **10**(1): 11-14.

International Multiple Sclerosis Genetics, C. (2013). "Network-based multiple sclerosis pathway analysis with GWAS data from 15,000 cases and 30,000 controls." Am J Hum Genet **92**(6): 854-865.

International Multiple Sclerosis Genetics, C., A. H. Beecham, N. A. Patsopoulos, D. K. Xifara, M. F. Davis, A. Kemppinen, C. Cotsapas, T. S. Shah, C. Spencer, D. Booth, A. Goris, A. Oturai, J. Saarela, B. Fontaine, B. Hemmer, C. Martin, F. Zipp, S. D'Alfonso, F. Martinelli-Boneschi, B. Taylor, H. F. Harbo, I. Kockum, J. Hillert, T. Olsson, M. Ban, J. R. Oksenberg, R. Hintzen, L. F. Barcellos, C. Wellcome Trust Case Control, I. B. D. G. C. International, C. Agliardi, L. Alfredsson, M. Alizadeh, C. Anderson, R. Andrews, H. B. Sondergaard, A. Baker, G. Band, S. E. Baranzini, N. Barizzone, J. Barrett, C. Bellenguez, L. Bergamaschi, L. Bernardinelli, A. Berthele, V. Biberacher, T. M. Binder, H. Blackburn, I. L. Bomfim, P. Brambilla, S. Broadley, B. Brochet, L. Brundin, D. Buck, H. Butzkueven, S. J. Caillier, W. Camu, W. Carpentier, P.

Cavalla, E. G. Celius, I. Coman, G. Comi, L. Corrado, L. Cosemans, I. Cournu-Rebeix, B. A. Cree, D. Cusi, V. Damotte, G. Defer, S. R. Delgado, P. Deloukas, A. di Sapio, A. T. Dilthey, P. Donnelly, B. Dubois, M. Duddy, S. Edkins, I. Elovaara, F. Esposito, N. Evangelou, B. Fiddes, J. Field, A. Franke, C. Freeman, I. Y. Frohlich, D. Galimberti, C. Gieger, P. A. Gourraud, C. Graetz, A. Graham, V. Grummel, C. Guaschino, A. Hadjixenofontos, H. Hakonarson, C. Halfpenny, G. Hall, P. Hall, A. Hamsten, J. Harley, T. Harrower, C. Hawkins, G. Hellenthal, C. Hillier, J. Hobart, M. Hoshi, S. E. Hunt, M. Jagodic, I. Jelcic, A. Jochim, B. Kendall, A. Kermode, T. Kilpatrick, K. Koivisto, I. Konidari, T. Korn, H. Kronsbein, C. Langford, M. Larsson, M. Lathrop, C. Lebrun-Frenay, J. Lechner-Scott, M. H. Lee, M. A. Leone, V. Leppa, G. Liberatore, B. A. Lie, C. M. Lill, M. Linden, J. Link, F. Luessi, J. Lycke, F. Macciardi, S. Mannisto, C. P. Manrique, R. Martin, V. Martinelli, D. Mason, G. Mazibrada, C. McCabe, I. L. Mero, J. Mescheriakova, L. Moutsianas, K. M. Myhr, G. Nagels, R. Nicholas, P. Nilsson, F. Piehl, M. Pirinen, S. E. Price, H. Quach, M. Reunanen, W. Robberecht, N. P. Robertson, M. Rodegher, D. Rog, M. Salvetti, N. C. Schnetz-Boutaud, F. Sellebjerg, R. C. Selter, C. Schaefer, S. Shaunak, L. Shen, S. Shields, V. Siffrin, M. Slee, P. S. Sorensen, M. Sorosina, M. Sospedra, A. Spurkland, A. Strange, E. Sundqvist, V. Thijs, J. Thorpe, A. Ticca, P. Tienari, C. van Duijn, E. M. Visser, S. Vucic, H. Westerlind, J. S. Wiley, A. Wilkins, J. F. Wilson, J. Winkelmann, J. Zajicek, E. Zindler, J. L. Haines, M. A. Pericak-Vance, A. J. Ivinson, G. Stewart, D. Hafler, S. L. Hauser, A. Compston, G. McVean, P. De Jager, S. J. Sawcer and J. L. McCauley (2013). "Analysis of immune-related loci identifies 48 new susceptibility variants for multiple sclerosis." Nat Genet **45**(11): 1353-1360.

Izquierdo, G., S. Angulo, J. M. Garcia-Moreno, M. A. Gamero, G. Navarro, J. M. Gata, J. L. Ruiz-Peña and M. D. Páramo (2002). "Intrathecal IgG synthesis: marker of progression in multiple sclerosis patients." Acta Neurol Scand **105**(3): 158-163.

Jäkel, S., E. Agirre, A. Mendanha Falcão, D. van Bruggen, K. W. Lee, I. Knuesel, D. Malhotra, C. Ffrench-Constant, A. Williams and G. Castelo-Branco (2019). "Altered human oligodendrocyte heterogeneity in multiple sclerosis." Nature **566**(7745): 543-547.

Jokubaitis, V. G., M. P. Campagna, O. Ibrahim, J. Stankovich, P. Kleinova, F. Matesanz, D. Hui, S. Eichau, M. Slee, J. Lechner-Scott, R. Lea, T. J. Kilpatrick, T. Kalincik, P. L. De Jager, A. Beecham, J. L. McCauley, B. V. Taylor, S. Vucic, L. Laverick, K. Vodehnalova, M. I. García-Sanchéz, A. Alcina, A. van der Walt, E. K. Havrdova, G. Izquierdo, N. Patsopoulos, D. Horakova and H. Butzkueven (2022). "Not all roads lead to the immune system: the genetic basis of multiple sclerosis severity." Brain.

Kalincik, T., G. Cutter, T. Spelman, V. Jokubaitis, E. Havrdova, D. Horakova, M. Trojano, G. Izquierdo, M. Girard, P. Duquette, A. Prat, A. Lugaresi, F. Grand'Maison, P. Grammond, R. Hupperts, C. Oreja-Guevara, C. Boz, E. Pucci, R. Bergamaschi, J. Lechner-Scott, R. Alroughani, V. Van Pesch, G. Iuliano, R. Fernandez-Bolaños, C. Ramo, M. Terzi, M. Slee, D. Spitaleri, F. Verheul, E. Cristiano, J. L. Sánchez-Menoyo, M. Fiol, O. Gray, J. A. Cabrera-Gomez, M. Barnett and H. Butzkueven (2015). "Defining reliable disability outcomes in multiple sclerosis." Brain **138**(Pt 11): 3287-3298.

Kappos, L., H. Butzkueven, H. Wiendl, T. Spelman, F. Pellegrini, Y. Chen, Q. Dong, H. Koendgen, S. Belachew and M. Trojano (2018). "Greater sensitivity to multiple sclerosis disability worsening and progression events using a roving versus a fixed reference value in a prospective cohort study." Mult Scler **24**(7): 963-973.

Kappos, L., J. S. Wolinsky, G. Giovannoni, D. L. Arnold, Q. Wang, C. Bernasconi, F. Model, H. Koendgen, M. Manfrini, S. Belachew and S. L. Hauser (2020). "Contribution of Relapse-Independent Progression vs Relapse-Associated Worsening to Overall Confirmed Disability Accumulation in Typical Relapsing Multiple Sclerosis in a Pooled Analysis of 2 Randomized Clinical Trials." JAMA Neurology **77**(9): 1132-1140.

Kearney, H., D. H. Miller and O. Ciccarelli (2015). "Spinal cord MRI in multiple sclerosis—diagnostic, prognostic and clinical value." Nature Reviews Neurology **11**(6): 327-338.

Kearney, H., D. R. Altmann, R. S. Samson, M. C. Yiannakas, C. A. Wheeler-Kingshott, O. Ciccarelli and D. H. Miller (2015). "Cervical cord lesion load is associated with disability independently from atrophy in MS." Neurology **84**(4): 367-373.

Kerbrat, A., C. Gros, A. Badji, E. Bannier, F. Galassi, B. Combès, R. Chouteau, P. Labauge, X. Ayrignac, C. Carra-Dalliere, J. Maranzano, T. Granberg, R. Ouellette, L. Stawiarz, J. Hillert, J. Talbott, Y. Tachibana, M. Hori, K. Kamiya, L. Chougar, J. Lefeuvre, D. S. Reich, G. Nair, P. Valsasina, M. A. Rocca, M. Filippi, R. Chu, R. Bakshi, V. Callot, J. Pelletier, B. Audoin, A. Maarouf, N. Collongues, J. De Seze, G. Edan and J. Cohen-Adad (2020). "Multiple sclerosis lesions in motor tracts from brain to cervical cord: spatial distribution and correlation with disability." Brain **143**(7): 2089-2105.

Khademi, M., I. Kockum, M. L. Andersson, E. Iacobaeus, L. Brundin, F. Sellebjerg, J. Hillert, F. Piehl and T. Olsson (2011). "Cerebrospinal fluid CXCL13 in multiple sclerosis: a suggestive prognostic marker for the disease course." Mult Scler **17**(3): 335-343.

Khaleeli, Z., O. Ciccarelli, K. Mizskiel, D. Altmann, D. H. Miller and A. J. Thompson (2010). "Lesion enhancement diminishes with time in primary progressive multiple sclerosis." Mult Scler **16**(3): 317-324.

Kiljan, S., P. Preziosa, L. E. Jonkman, W. D. van de Berg, J. Twisk, P. J. Pouwels, G. J. Schenk, M. A. Rocca, M. Filippi, J. J. Geurts and M. D. Steenwijk (2021). "Cortical axonal loss is associated with both gray matter demyelination and white matter tract pathology in progressive multiple sclerosis: Evidence from a combined MRI-histopathology study." Multiple Sclerosis Journal **27**(3): 380-390.

Kilsdonk, I. D., L. E. Jonkman, R. Klaver, S. J. van Veluw, J. J. M. Zwanenburg, J. P. A. Kuijer, P. J. W. Pouwels, J. W. R. Twisk, M. P. Wattjes, P. R. Luijten, F. Barkhof and J. J. G. Geurts (2016). "Increased cortical grey matter lesion detection in multiple sclerosis with 7 T MRI: a post-mortem verification study." Brain **139**(5): 1472-1481.

Klaver, R., V. Popescu, P. Voorn, Y. Galis-de Graaf, P. van der Valk, H. E. de Vries, G. J. Schenk and J. J. Geurts (2015). "Neuronal and axonal loss in normal-appearing gray matter and subpial lesions in multiple sclerosis." J Neuropathol Exp Neurol **74**(5): 453-458.

Koch, M., E. Kingwell, P. Rieckmann and H. Tremlett (2010). "The natural history of secondary progressive multiple sclerosis." J Neurol Neurosurg Psychiatry **81**(9): 1039-1043.

Kornek, B., M. K. Storch, R. Weissert, E. Wallstroem, A. Stefferl, T. Olsson, C. Linington, M. Schmidbauer and H. Lassmann (2000). "Multiple sclerosis and chronic autoimmune encephalomyelitis: a comparative quantitative study of axonal injury in active, inactive, and remyelinated lesions." Am J Pathol **157**(1): 267-276.

Kosa, P., C. Barbour, A. Wichman, M. Sandford, M. Greenwood and B. Bielekova (2018). "NeurEx: digitalized neurological examination offers a novel high-resolution disability scale." Ann Clin Transl Neurol **5**(10): 1241-1249.

Kosa, P., D. Ghazali, M. Tanigawa, C. Barbour, I. Cortese, W. Kelley, B. Snyder, J. Ohayon, K. Fenton, T. Lehky, T. Wu, M. Greenwood, G. Nair and B. Bielekova (2016). "Development of a Sensitive Outcome for Economical Drug Screening for Progressive Multiple Sclerosis Treatment." Frontiers in Neurology **7**.

Kosa, P., K. Lumbard, J. Wang, C. J. Liang, R. Masvekar, Y. Kim, M. Varosanec, L. Jennings and B. Bielekova (2022a). "Molecular mechanisms associated with multiple sclerosis progression, severity and phenotype." medRxiv: 2022.2010.2014.22281095.

Kosa, P., R. Masvekar, M. Komori, J. Phillips, V. Ramesh, M. Varosanec, M. Sandford and B. Bielekova (2022b). "Enhancing the clinical value of serum neurofilament light chain measurement." JCI Insight **7**(15).

Krieger, S. C., K. Cook, S. De Nino and M. Fletcher (2016). "The topographical model of multiple sclerosis." A dynamic visualization of disease course **3**(5): e279.

Kroksveen, A. C., J. A. Opsahl, A. Guldbrandsen, K. M. Myhr, E. Oveland, Ø. Torkildsen and F. S. Berven (2015). "Cerebrospinal fluid proteomics in multiple sclerosis." Biochim Biophys Acta **1854**(7): 746-756.

Kuhlmann, T., G. Lingfeld, A. Bitsch, J. Schuchardt and W. Brück (2002). "Acute axonal damage in multiple sclerosis is most extensive in early disease stages and decreases over time." Brain **125**(Pt 10): 2202-2212.

Kuhlmann, T., M. Moccia, T. Coetzee, J. A. Cohen, J. Correale, J. Graves, R. A. Marrie, X. Montalban, V. W. Yong, A. J. Thompson, D. S. Reich, M. P. Amato, B. Banwell, F. Barkhof, J. Chataway, T. Chitnis, G. Comi, T. Derfuss, M. Finlayson, M. Goldman, A. Green, K. Hellwig, D. Kos, A. Miller, E. Mowry, J. Oh, A. Salter, M. P. Sormani, M. Tintore, H. Tremlett, M.

Trojano, A. van der Walt, S. Vukusic and E. Waubant (2023). "Multiple sclerosis progression: time for a new mechanism-driven framework." The Lancet Neurology **22**(1): 78-88.

Kuhlmann, T., S. Ludwin, A. Prat, J. Antel, W. Brück and H. Lassmann (2017). "An updated histological classification system for multiple sclerosis lesions." Acta Neuropathol **133**(1): 13-24.

Kular, L., D. Klose, A. Urdánoz-Casado, E. Ewing, N. Planell, D. Gomez-Cabrero, M. Needhamsen and M. Jagodic (2022). "Epigenetic clock indicates accelerated aging in glial cells of progressive multiple sclerosis patients." Front Aging Neurosci **14**: 926468.

Kurtzke, J. F. (1983). "Rating neurologic impairment in multiple sclerosis: an expanded disability status scale (EDSS)." Neurology **33**(11): 1444-1452.

Langfelder, P. and S. Horvath (2008). "WGCNA: an R package for weighted correlation network analysis." BMC Bioinformatics **9**(1): 559.

Lassmann, H. (2005). "Multiple sclerosis pathology: evolution of pathogenetic concepts." Brain Pathol **15**(3): 217-222.

Lassmann, H. (2018). "Multiple Sclerosis Pathology." Cold Spring Harb Perspect Med **8**(3).

Leary, S. M., N. C. Silver, V. L. Stevenson, G. J. Barker, D. H. Miller and A. J. Thompson (1999). "Magnetisation transfer of normal appearing white matter in primary progressive multiple sclerosis." Multiple Sclerosis Journal **5**(5): 313-316.

Leone, M. A., N. Barizzone, F. Esposito, A. Lucenti, H. F. Harbo, A. Goris, I. Kockum, A. B. Oturai, E. G. Celius, I. L. Mero, B. Dubois, T. Olsson, H. B. Sondergaard, D. Cusi, S. Lupoli, B. K. Andreassen, C. International Multiple Sclerosis Genetics, C. Wellcome Trust Case Control, K. M. Myhr, F. R. Guerini, P. Group, P. Group, G. Comi, F. Martinelli-Boneschi and S. D'Alfonso (2013). "Association of genetic markers with CSF oligoclonal bands in multiple sclerosis patients." PLoS One **8**(6): e64408.

Lepore, V., C. Bosetti, C. Santucci, P. Iaffaldano, M. Trojano and P. Mosconi (2021). "Detection of disability worsening in relapsing-remitting multiple sclerosis patients: a real-world roving Expanded Disability Status Scale reference analysis from the Italian Multiple Sclerosis Register." Eur J Neurol **28**(2): 567-578.

Lindblom, R. P. F., S. Aeinehband, M. Ström, F. Al Nimer, K. Sandholm, M. Khademi, B. Nilsson, F. Piehl and K. N. Ekdahl (2016). "Complement Receptor 2 is increased in cerebrospinal fluid of multiple sclerosis patients and regulates C3 function." Clinical Immunology **166-167**: 89-95.

Lorscheider, J., K. Buzzard, V. Jokubaitis, T. Spelman, E. Havrdova, D. Horakova, M. Trojano, G. Izquierdo, M. Girard, P. Duquette, A. Prat, A. Lugaresi, F. Grand'Maison, P. Grammond, R.

Hupperts, R. Alroughani, P. Sola, C. Boz, E. Pucci, J. Lechner-Scott, R. Bergamaschi, C. Oreja-Guevara, G. Iuliano, V. Van Pesch, F. Granella, C. Ramo-Tello, D. Spitaleri, T. Petersen, M. Slee, F. Verheul, R. Ampapa, M. P. Amato, P. McCombe, S. Vucic, J. L. Sánchez Menoyo, E. Cristiano, M. H. Barnett, S. Hodgkinson, J. Olascoaga, M. L. Saladino, O. Gray, C. Shaw, F. Moore, H. Butzkueven, T. Kalincik and o. b. o. t. M. S. Group (2016). "Defining secondary progressive multiple sclerosis." Brain **139**(9): 2395-2405.

Lovas, G., N. Szilágyi, K. Majtényi, M. Palkovits and S. Komoly (2000). "Axonal changes in chronic demyelinated cervical spinal cord plaques." Brain **123 (Pt 2)**: 308-317.

Loveless, S., J. W. Neal, O. W. Howell, K. E. Harding, P. Sarkies, R. Evans, R. J. Bevan, S. Hakobyan, C. L. Harris, N. P. Robertson and B. P. Morgan (2018). "Tissue microarray methodology identifies complement pathway activation and dysregulation in progressive multiple sclerosis." Brain Pathol **28**(4): 507-520.

Lublin, F. D. and S. C. Reingold (1996). "Defining the clinical course of multiple sclerosis: results of an international survey. National Multiple Sclerosis Society (USA) Advisory Committee on Clinical Trials of New Agents in Multiple Sclerosis." Neurology **46**(4): 907-911.

Lublin, F. D., D. A. Häring, H. Ganjgahi, A. Ocampo, F. Hatami, J. Čuklina, P. Aarden, F. Dahlke, D. L. Arnold, H. Wiendl, T. Chitnis, T. E. Nichols, B. C. Kieseier and R. A. Bermel (2022). "How patients with multiple sclerosis acquire disability." Brain **145**(9): 3147-3161.

Lublin, F. D., S. C. Reingold, J. A. Cohen, G. R. Cutter, P. S. Sørensen, A. J. Thompson, J. S. Wolinsky, L. J. Balcer, B. Banwell, F. Barkhof, B. Bebo, Jr., P. A. Calabresi, M. Clanet, G. Comi, R. J. Fox, M. S. Freedman, A. D. Goodman, M. Inglese, L. Kappos, B. C. Kieseier, J. A. Lincoln, C. Lubetzki, A. E. Miller, X. Montalban, P. W. O'Connor, J. Petkau, C. Pozzilli, R. A. Rudick, M. P. Sormani, O. Stüve, E. Waubant and C. H. Polman (2014). "Defining the clinical course of multiple sclerosis: the 2013 revisions." Neurology **83**(3): 278-286.

Lucchinetti, C. F., B. F. Popescu, R. F. Bunyan, N. M. Moll, S. F. Roemer, H. Lassmann, W. Brück, J. E. Parisi, B. W. Scheithauer, C. Giannini, S. D. Weigand, J. Mandrekar and R. M. Ransohoff (2011). "Inflammatory cortical demyelination in early multiple sclerosis." N Engl J Med **365**(23): 2188-2197.

Lucchinetti, C., W. Brück, J. Parisi, B. Scheithauer, M. Rodriguez and H. Lassmann (2000). "Heterogeneity of multiple sclerosis lesions: implications for the pathogenesis of demyelination." Ann Neurol **47**(6): 707-717.

Luchetti, S., N. L. Fransen, C. G. van Eden, V. Ramaglia, M. Mason and I. Huitinga (2018). "Progressive multiple sclerosis patients show substantial lesion activity that correlates with clinical disease severity and sex: a retrospective autopsy cohort analysis." Acta Neuropathol **135**(4): 511-528.

Luchicchi, A., P. Preziosa and B. 't Hart (2021). "Editorial: “Inside-Out” vs “Outside-In” Paradigms in Multiple Sclerosis Etiopathogenesis." Frontiers in Cellular Neuroscience **15**.

Lukas, C., D. L. Knol, M. H. Sombekke, B. Bellenberg, H. K. Hahn, V. Popescu, K. Weier, E. W. Radue, A. Gass, L. Kappos, Y. Naegelin, B. M. Uitdehaag, J. J. Geurts, F. Barkhof and H. Vrenken (2015). "Cervical spinal cord volume loss is related to clinical disability progression in multiple sclerosis." J Neurol Neurosurg Psychiatry **86**(4): 410-418.

Ma, Y., D. Sannino, J. R. Linden, S. Haigh, B. Zhao, J. B. Grigg, P. Zumbo, F. Dündar, D. J. Butler, C. P. Profaci, K. M. Telesford, P. N. Winokur, K. R. Rumah, S. A. Gauthier, V. A. Fischetti, B. A. McClane, F. A. Uzal, L. Zexter, M. Mazzucco, R. Rudick, D. Danko, E. Balmuth, N. Nealon, J. Perumal, U. W. Kaunzner, I. L. Brito, Z. Chen, J. Z. Xiang, D. Betel, R. Daneman, G. F. Sonnenberg, C. E. Mason and T. Vartanian (2023). "Epsilon toxin-producing Clostridium perfringens colonize the MS gut and epsilon toxin overcomes immune privilege." The Journal of Clinical Investigation.

Magliozzi, R., G. Fadda, R. A. Brown, A. Bar-Or, O. W. Howell, S. Hametner, D. Marastoni, A. Poli, R. Nicholas, M. Calabrese, S. Monaco and R. Reynolds (2022). ""Ependymal-in" Gradient of Thalamic Damage in Progressive Multiple Sclerosis." Ann Neurol **92**(4): 670-685.

Magliozzi, R., O. Howell, A. Vora, B. Serafini, R. Nicholas, M. Puopolo, R. Reynolds and F. Aloisi (2007). "Meningeal B-cell follicles in secondary progressive multiple sclerosis associate with early onset of disease and severe cortical pathology." Brain **130**(Pt 4): 1089-1104.

Magliozzi, R., O. Howell, A. Vora, B. Serafini, R. Nicholas, M. Puopolo, R. Reynolds and F. Aloisi (2007). "Meningeal B-cell follicles in secondary progressive multiple sclerosis associate with early onset of disease and severe cortical pathology." Brain **130**(4): 1089-1104.

Magliozzi, R., O. W. Howell, C. Reeves, F. Roncaroli, R. Nicholas, B. Serafini, F. Aloisi and R. Reynolds (2010). "A Gradient of neuronal loss and meningeal inflammation in multiple sclerosis." Ann Neurol **68**(4): 477-493.

Magliozzi, R., O. W. Howell, R. Nicholas, C. Cruciani, M. Castellaro, C. Romualdi, S. Rossi, M. Pitteri, M. D. Benedetti, A. Gajofatto, F. B. Pizzini, S. Montemezzi, S. Rasia, R. Capra, A. Bertoldo, F. Facchiano, S. Monaco, R. Reynolds and M. Calabrese (2018). "Inflammatory intrathecal profiles and cortical damage in multiple sclerosis." Ann Neurol **83**(4): 739-755.

Magliozzi, R., S. Hametner, F. Facchiano, D. Marastoni, S. Rossi, M. Castellaro, A. Poli, F. Lattanzi, A. Visconti, R. Nicholas, R. Reynolds, S. Monaco, H. Lassmann and M. Calabrese (2019). "Iron homeostasis, complement, and coagulation cascade as CSF signature of cortical lesions in early multiple sclerosis." Annals of Clinical and Translational Neurology **6**(11): 2150-2163.

Manouchehrinia, A., E. Kingwell, F. Zhu, H. Tremlett, J. Hillert and R. Ramanujam (2021). "A multiple sclerosis disease progression measure based on cumulative disability." Mult Scler **27**(12): 1875-1883.

Manouchehrinia, A., H. Westerlind, E. Kingwell, F. Zhu, R. Carruthers, R. Ramanujam, M. Ban, A. Glaser, S. Sawcer, H. Tremlett and J. Hillert (2017). "Age Related Multiple Sclerosis Severity Score: Disability ranked by age." Mult Scler **23**(14): 1938-1946.

Marco, P., T.-O. Paula, H. Thorsten, L. Andreas, J. Ilijas, Z. Mario, J. H. Andreas, C. Carolina, F. Wolfgang, M. Roland and S. Mireia (2021). "Altered CSF Albumin Quotient Links Peripheral Inflammation and Brain Damage in MS." Neurology - Neuroimmunology Neuroinflammation **8**(2): e951.

Marrie, R. A., N. Reider, J. Cohen, O. Stuve, M. Trojano, G. Cutter, S. Reingold and P. S. Sorensen (2015). "A systematic review of the incidence and prevalence of cardiac, cerebrovascular, and peripheral vascular disease in multiple sclerosis." Mult Scler **21**(3): 318-331.

Marrie, R. A., R. Horwitz, G. Cutter, T. Tyry, D. Campagnolo and T. Vollmer (2009). "Comorbidity delays diagnosis and increases disability at diagnosis in MS." Neurology **72**(2): 117-124.

Marrie, R. A., R. Rudick, R. Horwitz, G. Cutter, T. Tyry, D. Campagnolo and T. Vollmer (2010). "Vascular comorbidity is associated with more rapid disability progression in multiple sclerosis." Neurology **74**(13): 1041-1047.

Martínez, M. A., B. Olsson, L. Bau, E. Matas, Á. Cobo Calvo, U. Andreasson, K. Blennow, L. Romero-Pinel, S. Martínez-Yélamos and H. Zetterberg (2015). "Glial and neuronal markers in cerebrospinal fluid predict progression in multiple sclerosis." Mult Scler **21**(5): 550-561.

Maver, A., P. Lavtar, S. Ristic, S. Stopinsek, S. Simcic, K. Hocevar, J. Sepcic, J. Drulovic, T. Pekmezovic, I. Novakovic, H. Alenka, G. Rudolf, S. Sega, N. Starcevic-Cizmarevic, A. Palandacic, G. Zamolo, M. Kapovic, T. Likar and B. Peterlin (2017). "Identification of rare genetic variation of NLRP1 gene in familial multiple sclerosis." Sci Rep **7**(1): 3715.

Mitrovic, M., N. Patsopoulos, A. Beecham, T. Dankowski, A. Goris, B. Dubois, M.-B. Dhooghe, R. Lemmens, P. Van Damme, K. Fitzgerald, H. Bach Sondergaard, F. Sellebjerg, P. S. Sorensen, H. Ullum, L. Wegner Thoerner, T. Werge, J. Saarela, I. Cournu-Rebeix, V. Damotte, B. Fontaine, L. Guillot-Noel, M. Lathrop, S. Vukusik, P.-A. Gourraud, T. Andlauer, V. Pongratz, D. Buck, C. Gasperi, C. Graetz, A. Bayas, C. Heesen, T. Kumpfel, R. Linker, F. Paul, M. Stangel, B. Tackenberg, F. Then Bergh, C. Warnke, H. Wiendl, B. Wildemann, U. Zettl, U. Ziemann, H. Tumani, R. Gold, V. Grummel, B. Hemmer, B. Knier, C. Lill, E. Luessi, E. Dardiotis, C. Agliardi, N. Barizzone, E. Mascia, L. Bernardinelli, G. Comi, D. Cusi, F. Esposito, L. Ferre, C. Comi, D. Galimberti, M. Leone, M. Sorosina, J. Y. Mescheriakova, R. Hintzen, C. Van Duijn, S. Bos, K.-M. Myhr, E. G. Celius, B. Lie, A. Spurkland, M. Comabella, X.

Montalban, L. Alfredsson, P. Stridh, J. Hillert, M. Jagodic, F. Piehl, I. Jelcic, R. Martin, M. Sospedra, M. Ban, C. Hawkins, P. Hysi, S. Kalra, F. Karpe, J. Khadake, G. Lachance, M. Neville, A. Santaniello, S. Caillier, P. Calabresi, B. Cree, A. Cross, M. Davis, J. Haines, P. de Bakker, S. Delgado, M. Dembele, K. Edwards, H. Hakonarson, I. Konidari, E. Lathi, C. Manrique, M. Pericak-Vance, L. Piccio, C. Schaefer, C. McCabe, H. Weiner, T. Olsson, G. Hadjigeorgiou, B. Taylor, L. Tajoori, J. Charlesworth, D. Booth, H. F. Harbo, A. Ivinson, S. Hauser, A. Compston, G. Stewart, F. Zipp, L. Barcellos, S. Baranzini, F. Martinelli Boneschi, S. D'Alfonso, A. Ziegler, A. Oturai, J. McCauley, S. Sawcer, J. Oksenberg, P. De Jager, I. Kockum, D. Hafler and C. Cotsapas (2018). "Low frequency and rare coding variation contributes to multiple sclerosis risk."

Moccia, M., F. Prados, M. Filippi, M. A. Rocca, P. Valsasina, W. J. Brownlee, C. Zecca, A. Gallo, A. Rovira, A. Gass, J. Palace, C. Lukas, H. Vrenken, S. Ourselin, C. A. M. Gandini Wheeler-Kingshott, O. Ciccarelli, F. Barkhof and f. t. M. S. Group (2019a). "Longitudinal spinal cord atrophy in multiple sclerosis using the generalized boundary shift integral." Annals of Neurology **86**(5): 704-713.

Moccia, M., N. Valsecchi, O. Ciccarelli, R. Van Schijndel, F. Barkhof and F. Prados (2020). "Spinal cord atrophy in a primary progressive multiple sclerosis trial: Improved sample size using GBSI." NeuroImage: Clinical **28**: 102418.

Moccia, M., S. Ruggieri, A. Ianniello, A. Toosy, C. Pozzilli and O. Ciccarelli (2019b). "Advances in spinal cord imaging in multiple sclerosis." Ther Adv Neurol Disord **12**: 1756286419840593.

Muñoz, U., C. Sebal, E. Escudero, M. Esiri, J. Tzartos, C. Sloan and M. C. Sadaba (2022). "Main Role of Antibodies in Demyelination and Axonal Damage in Multiple Sclerosis." Cell Mol Neurobiol **42**(6): 1809-1827.

Neumann, B., S. Foerster, C. Zhao, B. Bodini, D. S. Reich, D. E. Bergles, R. T. Káradóttir, C. Lubetzki, L. L. Lairson, B. Zalc, B. Stankoff and R. J. M. Franklin (2020). "Problems and Pitfalls of Identifying Remyelination in Multiple Sclerosis." Cell Stem Cell **26**(5): 617-619.

Norgren, N., P. Sundström, A. Svenningsson, L. Rosengren, T. Stigbrand and M. Gunnarsson (2004). "Neurofilament and glial fibrillary acidic protein in multiple sclerosis." Neurology **63**(9): 1586-1590.

O'Donovan, B., C. Mandel-Brehm, S. E. Vazquez, J. Liu, A. V. Parent, M. S. Anderson, T. Kassimatis, A. Zekeridou, S. L. Hauser, S. J. Pittock, E. Chow, M. R. Wilson and J. L. DeRisi (2020). "High-resolution epitope mapping of anti-Hu and anti-Yo autoimmunity by programmable phage display." Brain Communications **2**(2).

Oechtering, J., S. Schaedelin, P. Benkert, S. Müller, L. Achtnichts, J. Vehoff, G. Disanto, O. Findling, B. Fischer-Barnicol, A. Orleth, A. Chan, C. Pot, M. Barakovic, R. Rahmanzadeh, R. Galbusera, I. Heijnen, P. H. Lalive, J. Wuerfel, S. Subramaniam, S. Aeschbacher, D. Conen, Y.

Naegelin, A. Maceski, S. Meier, K. Berger, H. Wiendl, T. Lincke, J. Lieb, Ö. Yaldizli, T. Sinnecker, T. Derfuss, A. Regeniter, C. Zecca, C. Gobbi, L. Kappos, C. Granziera, D. Leppert and J. Kuhle (2021). "Intrathecal Immunoglobulin M Synthesis is an Independent Biomarker for Higher Disease Activity and Severity in Multiple Sclerosis." Ann Neurol **90**(3): 477-489.

Oechtering, J., T. Lincke, S. Schaedelin, B. F. Décard, A. Maceski, A. Orleth, S. Meier, E. Willemse, A. Buchmann, M. Khalil, T. Derfuss, P. Benkert, I. Heijnen, A. Regeniter, S. Müller, L. Achtnichts, P. Lalive, A. Salmen, C. Pot, C. Gobbi, L. Kappos, C. Granziera, D. Leppert, R. Schlaeger, J. M. Lieb and J. Kuhle (2022). "Intrathecal IgM Synthesis Is Associated with Spinal Cord Manifestation and Neuronal Injury in Early MS." Ann Neurol **91**(6): 814-820.

Oldham, M. C., G. Konopka, K. Iwamoto, P. Langfelder, T. Kato, S. Horvath and D. H. Geschwind (2008). "Functional organization of the transcriptome in human brain." Nature neuroscience **11**(11): 1271-1282.

Oppenheimer, D. R. (1978). "The cervical cord in multiple sclerosis." Neuropathol Appl Neurobiol **4**(2): 151-162.

Ozakbas, S., B. P. Cinar, P. Özcelik, H. Baser and G. Kosehasanoğullari (2017). "Intrathecal IgM index correlates with a severe disease course in multiple sclerosis: Clinical and MRI results." Clin Neurol Neurosurg **160**: 27-29.

Pagani, E., M. A. Rocca, A. Gallo, M. Rovaris, V. Martinelli, G. Comi and M. Filippi (2005). "Regional brain atrophy evolves differently in patients with multiple sclerosis according to clinical phenotype." AJNR Am J Neuroradiol **26**(2): 341-346.

Park, C., G. Ponath, M. Levine-Ritterman, E. Bull, E. C. Swanson, P. L. De Jager, B. M. Segal and D. Pitt (2019). "The landscape of myeloid and astrocyte phenotypes in acute multiple sclerosis lesions." Acta Neuropathol Commun **7**(1): 130.

Perini, P., F. Ranzato, M. Calabrese, L. Battistin and P. Gallo (2006). "Intrathecal IgM production at clinical onset correlates with a more severe disease course in multiple sclerosis." J Neurol Neurosurg Psychiatry **77**(8): 953-955.

Petrova, N., D. Carassiti, D. R. Altmann, D. Baker and K. Schmierer (2018). "Axonal loss in the multiple sclerosis spinal cord revisited." Brain Pathol **28**(3): 334-348.

Petrova, N., E. Nutma, D. Carassiti, J. Rs Newman, S. Amor, D. R. Altmann, D. Baker and K. Schmierer (2020). "Synaptic Loss in Multiple Sclerosis Spinal Cord." Annals of Neurology **n/a**(n/a).

Petzold, A., D. Gveric, M. Groves, K. Schmierer, D. Grant, M. Chapman, G. Keir, L. Cuzner and E. J. Thompson (2008). "Phosphorylation and compactness of neurofilaments in multiple sclerosis: indicators of axonal pathology." Exp Neurol **213**(2): 326-335.

Petzold, A., D. J. Tozer and K. Schmierer (2011). "Axonal damage in the making: neurofilament phosphorylation, proton mobility and magnetisation transfer in multiple sclerosis normal appearing white matter." Exp Neurol **232**(2): 234-239.

Petzold, A., M. J. Eikelenboom, D. Gveric, G. Keir, M. Chapman, R. H. Lazeron, M. L. Cuzner, C. H. Polman, B. M. Uitdehaag, E. J. Thompson and G. Giovannoni (2002). "Markers for different glial cell responses in multiple sclerosis: clinical and pathological correlations." Brain **125**(Pt 7): 1462-1473.

Popescu, B. F. and C. F. Lucchinetti (2012). "Meningeal and cortical grey matter pathology in multiple sclerosis." BMC Neurol **12**: 11.

Poser, C. M., D. W. Paty, L. Scheinberg, W. I. McDonald, F. A. Davis, G. C. Ebers, K. P. Johnson, W. A. Sibley, D. H. Silberberg and W. W. Tourtellotte (1983). "New diagnostic criteria for multiple sclerosis: guidelines for research protocols." Ann Neurol **13**(3): 227-231.

Poulsen, E. N., A. Olsson, S. Gustavsen, A. R. Langkilde, A. B. Oturai and J. F. Carlsen (2021). "MRI of the Entire Spinal Cord—Worth the While or Waste of Time? A Retrospective Study of 74 Patients with Multiple Sclerosis." Diagnostics **11**(8).

Prados, F., M. Moccia, A. Johnson, M. Yiannakas, F. Grussu, M. J. Cardoso, O. Ciccarelli, S. Ourselin, F. Barkhof and C. Wheeler-Kingshott (2020). "Generalised boundary shift integral for longitudinal assessment of spinal cord atrophy." Neuroimage **209**: 116489.

Ramaglia, V., S. Sheikh-Mohamed, K. Legg, C. Park, O. L. Rojas, S. Zandee, F. Fu, O. Ornatsky, E. C. Swanson, D. Pitt, A. Prat, T. D. McKee and J. L. Gommerman (2019). "Multiplexed imaging of immune cells in staged multiple sclerosis lesions by mass cytometry." Elife **8**.

Ramagopalan, S. V., D. A. Dyment, M. Z. Cader, K. M. Morrison, G. Disanto, J. M. Morahan, A. J. Berlanga-Taylor, A. Handel, G. C. De Luca, A. D. Sadovnick, P. Lepage, A. Montpetit and G. C. Ebers (2011). "Rare variants in the CYP27B1 gene are associated with multiple sclerosis." Ann Neurol **70**(6): 881-886.

Rashid, W., G. R. Davies, D. T. Chard, C. M. Griffin, D. R. Altmann, R. Gordon, A. J. Thompson and D. H. Miller (2006). "Increasing cord atrophy in early relapsing-remitting multiple sclerosis: a 3 year study." J Neurol Neurosurg Psychiatry **77**(1): 51-55.

Reali, C., R. Magliozzi, F. Roncaroli, R. Nicholas, O. W. Howell and R. Reynolds (2020). "B cell rich meningeal inflammation associates with increased spinal cord pathology in multiple sclerosis." Brain Pathology **30**(4): 779-793.

Reich, D. S., C. F. Lucchinetti and P. A. Calabresi (2018). "Multiple Sclerosis." N Engl J Med **378**(2): 169-180.

Reich, D. S., C. F. Lucchinetti and P. A. Calabresi (2018). "Multiple Sclerosis." New England Journal of Medicine **378**(2): 169-180.

Revesz, T., D. Kidd, A. J. Thompson, R. O. Barnard and W. I. McDonald (1994). "A comparison of the pathology of primary and secondary progressive multiple sclerosis." Brain **117 (Pt 4)**: 759-765.

Rindfleisch, E. (1863). "Histologisches Detail zu der grauen Degeneration von Gehirn und Rückenmark. (Zugleich ein Beitrag zu der Lehre von der Entstehung und Verwandlung der Zelle.)." Archiv für pathologische Anatomie und Physiologie und für klinische Medicin **26**(5): 474-483.

Rocca, M. A., G. Comi and M. Filippi (2017). "The Role of T1-Weighted Derived Measures of Neurodegeneration for Assessing Disability Progression in Multiple Sclerosis." Front Neurol **8**: 433.

Rovaris, M., M. Bozzali, G. Santuccio, G. Iannucci, M. P. Sormani, B. Colombo, G. Comi and M. Filippi (2000). "Relative contributions of brain and cervical cord pathology to multiple sclerosis disability: a study with magnetisation transfer ratio histogram analysis." J Neurol Neurosurg Psychiatry **69**(6): 723-727.

Roxburgh, R. H., S. R. Seaman, T. Masterman, A. E. Hensiek, S. J. Sawcer, S. Vukusic, I. Achiti, C. Confavreux, M. Coustans, E. le Page, G. Edan, G. V. McDonnell, S. Hawkins, M. Trojano, M. Liguori, E. Cocco, M. G. Marrosu, F. Tesser, M. A. Leone, A. Weber, F. Zipp, B. Miterski, J. T. Epplen, A. Oturai, P. S. Sørensen, E. G. Celius, N. T. Lara, X. Montalban, P. Villoslada, A. M. Silva, M. Marta, I. Leite, B. Dubois, J. Rubio, H. Butzkueven, T. Kilpatrick, M. P. Mycko, K. W. Selmaj, M. E. Rio, M. Sá, G. Salemi, G. Savettieri, J. Hillert and D. A. Compston (2005). "Multiple Sclerosis Severity Score: using disability and disease duration to rate disease severity." Neurology **64**(7): 1144-1151.

Rumah, K. R., J. Linden, V. A. Fischetti and T. Vartanian (2013). "Isolation of Clostridium perfringens type B in an individual at first clinical presentation of multiple sclerosis provides clues for environmental triggers of the disease." PLoS One **8**(10): e76359.

Sádaba, M. C., J. Tzartos, C. Paíno, M. García-Villanueva, J. C. Álvarez-Cermeño, L. M. Villar and M. M. Esiri (2012). "Axonal and oligodendrocyte-localized IgM and IgG deposits in MS lesions." Journal of Neuroimmunology **247**(1): 86-94.

Salzer, J., A. Svenningsson and P. Sundström (2010). "Neurofilament light as a prognostic marker in multiple sclerosis." Mult Scler **16**(3): 287-292.

Sastre-Garriga, J., A. Rovira, A. García-Vidal, P. Carbonell-Mirabent, M. Alberich, A. Vidal-Jordana, C. Auger, M. Tintore, X. Montalban and D. Pareto (2023). "Spinal cord reserve in multiple sclerosis." Journal of Neurology, Neurosurgery & Psychiatry: jnnp-2022-330613.

Sastre-Garriga, J., D. Pareto, M. Battaglini, M. A. Rocca, O. Ciccarelli, C. Enzinger, J. Wuerfel, M. P. Sormani, F. Barkhof, T. A. Yousry, N. De Stefano, M. Tintoré, M. Filippi, C. Gasperini, L. Kappos, J. Río, J. Frederiksen, J. Palace, H. Vrenken, X. Montalban, À. Rovira and M. s. g. on behalf of the (2020). "MAGNIMS consensus recommendations on the use of brain and spinal cord atrophy measures in clinical practice." Nature Reviews Neurology **16**(3): 171-182.

Sati, P., J. Oh, R. T. Constable, N. Evangelou, C. R. G. Guttmann, R. G. Henry, E. C. Klawiter, C. Mainero, L. Massacesi, H. McFarland, F. Nelson, D. Ontaneda, A. Rauscher, W. D. Rooney, A. P. R. Samaraweera, R. T. Shinohara, R. A. Sobel, A. J. Solomon, C. A. Treaba, J. Wuerfel, R. Zivadinov, N. L. Sicotte, D. Pelletier, D. S. Reich and N. C. on behalf of the (2016). "The central vein sign and its clinical evaluation for the diagnosis of multiple sclerosis: a consensus statement from the North American Imaging in Multiple Sclerosis Cooperative." Nature Reviews Neurology **12**(12): 714-722.

Scalfari, A., A. Neuhaus, M. Daumer, P. A. Muraro and G. C. Ebers (2014). "Onset of secondary progressive phase and long-term evolution of multiple sclerosis." Journal of Neurology, Neurosurgery & Psychiatry **85**(1): 67-75.

Schirmer, L., D. Velmeshev, S. Holmqvist, M. Kaufmann, S. Werneburg, D. Jung, S. Vistnes, J. H. Stockley, A. Young, M. Steindel, B. Tung, N. Goyal, A. Bhaduri, S. Mayer, J. B. Engler, O. A. Bayraktar, R. J. M. Franklin, M. Haeussler, R. Reynolds, D. P. Schafer, M. A. Friese, L. R. Shiow, A. R. Kriegstein and D. H. Rowitch (2019). "Neuronal vulnerability and multilineage diversity in multiple sclerosis." Nature **573**(7772): 75-82.

Schirmer, L., J. P. Antel, W. Brück and C. Stadelmann (2011). "Axonal loss and neurofilament phosphorylation changes accompany lesion development and clinical progression in multiple sclerosis." Brain Pathol **21**(4): 428-440.

Schwanhäusser, B., D. Busse, N. Li, G. Dittmar, J. Schuchhardt, J. Wolf, W. Chen and M. Selbach (2011). "Global quantification of mammalian gene expression control." Nature **473**(7347): 337-342.

Searle, S. R., F. M. Speed and G. A. Milliken (1980). "Population Marginal Means in the Linear Model: An Alternative to Least Squares Means." The American Statistician **34**(4): 216-221.

Seeker, L. A., N. Bestard-Cuche, S. Jäkel, N.-L. Kazakou, S. M. K. Bøstrand, A. M. Kilpatrick, D. Van Bruggen, M. Kabbe, F. B. Pohl, Z. Moslehi, N. C. Henderson, C. A. Vallejos, G. L. Manno, G. Castelo-Branco and A. Williams (2022). "Marked regional glial heterogeneity in the human white matter of the central nervous system." bioRxiv: 2022.2003.2022.485367.

Sen, M. K., M. S. M. Almuslehi, P. J. Shortland, D. A. Mahns and J. R. Coorssen (2021). "Proteomics of Multiple Sclerosis: Inherent Issues in Defining the Pathoetiology and Identifying (Early) Biomarkers." Int J Mol Sci **22**(14).

Serafini, B., B. Rosicarelli, D. Franciotta, R. Magliozzi, R. Reynolds, P. Cinque, L. Andreoni, P. Trivedi, M. Salvetti, A. Faggioni and F. Aloisi (2007). "Dysregulated Epstein-Barr virus infection in the multiple sclerosis brain." J Exp Med **204**(12): 2899-2912.

Serafini, B., B. Rosicarelli, R. Magliozzi, E. Stigliano and F. Aloisi (2004). "Detection of ectopic B-cell follicles with germinal centers in the meninges of patients with secondary progressive multiple sclerosis." Brain Pathol **14**(2): 164-174.

Simonsen, C. S., H. Flemmen, T. Lauritzen, P. Berg-Hansen, S. M. Moen and E. G. Celius (2020). "The diagnostic value of IgG index versus oligoclonal bands in cerebrospinal fluid of patients with multiple sclerosis." Mult Scler J Exp Transl Clin **6**(1): 2055217319901291.

Sinah, E., S. Falk, U. Timo, S.-K. Peter, Z. Frauke, B. Stefan and L. Felix (2020). "Association of intrathecal pleocytosis and IgG synthesis with axonal damage in early MS." Neurology - Neuroimmunology Neuroinflammation **7**(3): e679.

Singh, S., T. Dallenga, A. Winkler, S. Roemer, B. Maruschak, H. Siebert, W. Brück and C. Stadelmann (2017). "Relationship of acute axonal damage, Wallerian degeneration, and clinical disability in multiple sclerosis." J Neuroinflammation **14**(1): 57.

Solomon, A. J., R. T. Naismith and A. H. Cross (2019). "Misdiagnosis of multiple sclerosis." Impact of the 2017 McDonald criteria on clinical practice **92**(1): 26-33.

Sombekke, M. H., M. P. Wattjes, L. J. Balk, J. M. Nielsen, H. Vrenken, B. M. Uitdehaag, C. H. Polman and F. Barkhof (2013). "Spinal cord lesions in patients with clinically isolated syndrome: a powerful tool in diagnosis and prognosis." Neurology **80**(1): 69-75.

Stendahl-Brodin, L. and H. Link (1980). "Relation between benign course of multiple sclerosis and low-grade humoral immune response in cerebrospinal fluid." J Neurol Neurosurg Psychiatry **43**(2): 102-105.

Storch, M. K., S. Piddlesden, M. Haltia, M. Iivanainen, P. Morgan and H. Lassmann (1998). "Multiple sclerosis: In situ evidence for antibody- and complement-mediated demyelination." Annals of Neurology **43**(4): 465-471.

Stratton, K. G., B.-J. M. Webb-Robertson, L. A. McCue, B. Stanfill, D. Claborne, I. Godinez, T. Johansen, A. M. Thompson, K. E. Burnum-Johnson, K. M. Waters and L. M. Bramer (2019). "pmartR: Quality Control and Statistics for Mass Spectrometry-Based Biological Data." Journal of Proteome Research **18**(3): 1418-1425.

Sumowski, J. F., M. A. Rocca, V. M. Leavitt, A. Meani, S. Mesaros, J. Drulovic, P. Preziosa, C. G. Habeck and M. Filippi (2016). "Brain reserve against physical disability progression over 5 years in multiple sclerosis." Neurology **86**(21): 2006-2009.

Tallantyre, E. C., L. Bø, O. Al-Rawashdeh, T. Owens, C. H. Polman, J. Lowe and N. Evangelou (2009). "Greater loss of axons in primary progressive multiple sclerosis plaques compared to secondary progressive disease." Brain **132**(5): 1190-1199.

Tallantyre, E. C., L. Bø, O. Al-Rawashdeh, T. Owens, C. H. Polman, J. S. Lowe and N. Evangelou (2010). "Clinico-pathological evidence that axonal loss underlies disability in progressive multiple sclerosis." Mult Scler **16**(4): 406-411.

Tedeholm, H., F. Piehl, J. Lycke, J. Link, L. Stawiarz, J. Burman, P. de Flon, K. Fink, M. Gunnarsson, J. Mellergård, P. Nilsson, P. Sundström, A. Svenningsson, H. Johansson and O. Andersen (2022). "Effectiveness of first generation disease-modifying therapy to prevent conversion to secondary progressive multiple sclerosis." Multiple Sclerosis and Related Disorders **68**: 104220.

Teunissen, C. E. and M. Khalil (2012). "Neurofilaments as biomarkers in multiple sclerosis." Mult Scler **18**(5): 552-556.

Theodoropoulou, E., L. Alfredsson, F. Piehl, F. Marabita and M. Jagodic (2019). "Different epigenetic clocks reflect distinct pathophysiological features of multiple sclerosis." Epigenomics **11**(12): 1429-1439.

Thompson, A. J., B. L. Banwell, F. Barkhof, W. M. Carroll, T. Coetzee, G. Comi, J. Correale, F. Fazekas, M. Filippi, M. S. Freedman, K. Fujihara, S. L. Galetta, H. P. Hartung, L. Kappos, F. D. Lublin, R. A. Marrie, A. E. Miller, D. H. Miller, X. Montalban, E. M. Mowry, P. S. Sorensen, M. Tintoré, A. L. Traboulsee, M. Trojano, B. M. J. Uitdehaag, S. Vukusic, E. Waubant, B. G. Weinshenker, S. C. Reingold and J. A. Cohen (2018). "Diagnosis of multiple sclerosis: 2017 revisions of the McDonald criteria." The Lancet Neurology **17**(2): 162-173.

Tiftikçioğlu, B. (2018). "Multiple Sclerosis Functional Composite (MSFC): Scoring Instructions." Noro Psikiyatr Ars **55**(Suppl 1): S46-s48.

Tintore, M., À. Rovira, J. Río, S. Otero-Romero, G. Arrambide, C. Tur, M. Comabella, C. Nos, M. J. Arévalo, L. Negrotto, I. Galán, A. Vidal-Jordana, J. Castilló, F. Palavra, E. Simon, R. Mitjana, C. Auger, J. Sastre-Garriga and X. Montalban (2015). "Defining high, medium and low impact prognostic factors for developing multiple sclerosis." Brain **138**(Pt 7): 1863-1874.

Traboulsee, A. L., C. Q. Bernales, J. P. Ross, J. D. Lee, A. D. Sadovnick and C. Vilarino-Guell (2014). "Genetic variants in IL2RA and IL7R affect multiple sclerosis disease risk and progression." Neurogenetics **15**(3): 165-169.

Trapp, B. D., J. Peterson, R. M. Ransohoff, R. Rudick, S. Mörk and L. Bö (1998). "Axonal transection in the lesions of multiple sclerosis." N Engl J Med **338**(5): 278-285.

Trapp, B. D., M. Vignos, J. Dudman, A. Chang, E. Fisher, S. M. Staugaitis, H. Battapady, S. Mork, D. Ontaneda, S. E. Jones, R. J. Fox, J. Chen, K. Nakamura and R. A. Rudick (2018).

"Cortical neuronal densities and cerebral white matter demyelination in multiple sclerosis: a retrospective study." Lancet Neurol **17**(10): 870-884.

Tremlett, H., M. Yousefi, V. Devonshire, P. Rieckmann and Y. Zhao (2009). "Impact of multiple sclerosis relapses on progression diminishes with time." Neurology **73**(20): 1616-1623.

Tur, C., P. Carbonell-Mirabent, Á. Cobo-Calvo, S. Otero-Romero, G. Arrambide, L. Midaglia, J. Castilló, Á. Vidal-Jordana, B. Rodríguez-Acevedo, A. Zabalza, I. Galán, C. Nos, A. Salerno, C. Auger, D. Pareto, M. Comabella, J. Río, J. Sastre-Garriga, À. Rovira, M. Tintoré and X. Montalban (2023). "Association of Early Progression Independent of Relapse Activity With Long-term Disability After a First Demyelinating Event in Multiple Sclerosis." JAMA Neurology **80**(2): 151-160.

Uhlén, M., L. Fagerberg, B. M. Hallström, C. Lindskog, P. Oksvold, A. Mardinoglu, Å. Sivertsson, C. Kampf, E. Sjöstedt, A. Asplund, I. Olsson, K. Edlund, E. Lundberg, S. Navani, C. A. Szigyarto, J. Odeberg, D. Djureinovic, J. O. Takanen, S. Hober, T. Alm, P. H. Edqvist, H. Berling, H. Tegel, J. Mulder, J. Rockberg, P. Nilsson, J. M. Schwenk, M. Hamsten, K. von Feilitzen, M. Forsberg, L. Persson, F. Johansson, M. Zwahlen, G. von Heijne, J. Nielsen and F. Pontén (2015). "Proteomics. Tissue-based map of the human proteome." Science **347**(6220): 1260419.

University of California, S. F. M. S. E. T., B. A. C. Cree, J. A. Hollenbach, R. Bove, G. Kirkish, S. Sacco, E. Caverzasi, A. Bischof, T. Gundel, A. H. Zhu, N. Papinutto, W. A. Stern, C. Bevan, A. Romeo, D. S. Goodin, J. M. Gelfand, J. Graves, A. J. Green, M. R. Wilson, S. S. Zamvil, C. Zhao, R. Gomez, N. R. Ragan, G. Q. Rush, P. Barba, A. Santaniello, S. E. Baranzini, J. R. Oksenberg, R. G. Henry and S. L. Hauser (2019). "Silent progression in disease activity–free relapsing multiple sclerosis." Annals of Neurology **85**(5): 653-666.

Valsasina, P., M. A. Rocca, M. A. Horsfield, M. Copetti and M. Filippi (2015). "A longitudinal MRI study of cervical cord atrophy in multiple sclerosis." J Neurol **262**(7): 1622-1628.

van den Bosch, A., N. Fransen, M. Mason, A. J. Rozemuller, C. Teunissen, J. Smolders and I. Huitinga (2022). "Neurofilament Light Chain Levels in Multiple Sclerosis Correlate With Lesions Containing Foamy Macrophages and With Acute Axonal Damage." Neurology - Neuroimmunology Neuroinflammation **9**(3): e1154.

van Walderveen, M. A., W. Kamphorst, P. Scheltens, J. H. van Waesberghe, R. Ravid, J. Valk, C. H. Polman and F. Barkhof (1998). "Histopathologic correlate of hypointense lesions on T1-weighted spin-echo MRI in multiple sclerosis." Neurology **50**(5): 1282-1288.

Vecchio, D., I. Crespi, E. Virgilio, P. Naldi, M. P. Campisi, R. Serino, U. Dianzani, G. Bellomo, R. Cantello and C. Comi (2019). "Kappa free light chains could predict early disease course in multiple sclerosis." Mult Scler Relat Disord **30**: 81-84.

Villar, L. M., J. Masjuan, P. González-Porqué, J. Plaza, M. C. Sádaba, E. Roldán, A. Bootello and J. C. Alvarez-Cermeño (2003). "Intrathecal IgM synthesis is a prognostic factor in multiple sclerosis." Ann Neurol **53**(2): 222-226.

Villar, L., N. García-Barragán, M. Espiño, E. Roldán, M. Sádaba, J. Gómez-Rial, P. González-Porqué and J. Alvarez-Cermeño (2008). "Influence of oligoclonal IgM specificity in multiple sclerosis disease course." Mult Scler **14**(2): 183-187.

Vulpian, E. (1866). "Note sur la sclérose en plaques de la moelle épinière." L'Union Médicale **30**: 459-465.

Wagley, S., M. Bokori-Brown, H. Morcrette, A. Malaspina, C. D'Arcy, S. Gnanapavan, N. Lewis, M. R. Popoff, D. Raciborska, R. Nicholas, B. Turner and R. W. Titball (2019). "Evidence of Clostridium perfringens epsilon toxin associated with multiple sclerosis." Mult Scler **25**(5): 653-660.

Wallin, M. T., W. J. Culpepper, J. D. Campbell, L. M. Nelson, A. Langer-Gould, R. A. Marrie, G. R. Cutter, W. E. Kaye, L. Wagner, H. Tremlett, S. L. Buka, P. Dilokthornsakul, B. Topol, L. H. Chen and N. G. LaRocca (2019). "The prevalence of MS in the United States." A population-based estimate using health claims data **92**(10): e1029-e1040.

Walton, C., R. King, L. Rechtman, W. Kaye, E. Leray, R. A. Marrie, N. Robertson, N. La Rocca, B. Uitdehaag, I. van der Mei, M. Wallin, A. Helme, C. Angood Napier, N. Rijke and P. Baneke (2020). "Rising prevalence of multiple sclerosis worldwide: Insights from the Atlas of MS, third edition." Multiple Sclerosis Journal **26**(14): 1816-1821.

Watkins, L. M., J. W. Neal, S. Loveless, I. Michailidou, V. Ramaglia, M. I. Rees, R. Reynolds, N. P. Robertson, B. P. Morgan and O. W. Howell (2016). "Complement is activated in progressive multiple sclerosis cortical grey matter lesions." J Neuroinflammation **13**(1): 161.

Wattjes, M. P., O. Ciccarelli, D. S. Reich, B. Banwell, N. de Stefano, C. Enzinger, F. Fazekas, M. Filippi, J. Frederiksen, C. Gasperini, Y. Hacohen, L. Kappos, D. K. B. Li, K. Mankad, X. Montalban, S. D. Newsome, J. Oh, J. Palace, M. A. Rocca, J. Sastre-Garriga, M. Tintoré, A. Traboulsee, H. Vrenken, T. Yousry, F. Barkhof, À. Rovira, M. P. Wattjes, O. Ciccarelli, N. de Stefano, C. Enzinger, F. Fazekas, M. Filippi, J. Frederiksen, C. Gasperini, Y. Hacohen, L. Kappos, K. Mankad, X. Montalban, J. Palace, M. A. Rocca, J. Sastre-Garriga, M. Tintore, H. Vrenken, T. Yousry, F. Barkhof, A. Rovira, D. K. B. Li, A. Traboulsee, S. D. Newsome, B. Banwell, J. Oh, D. S. Reich, D. S. Reich and J. Oh (2021). "2021 MAGNIMS–CMSC–NAIMS consensus recommendations on the use of MRI in patients with multiple sclerosis." The Lancet Neurology **20**(8): 653-670.

Wei, R., J. Wang, M. Su, E. Jia, S. Chen, T. Chen and Y. Ni (2018). "Missing Value Imputation Approach for Mass Spectrometry-based Metabolomics Data." Scientific Reports **8**(1): 663.

Weideman, A. M., C. Barbour, M. A. Tapia-Maltos, T. Tran, K. Jackson, P. Kosa, M. Komori, A. Wichman, K. Johnson, M. Greenwood and B. Bielekova (2017a). "New Multiple Sclerosis Disease Severity Scale Predicts Future Accumulation of Disability." Front Neurol **8**: 598.

Weideman, A. M., M. A. Tapia-Maltos, K. Johnson, M. Greenwood and B. Bielekova (2017b). "Meta-analysis of the Age-Dependent Efficacy of Multiple Sclerosis Treatments." Front Neurol **8**: 577.

Weier, K., J. Mazraeh, Y. Naegelin, A. Thoeni, J. G. Hirsch, T. Fabbro, N. Bruni, H. Duyar, K. Bendfeldt, E. W. Radue, L. Kappos and A. Gass (2012). "Biplanar MRI for the assessment of the spinal cord in multiple sclerosis." Mult Scler **18**(11): 1560-1569.

Weinshenker, B. G., G. P. Rice, J. H. Noseworthy, W. Carriere, J. Baskerville and G. C. Ebers (1991). "The natural history of multiple sclerosis: a geographically based study. 3. Multivariate analysis of predictive factors and models of outcome." Brain **114 (Pt 2)**: 1045-1056.

Wheeler, M. A., I. C. Clark, E. C. Tjon, Z. Li, S. E. J. Zandee, C. P. Couturier, B. R. Watson, G. Scalisi, S. Alkwai, V. Rothhammer, A. Rotem, J. A. Heyman, S. Thaploo, L. M. Sanmarco, J. Ragoussis, D. A. Weitz, K. Petrecca, J. R. Moffitt, B. Becher, J. P. Antel, A. Prat and F. J. Quintana (2020). "MAFG-driven astrocytes promote CNS inflammation." Nature **578**(7796): 593-599.

Wishart, D. S., C. Knox, A. C. Guo, S. Shrivastava, M. Hassanali, P. Stothard, Z. Chang and J. Woolsey (2006). "DrugBank: a comprehensive resource for in silico drug discovery and exploration." Nucleic Acids Res **34**(Database issue): D668-672.

Yates, R. L., M. M. Esiri, J. Palace, B. Jacobs, R. Perera and G. C. DeLuca (2017). "Fibrin(ogen) and neurodegeneration in the progressive multiple sclerosis cortex." Ann Neurol **82**(2): 259-270.

Zamecnik, C. R., J. V. Rajan, K. A. Yamauchi, S. A. Mann, R. P. Loudermilk, G. M. Sowa, K. C. Zorn, B. D. Alvarenga, C. Gaebler, M. Caskey, M. Stone, P. J. Norris, W. Gu, C. Y. Chiu, D. Ng, J. R. Byrnes, X. X. Zhou, J. A. Wells, D. F. Robbiani, M. C. Nussenzweig, J. L. DeRisi and M. R. Wilson (2020). "ReScan, a Multiplex Diagnostic Pipeline, Pans Human Sera for SARS-CoV-2 Antigens." Cell Reports Medicine **1**(7): 100123.

Zhang, X., A. H. Smits, G. B. A. van Tilburg, H. Ovaa, W. Huber and M. Vermeulen (2018). "Proteome-wide identification of ubiquitin interactions using UbIA-MS." Nature Protocols **13**(3): 530-550.

Ziemssen, T., K. Akgün and W. Brück (2019). "Molecular biomarkers in multiple sclerosis." Journal of Neuroinflammation **16**(1): 272.

Zrzavy, T., S. Hametner, I. Wimmer, O. Butovsky, H. L. Weiner and H. Lassmann (2017). "Loss of 'homeostatic' microglia and patterns of their activation in active multiple sclerosis." Brain **140**(7): 1900-1913.